# FOULING AND WETTING IN MEMBRANE DISTILLATION: MECHANISMS AND MITIGATION STRATEGIES

By

Zhangxin Wang

Dissertation
Submitted to the Faculty of the
Graduate School of Vanderbilt University
in partial fulfillment of the requirements
for the degree of

DOCTOR OF PHILOSOPHY
in

Environmental Engineering

September 30, 2018
Nashville, Tennessee

Approved:

Shihong Lin, Ph.D.
Florence Sanchez, Ph.D.
Alan Bowers, Ph.D.
Paul E. Laibinis, Ph.D.
G. Kane Jennings, Ph.D.

*To my parents,*

*For their love, encouragement, and support*

ACKNOWLEDGEMENTS

I would like to express my great thankfulness to Dr. Shihong Lin, who has been an excellent advisor and mentor throughout my Ph.D. study. Without his guidance and support, I would not be able to have such fulfillments in the past 4 years. I also want to thank Dr. Florence Sanchez, Dr. Alan Bowers, Dr. Paul Laibinis, and Dr. Kane Jennings for serving on my dissertation committee and giving me valuable suggestions.

I would like to give thanks to my colleagues in Dr. Lin's group, including Deyin Hou, Yuxi Huang, Yuanmiaoliang Chen, Thomas Horseman, Kofi Christie, Li Wang, Yuanzhe Liang and so on. These people are not only my teammates who have lent me hands in my academic journey, but also my friends who have decorated my life at Vanderbilt University more colorful. Best luck to all of you and I hope we can have our paths crossing again in the future.

I want to thank Rossane Delapp and Dalesha Blackwell, the CEE lab managers who have offered me a lot of help in my experiments. I also want to thank the ViNSE faculty members for training and helping me to use the lab instruments.

Last but not the least, I want to express my deepest gratitude to my parents for their love and encouragement. They always stand with me as my strongest backup upon every decision I made. Without their support, I would not become the person I am today.

TABLE OF CONTENTS

Page

LIST OF FIGURES

Figure Page

LIST OF TABLES

Table Page

# CHAPTER 1

# INTRODUCTION

## 1.1. The Emerging Need for Hypersaline Industrial Wastewater Desalination

Intensified freshwater scarcity and growing public environmental awareness have progressively lead to stricter regulations on industrial wastewater disposal. As a consequence, disposal of industrial wastewater has become increasingly costly and in some cases even prohibited. Global interest in zero liquid discharge (ZLD) has thus been increasing in both developed and developing countries[1]. Since many types of industrial wastewater contain significant amount of salts, achieving ZLD will involve desalinating the saline wastewater, concentrating the brine to the greatest extent possible, and eventually crystallizing the brine to obtain solid waste. Regardless what initial salinity the industrial wastewater has, desalination/concentration of the hypersaline brine is an inevitable step toward ZLD.

Another area that would foresee an appreciable growth in wastewater desalination is the industry of shale oil/gas production[2]. The development of horizontal drilling and hydraulic fracturing (fracking) has enabled economical exploitation of oil and gas from shale formations—a tremendous source that was once hardly accessible with the conventional extraction technologies[3]. As a result, the production of shale oil/gas has drastically altered the energy portfolio of U.S. in recent years[4] and has appreciably impacted the global energy production landscape[5]. However, shale oil/gas production faces multiple significant environmental and public health challenges[3,6–8]. Environmentally responsible management of the tremendous amount of wastewater is key to the sustainability of the fracking industry.

Fracking wastewater is composed of both the flow-back and the produced water[9]. The flow-back water is the aqueous solution that flows back to the surface upon the completion of fracking. The produced water is the water that originates from the shale formation and flows to the surface during the oil/gas production. Collectively, fracking wastewater presents significant environmental challenges as it contains a wide variety of contaminants that are detrimental to the surface and ground water quality[2]. These waters are usually rich in mineral ions, colloids, hydrocarbon, a variety of chemical additives, and in many cases, radionuclides. Existing practices

for managing fracking wastewater include underground injection[10], disposal to surface water or POTW, onsite treatment, and reuse within and outside the shale oil/gas industry[11].

While reuse within the shale oil/gas industry is currently the most practical management approach, there are multiple reasons for the growing need of onsite treatment of these wastewaters for beneficial reuse outside the oil/gas industry or for safe discharge. These reasons include, but are not limited to, tightening environmental regulations on direct disposal, growing fresh water scarcity in certain areas (e.g. California)[12], and the expectable diminishing opportunities for local reuse as fracturing fluid[13]. Therefore, appropriate treatment of fracking wastewater is required to meet the water quality standards for surface discharge or beneficial reuses outside the oil/gas industry. Depending on the specific shale formation, some of the fracking wastewater is highly saline with a total dissolved solid (TDS) several times as high as that of seawater in certain cases[4]. Desalination is thus required to reduce the TDS to an acceptable level for reuse or discharge of these wastewaters.

For these reasons, viable technologies are in need for the desalination of industrial wastewater and fracking wastewater, not only to comply with growingly stringent regulations but also to recover valuable resources from waste streams.

### 1.2. Membrane Distillation as a Promising Solution

Reverse osmosis (RO) is a pressure-driven desalination technology that currently dominates the market of desalination[14,15]. Although from the energy efficiency perspective, RO is almost unbeatable, it still has some limitations in application. For hypersaline wastewaters that have extremely high osmotic pressures, such as produced wastewater, RO cannot be utilized as the allowable operating pressure is far exceeded. For the desalination of these wastewaters, thermal desalination is by far the most practical choice[13].

Membrane distillation (MD) is an emerging thermal desalination technology using a microporous hydrophobic membrane[16–19]. As shown in Figure 1.1, the microporous hydrophobic membrane was used to isolate a hot salty stream (feed) and a cold fresh stream (distillate). Driven by the partial vapor pressure difference generated from temperature difference, fresh water vapor would permeate through the membrane pores from the feed side to the distillate

side and condense as liquid water. In the meantime, the hydrophobicity of the membrane keeps the salty liquid water from the fresh water and thereby realizes the salty water desalination.

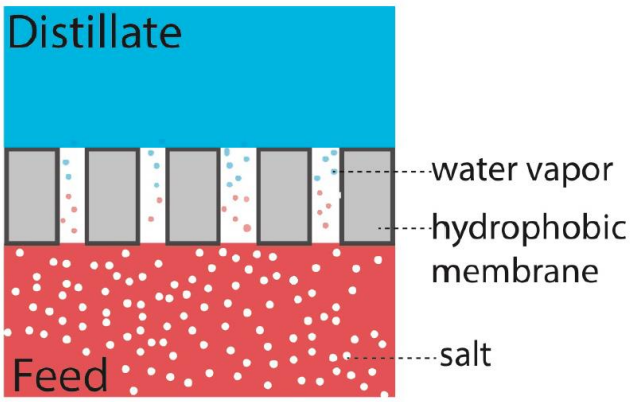


Figure 1.1 The mechanism of direct contact membrane distillation (DCMD): a hydrophobic membrane, separating the hot salty feed stream and the cold pure distillate stream, only allows water vapor to pass through its pores and condense on the distillate-membrane interface. The transport of vapor through the pores is driven by the partial vapor pressure difference across the membrane.

Compared with RO, the state-of-the-art desalination technology, MD has several advantages. First, MD can be used to desalinate hypersaline wastewater, such as RO brine and shale gas/oil produced water, whose salinity is too high for RO to deal with[20]. Second, as a low-temperature desalination technology, MD is able to harness low-quality energy such as waste heat, solar energy, and geothermal energy[21]. Third, the capital cost of MD is relatively low, which renders MD an appealing process for sustainable and off-grid desalination[22].

### 1.3. Challenges with Conventional Hydrophobic MD Membranes

The MD membrane is the critical component in an MD system. Conventional MD membranes are hydrophobic and made of common polymeric materials such as polyvinylidene fluoride (PVDF), polypropylene (PP), and polytetrafluroethylene (PTFE). The hydrophobicity is required to prevent direct liquid permeation through the micropores. However, when hydrophobic membranes are used in MD to treat hypersaline wastewater of a complex composition, two potential problems may lead to MD operation failures[23].

*1.3.1. Membrane fouling*

The first potential problem is membrane fouling. Membrane fouling is a universal problem in all membrane processes[23–26]. It refers to the accumulation of unwanted materials on the membrane surface or inside the membrane pores during operation, which leads to detrimental effect of the overall membrane performance[23]. In MD operations, membrane fouling can be induced by a variety of foulants including salt scalants (e.g. $CaSO_4$ and $CaCO_3$), particulates and colloids (e.g. silica and silts), and biofoulants (e.g. biofilms and natural organic matters)[23,27,28].

In particular, membrane fouling is a critical concern when a hydrophobic membrane is used in MD to treat feed waters with an abundance of hydrophobic contaminants (e.g. oil, hydrophobic organics) due to the strong hydrophobic-hydrophobic interaction[27,29–31]. As shown in Figure 1.2, with the presence of oil droplets in the feed solution of an MD operation, the membrane pore would be readily blocked leading to a significant vapor flux decline[32]. Recent studies using hydrophobic MD membranes for desalinating brine water rich in oil or organics have shown the rapid and severe flux decline as a result of membrane fouling[33].

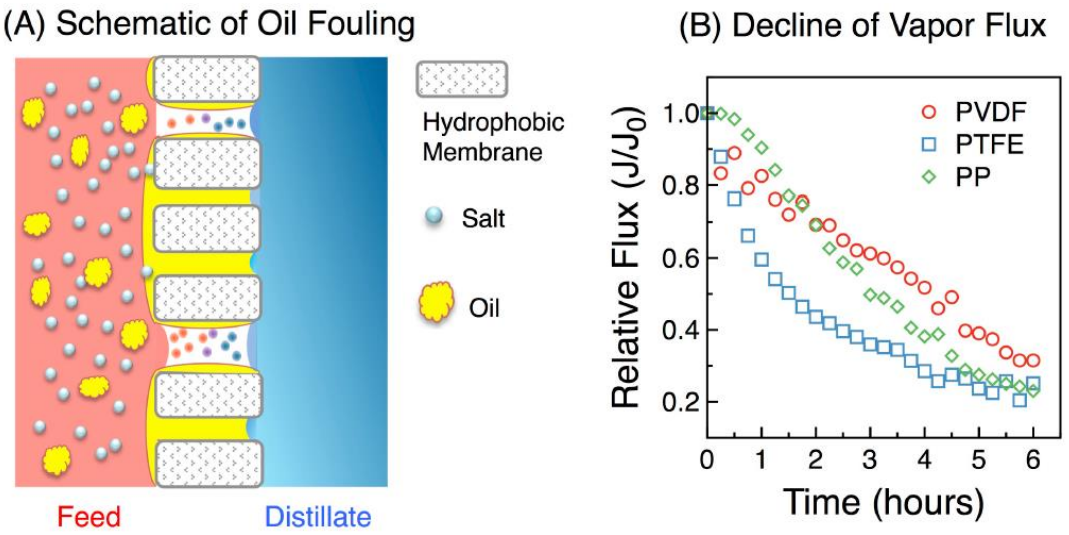


Figure 1.2 (A) Oil fouling of a hydrophobic membrane: the hydrophobic oil droplets accumulate at the hydrophobic membrane surface, blocking the pores for vapor transfer. (B) Experimental results showing rapid flux decline as evidence of the membrane oil-fouling.

To mitigate the membrane fouling problem in MD, numerous strategies have been proposed and tested. For instance, pretreating the feed solution using microfiltration (MF), ultrafiltration (UF), or nanofiltration (NF) can effectively remove the potential foulants such as particulates,

colloids, and microorganisms[23,34]; implementing regular membrane flushing or gas bubbling in MD operation can prevent salt scalant-induced fouling[35,36]; modifying the membrane surface to be more hydrophobic can significantly lessen biofouling[37]; adding chemicals such as antiscalants, cleaning agents, and biocides can also successfully improve alleviate the corresponding membrane fouling problems[38,39]. Unfortunately, in MD with membrane fouling by hydrophobic contaminants, the strategies mentioned above would either drastically increase the treatment cost or are not efficient at all. Thus, for desalinating shale/gas wastewater or industrial brines, which are enriched in hydrophobic contaminants, novel membrane fouling mitigation strategies are needed.

### *1.3.2. Membrane wetting*

The second major problem that may lead to MD operation failure is membrane wetting[16,40–42]. It refers to the intrusion of liquid water into the membrane pore, which establishes a pathway for liquid water transfer across the membrane. Different from membrane fouling, membrane wetting is a unique problem in MD operations, as for other membrane processes such as MF, UF, NF, and reverse osmosis (RO), the membranes are wetted by default.

Previous studies have shown that membrane wetting can be induced by various contaminants such as low-surface-tension and water miscible liquids (e.g. alcohols), amphiphilic molecules (e.g. surfactants), or other natural surface active agents[40,43–45]. Figure 1.3 shows the schematic of membrane wetting process induced by surfactants. With the presence of surfactants in the feed solution, the surface tension of the feed solution would be reduced, leading to a reduced liquid entry pressure, and thereby driving the feed solution to intrude the membrane pore. Meanwhile, in the membrane wetting process, the hydrophobic tails of the surfactant molecules will attach onto the hydrophobic membrane pore surface, leaving the hydrophilic head exposed and eventually rendering the membrane pores hydrophilic. The consequence of membrane wetting in MD is the direct permeation of feed water into the distillate stream and significantly undermined salt rejection rate[44,46–49].

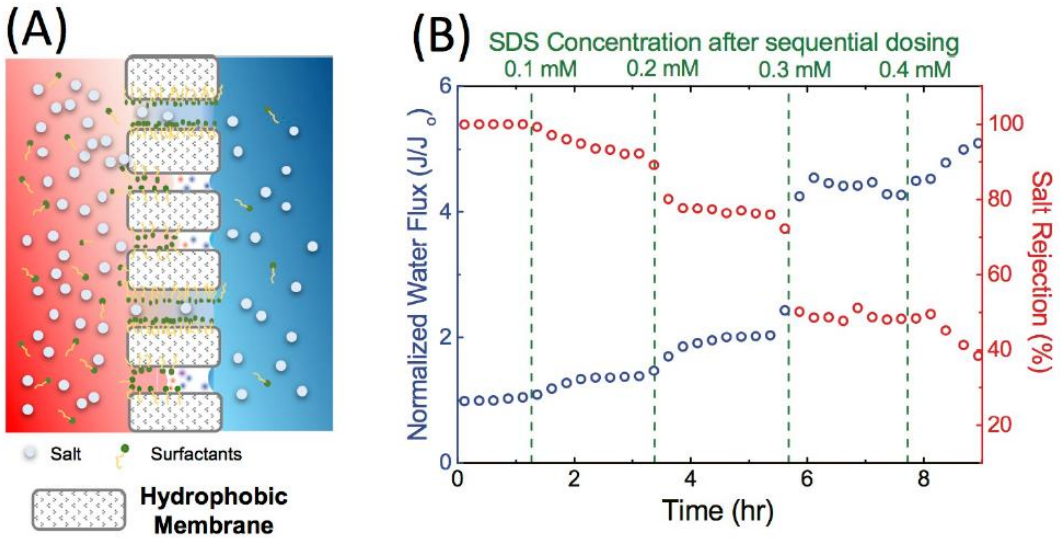


Figure 1.3 (A) Membrane pore wetting by surfactants: the attachment of surfactants onto the pore surface rendered the pore hydrophilic, providing channels for direct liquid passage (B) Experimental results showing significant reduction in rejection as evidence of membrane pore wetting.

So far, much effort has been made to mitigate membrane pore wetting in MD, such as the development of omniphobic membranes[44,48,50,51], composite membranes with hydrophilic surface layers[52,53], and superhydrophobic membranes with air-recharging during operation[43,54]. However, in spite of the achievements in membrane pore wetting mitigation, the mechanism of membrane pore wetting remains not fully understood, especially for surfactant-induced pore wetting phenomena.

### 1.4. The Applications of Membranes with Special Wettability

The wettability of a solid surface is a macroscopic representation of the interaction between the liquid and the substrate solid material. The most common way to quantify surface wettability is contact angle (CA) measurement. Either sessile drop method in air (Figure 1.4A) or captive bubble method in water (Figure 1.4B) has been utilized in contact angle measurements. A surface is typically considered hydrophobic if the water CA is higher than 90° or hydrophilic if the water CA is lower than 90°. Similarly, a surface can be determined as oleophobic if the oil CA is higher than 90° or oleophilic if the oil CA is lower than 90°. CA alone, however, does not fully capture the wetting behavior of a surface. The maximum and minimum CA of a liquid droplet with a given solid−liquid boundary are defined as the advancing CA, $\theta_A$ (Figure 1.4C), and the receding CA,

$\theta_R$ (Figure 1.4D), respectively[55–57]. CA hysteresis (CAH) is usually defined as the difference between $\theta_A$ and $\theta_R$ (i.e., $\theta_A - \theta_R$)[58,59]. By tradition, if the CA is higher than 150°, and the CAH is smaller than 5° or 10°, the surface would be considered as superhydrophobic/superoleophobic[60,61]. In constrast, the definition of superhydrophilic surface is controversial. While some suggest a maximum water CA of 5° as the upper limit[62,63], others confine the definition of superhydrophilicity to only a rough or porous surface[64].

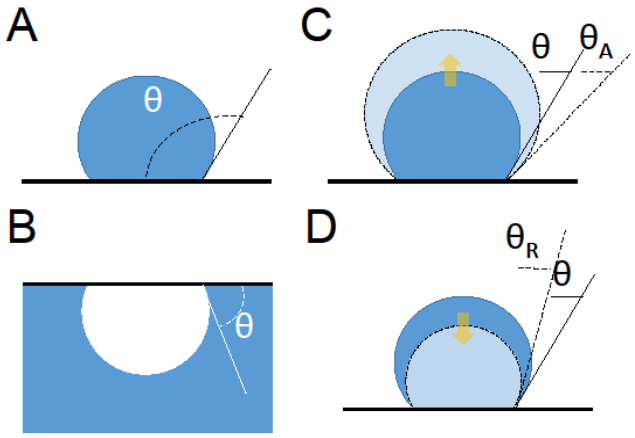


Figure 1.4 (A) Definition of contact angle (CA), θ, based on a sessile liquid drop on a solid surface. (B) Definition of CA based on a captive bubble. (C) Advancing CA, $\theta_A$(>θ): the maximum CA of a sessile drop before its boundary expands upon increase of drop volume. (D) Receding CA, $\theta_R$(<θ): the minimum CA of sessile drop before its boundary shrinks upon reduction of drop volume.

Special wettability typically refers to surface wetting properties that are not commonly encountered in daily life. Some of the most investigated surfaces of special wettability include those that are extremely repellent to water (superhydrophobic)[61], to oil (superoleophobic)[65–67], or simultaneously repellent to both water and oil (omniphobic)[68,69]. There are also surfaces that are in-air hydrophilic but oleophobic (i.e., wetted by water but not oil in air)[66]; such surfaces are more challenging to develop because liquids of a lower surface tension, such as oil, usually wet a surface more readily than water which has a very high surface tension. In addition to surfaces of homogeneous wettability, there exist surfaces of patterned wettability that are partially hydrophobic and partially hydrophilic[70–73]. Smart surfaces that can switch wettability in response to a variety of environmental stimuli have also been developed[74,75]. A schematic

diagram illustrating the concepts and relations between different types of surface wettability is given in Figure 1.5.

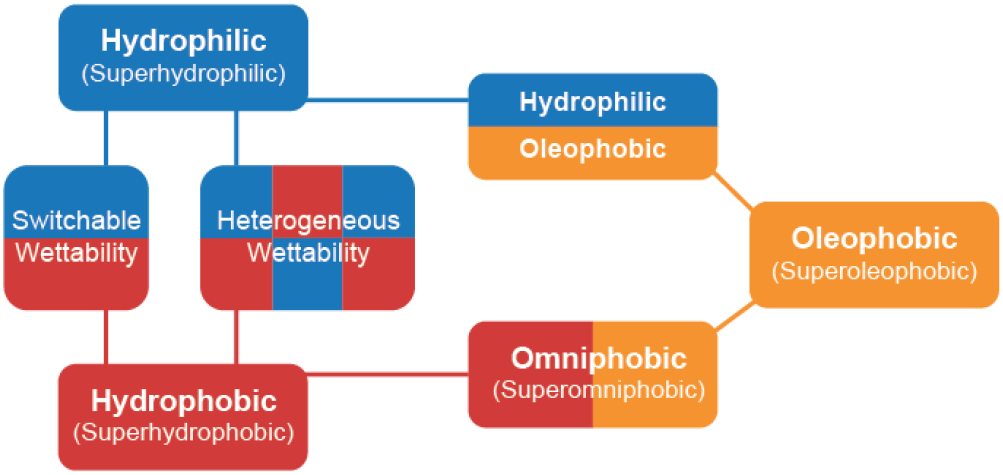


Figure 1.5 The relationships between different types of most investigated surfaces with special wettability. A surface is considered specially wettable if it has wetting properties that are not usually observed in daily life materials, which include not only those that are super wetting or nonwetting but also those with heterogeneous and stimuli-responsive switchable wetting properties. We note that oleophilicity is not explicitly listed here, as most materials are oleophilic due to the low surface tension of oil.

Recently, a variety of membranes with special wettability have been developed by the material science community. These membranes are applied in various membrane processes. For instance, omniphobic membranes have been proposed to be utilized in MD processes for resisting membrane wetting by surfactants[44,48,49]; superhydrophilic membranes are employed in ultrafiltration[76,77], nanofiltration[78,79], reverse osmosis[80,81], and forward osmosis for mitigating organic or biological fouling[82–84]; some recent studies also suggest that novel ultrafiltration membranes with in-air hydrophilicity and oleophobicity offer antifouling performance that is unmatched by membranes that are in-air oleophilic[85,86].

However, to date, few studies have been reported to employ membrane with special wettability to solve the membrane wetting problem. In addition, although the omniphobic membranes show excellent anti-wetting property, the exact mechanism of membrane pore wetting still remains unclear, which in turn imposes confusion about the anti-wetting mechanism of the omniphobic membranes.

## 1.5. Objectives and Hypothesis

The overall objective of this dissertation is to elucidate the failure mechanisms and mitigation strategies in MD operations in regards to membrane fouling and wetting problems. There are five specific objectives in details as below:

The first objective is to investigate the impact of surface wettability on fouling resistance of MD membranes. We fabricated a composite membrane with asymmetric wettability for MD operation with oily feed solution. The composite membrane was composed of an in-air superhydrophilic/underwater oleophobic surface layer and a hydrophobic substrate. Our hypothesis is that compared to the conventional hydrophobic MD membrane, this composite membrane is able to sustain stable MD operation in the presence of oily contaminants in feed as the in-air superhydrophilic/underwater oleophobic surface layer can eliminate the hydrophobic-hydrophobic interaction between the oil droplet and hydrophobic MD membrane surface underwater.

The second objective is to explore the influence of surface charge on the fouling resistance of MD membranes besides surface wettability. Since both the oil droplet and MD membrane are surface charged underwater, our hypothesis is that although the membrane surface wettability dominates the fouling resistance of the membrane, the membrane surface charge would also impact the membrane performance.

The third objective is to study the mechanism of MD membrane pore wetting. As is well known, the membrane pore wetting can be induced by different wetting agents, such as low-surface-tension and water miscible liquids (e.g. alcohols), and amphiphilic molecules (e.g. surfactants). Our hypothesis is that for membrane pore wetting resulting from ethanol and surfactants, albeit the wetting criterions are the same, the wetting dynamics are different due to surfactant adsorption onto the membrane pore surface.

The fourth objective is to develop a mathematical model that can comprehensively elucidate the kinetics of MD membrane pore wetting induced by surfactant. Our hypothesis is that the kinetics of membrane pore wetting induced by surfactant is controlled by the surfactant adsorption, and it can be predicted with the operation conditions and surfactant properties.

The fifth objective is to provide the mitigation strategies for fouling and wetting in MD operations employing membranes with special wettability. Our hypothesis is that although the

composite membranes can resist oil fouling, they will still be wetted by surfactants. Likewise, we hypothesize that albeit the omniphobic membranes exhibit good resistance to membrane pore wetting by surfactants, they will still be fouled by oils.

### 1.6. Structure of the Dissertation

This dissertation is organized into seven chapters. Chapter 2 discusses the implementation of composite membrane with asymmetric wettability in MD operation with oily contaminants as well as the corresponding anti-fouling mechanism. Chapter 3 presents the synergistic effects of surface wettability and surface charge on fouling resistance of MD membranes. Chapter 4 shows the comparison of mechanisms of membrane pore wetting induced by different wetting agents including ethanol and surfactant in MD operations with a novel impedance-based membrane pore wetting monitoring technique. Chapter 5 presents a theoretical model that is able to comprehensively describe the kinetics of MD membrane pore wetting induced by surfactants with regards to operation conditions and surfactant properties. Chapter 6 systematically investigates the performances of composite membrane and omniphobic membrane on MD operations with different types of feed and provides the strategy of MD membrane selection for robust MD operation based on feed type. Finally, Chapter 7 summarizes the results of this research and presents recommendations for future work.

# CHAPTER 2

# IMPACT OF SURFACE WETTABILITY ON FOULING RESISTANCE OF MD MEMBRANES

This chapter has been published in the journal Environmental Science & Technology as the following peer-reviewed manuscript: Wang Z., Hou D., and Lin S., Composite membrane with Underwater-oleophobic surface for anti-oil-fouling membrane distillation. Environmental Science & Technology **50** (2016). p. 3866-3874. doi: 10.1021/acs.est.5b05976.

## 2.1. Introduction

Membrane distillation (MD) is a thermal desalination process using a micro-porous hydrophobic membrane[16,18,19,87]. In an MD process, a hydrophobic membrane is employed to create a vapor gap that separates the cold distilled water (the distillate) from the hot salty water (the feed solution). The partial vapor pressure difference induced by trans-membrane temperature difference drives the water vapor to transport across the hydrophobic membrane from the feed stream to the distillate stream, rejecting most of the non-volatile species and producing high quality distillate water. As a low-temperature, low-pressure, and low capital cost membrane-based process that can desalinate highly saline feed water with low-grade thermal energy, MD is a promising desalination technology for small-scale and off-grid applications, especially when low-grade thermal energy such as waste heat, solar thermal, or geothermal energy is available[88–92]. Recently, MD has also been suggested as one of the few viable technological candidates for onsite desalination of shale oil and gas wastewater[13,44,93].

The production of shale oil and gas with hydraulic fracturing generates a tremendous volume of wastewater[2,3,8,94,95]. Managing this wastewater from shale oil and gas production is very challenging, with the optimal approach highly dependent on the geologic condition of the production sites and the chemical composition of the wastewater. Hypersaline shale oil and gas wastewater might eventually need to be desalinated for environmentally responsible discharge or beneficial reuse outside the oil and gas industry, as opportunities of reuse for hydraulic fracturing will eventually diminish. Reverse osmosis (RO), the state-of-the-art technology for seawater desalination[14], is not applicable to treat hypersaline wastewater in many cases as the osmotic pressure of the wastewater can far exceed the maximum working pressure of existing RO

systems[2,96]. In this scenario, MD, a thermal desalination process the performance of which is relatively independent of salinity, becomes one of the few viable options[13].

Commercially available MD membranes are typically made of hydrophobic materials[97], such as polyvinylidene fluoride (PVDF), polypropylene (PP), and polytetrafluoroethylene (PTFE). However, hydrophobic membranes used for MD are inherently prone to fouling by oil and hydrophobic organics[27,98–100] due to the long-range hydrophobic-hydrophobic interaction[29–31]. Depending on the production sites, the shale oil/gas wastewater can be rich in organic constituents. In certain cases, the total organic carbon (TOC) can be as high as 5,000 to 6,000 ppm[12,101]. The necessity of using hydrophobic membranes in MD and the abundance of hydrophobic contaminants in shale oil/gas wastewaters, pose a challenging dilemma that prevents MD—an otherwise highly promising technology—from desalinating shale oil and gas wastewater.

To develop underwater anti-oil-adhesion surfaces, or surfaces with underwater oelophobicity (oleophobic means "oil repelling"), the materials science community has been resorting to biological systems for hints[102]. Biological surfaces such as fish scales, clamshell, and sharkskin can resist marine fouling by organic matter, microorganisms, or even by oil in seawater polluted by oil spill[103,104]. Investigating these natural underwater oleophobic surfaces reveals that this remarkable anti-oil-adhesion surface property is attributable to the combination of both rough surface morphology and surpehydrophilic surface chemistry. Following this principle, a wide variety of the underwater superoleophobic surfaces have been prepared using different approaches on different substrate materials[105–111]. In particular, underwater superoleophobic meshes and membranes have been developed for effective oil-water separation[112].

While these proven techniques can definitely offer insights to the fabrication of anti-oil-fouling MD membranes, techniques that modify the wetting property of the entire membrane (e.g. dip coating, in-situ modification) are not directly applicable, because a hydrophobic substrate needs to be preserved as a barrier for liquid transfer in MD operations. The key requirement for developing an anti-oil-fouling MD membrane is the construction of a composite membrane structure with a hydrophilic-underwater oleophobic surface coating to impart fouling resistance, and a hydrophobic substrate to serve as the liquid barrier and vapor gap for the MD process. In other words, a composite membrane with asymmetric wetting properties is required.

A plethora of composite MD membranes has been developed in previous studies. Several of those studies focused on achieving surface superhydrophobicity by decorating the membrane surface with nanoparticles[46,47,113,114]. Composite membranes with asymmetric wettability have also been fabricated for enhancing water vapor flux, with the rationale that a thin hydrophobic layer with hydrophilic support has a lower overall resistance for vapor transfer[115–118]. It has been found that certain composite MD membranes, including the superhydrophobic[46,114], omniphobic[44], and hydrophilic/hydrophobic membranes[52], can enhance the membrane anti-wetting property to different degrees. A recent study reported a PVDF membrane with both surfaces modified either by polyethylene glycol (PEG) along or by both PEG coated titanium dioxide nanoparticles and showed that the modified membrane exhibited good resistance against both wetting and fouling by an emulsified feed solution with 100 ppm mineral oil[100].

In this study, we fabricate a composite membrane with asymmetric wetting properties for anti-oil-fouling MD operation. The composite membrane has a PVDF hydrophobic substrate and a nanoparticle-polymer composite surface coating that is in-air superhydrophilic and underwater oleophobic. We compare the morphology and wetting properties of the composite membrane and the pristine PVDF membrane. We then conducted comparative direct contact MD (DCMD) experiments with saline feed solution containing a high concentration of crude oil (1,000 ppm) to show the different fouling propensities between the two membranes. Finally, we conducted force spectroscopy for the underwater interaction of both the composite membrane and the pristine PVDF membrane with an oil droplet to unravel the mechanism for the different fouling behaviors observed in DCMD experiments.

## 2.2. Materials and Methods

### *2.2.1. Materials and Chemicals*

The substrate membrane was a hydrophobic PVDF microfiltration membrane with symmetric surface wetting property and a nominal pore size of 0.45 μm (GE Healthcare Life Sciences, Pittsburg, PA). Chitosan (CTS, 90% Deacetylated) was obtained from Chemsavers (Bluefield, WV). Perfluorooctanoic acid, sodium hydroxide (NaOH), sodium chloride (NaCl), acetic acid (>99%), and silica nanoparticles (Ludox, HS-40, 40 wt.% aqueous suspension) were purchased

from Sigma Aldrich (St. Louis, MO). The crude oil, as the fouling agent, was acquired from Texas Raw Crude Oil (Midland, TX).

### *2.2.2. Composite Membrane Fabrication*

The in-air superhydrophilic and underwater oleophobic coating was synthesized using a 4-step procedure[119,120]. First, 0.2 g chitosan (CTS) was dissolved in 100 mL of 1 % acetic acid solution with a mixer. Second, 0.3 g silica nanoparticles (SiNPs) with an average diameter of 20 nm were dispersed in the CTS suspension under sonication for 15 min to form a dispersion of CTS-SiNPs. After that, 20 mL aqueous solution of sodium perfluorooctanoate (PFO, 0.1M), resulting from the reaction of perfluorooctanonic acid with NaOH, was added to the CTS-SiNPs solution dropwise under stirring. The PFO anions coordinate to the amino groups of the CTS, forming a white suspension of SiNPs coated with a mixture of CTS and PFO (CTS-PFO/SiNPs). Finally, the resulting product was filtered and rinsed, first with deionized water, and then ethanol before drying at room temperature.

To prepare the coating suspension, 0.3 g of the synthesized nanocomposite particles (CTS-PFO/SiNPs) were dispersed in 20 mL of ethanol using bath sonication. The nanocomposite suspension was spray-coated onto one side of the hydrophobic PVDF membrane substrate with an area of 20 cm × 20 cm using a spray gun with an operating pressure of 0.2 MPa air. Special caution was taken to ensure that the hydrophobic PVDF membrane was not fully wetted by the ethanol based suspension, so that only the wetting property of the top surface but not that of the entire porous structure was modified. The coated membrane was heat treated at 80 °C for 1 hour to thoroughly remove any remaining solvent.

### *2.2.3. Membrane Characterizations*

The surface morphology of the pristine PVDF membrane and fabricated composite membrane was observed using scanning electron microscopy (SEM, Merlin, Zeiss, Thornwood, NY). The porosity of the pristine and modified membrane was measured by gravimetric method with a wetting agent (Porefil, IB-GT GmbH, Germany) of a low surface tension of 16 mN/m. Furthermore, we measured the pore size distributions for both membranes with a capillary flow porometer (Poroflux 1000, IB-FT GmbH, Germany) following a procedure described in literature[121]. In addition to characterizing the membrane morphology and structure, we also

conducted polarization modulation-infrared reflection-adsorption spectroscopy (PM-IRRAS, PMA 50, Bruker, Billerica, MA) to verify changes in surface chemical composition.

To compare the surface wetting properties of the two membranes, we measured their static contact angle (CA) using an optical tensiometer (TL100, Attension, Finland). Both the in-air sessile drop CA with water and underwater CA with crude oil were measured. Before measuring the in-air water CA, we immersed the membranes in water for 2 minutes, removed the membranes from water, and then carefully removed any water puddle remaining on the membrane surfaces using blotting paper. Sessile drop CA measurements using this approach yield more relevant information compared to those conducted without conditioning the membrane surfaces with water, because in actual MD operations the membrane surfaces are in constant contact with the feed and distillate solutions. The measurement of underwater CA is similar to that of measuring the captive bubble CA but with the bubble being replaced by a crude oil droplet. We note that the density of the crude oil is lower than that of water. Finally, the liquid entry pressure (LEP), which is a parameter highly relevant to MD operation, was also measured using a well-established method[122].

### *2.2.4. Preparation and Characterizations of Oil Feed Solution*

The oily feed solution was prepared by vigorously mixing 2 g of crude oil and 2 L of NaCl aqueous solution (600 mM) using a laboratory homogenizer (Fisher Scientific, Pittsburgh, PA) at 16,000 rpm for 15 minutes. The crude oil concentration of the prepared feed solution was 1,000 ppm (by weight). The morphology of oil droplets in the suspension was observed using an optical microscopy (Nikon LV100, Japan). The size distribution of the oil droplets in the emulsion was determined by dynamic light scattering using a Zetasizer (Malvern Nano ZS, UK).

### *2.2.5. Membrane Fouling Test*

DCMD experiments with oily and saline feed solution were conducted to compare the fouling behavior of the pristine PVDF membrane and the fabricated composite membrane. In these experiments, small membrane coupons (2.5 cm × 8 cm) were used in a cross-flow test cell in co-current flow configuration. The influent temperatures of the oily feed stream and the deionized distillate stream were 60 °C and 20 °C, respectively. In the experiments with the composite membrane, the modified surface of the membrane faced the oily feed solution and the unmodified

surface was in contact with the distillate. The mass and conductivity of the solution in the distillate reservoir were constantly measured and recorded. The salinity of the solution was calculated from the measured conductivity based on a pre-established calibration curve. The water vapor flux and the salt rejection were calculated from the rates of change of the distillate mass and salinity.

The flowrates of feed and distillate streams were controlled to be 0.45 L/min (9.6 cm/s in our test cell) and 0.2 L/min (4.3 cm/s), respectively, so that the hydraulic pressure of the feed stream was slightly higher than that of the distillate stream in our specific system. It was visually observable that the MD membranes were pushed from feed channel to the distillate channel. Such an experimental setup facilitated the detection of the membrane wetting: if certain membrane pores were wetted and thus served as channels for liquid water transport as in microfiltration, water would transport from the feed stream to the distillate stream due to the trans-membrane pressure difference, resulting in a clearly observable increase of the distillate salinity caused by reduced salt rejection.

*2.2.6. Force Measurement of Underwater Oil-Membrane Interaction*

To mechanistically elucidate the different fouling propensities of the pristine PVDF membrane and the composite membrane, we measured the force curves for the interaction between an oil droplet and membrane surfaces underwater using a force tensiometer (Sigma701, Attension, Finland)[104,123–125]. In these measurements, the membrane was fixed to the bottom of a transparent cell using double-sided tape before the cell was filled with water. A small droplet of mineral oil droplet (~6 μL, Sigma Aldrich, MO) was carefully hung onto an adhesion force probe (T114, Attension, Finland) underwater. The adhesion force probe, with an oil droplet attached, approached the membrane surface at a constant speed of 0.3 mm/min until the oil droplet contacted the membrane surface, and then retracted from the membrane surface at the same speed. The results from the force spectroscopy are presented as force being a function of displacement of the adhesion force probe.

Although our ultimate intention was to probe the interaction between the oil droplet and the membrane surface, what the force tensiometer factually measured was the force sensed by the microelectro-mechanical system pulled by the adhesion force probe (similar to a small version of a Du Noüy ring) hanging the oil droplet. When acquiring the force curves, the initiation point of the retraction, which demarcated the advancing and receding stages, was set to be the moment

right after the advancing oil droplet contacted the membrane surface. The measurement was conducted in this way to avoid actively pressing the oil droplet by the force probe after the oil was in contact with the membrane surface, as the ring-shaped force probe could be forced into the oil droplet and generate irrelevant information that complicates the data interpretation.

## 2.3. Results and Discussions

### *2.3.1. Morphology and Wetting Properties of the Pristine and Modified Membranes*

The modified surface of the composite membrane (Figure 2.1B) exhibits a different surface morphology compared to that of the pristine PVDF membrane (Figure 2.1A) due to the presence of the CTS-PFO/SiNPs nanocomposite coating. The comparison of the PM-IRRAS spectra for the pristine and the modified membranes also provides compositional evidence of surface modification (Supporting Information). Figure 2.1B suggests that the nanocomposite coating thoroughly covered the surface of the PVDF substrate and formed agglomerates that blocked some of the membrane pores. These nanocomposite agglomerates, together with the inherent roughness of the pristine membrane, created a hierarchical structure with a high degree of surface roughness. According to the Wenzel theory, roughness is of critical importance in enhancing the intrinsic wetting property of a surface[126,127].

The measured porosity of the modified membrane was 72.5 $\pm$ 0.2%, which was only slightly lower than that of the pristine membrane (75.1 $\pm$ 0.1%). Similarly, the pore size distribution was not significantly affected by the modification (Figure 2.1C), with the average pore size of pristine PVDF membrane being 392 $\pm$ 23 nm and that of the modified membrane being 388 $\pm$ 28 nm. The relatively small change in the structural property of the porous membrane is expected, as the modification only affected the top surface of the membrane by adding about 4% to the overall thickness of pristine the membrane (172.6 $\pm$ 7.6 μm for pristine membrane vs. 180.1$\pm$ 7.1 μm for the modified membrane).

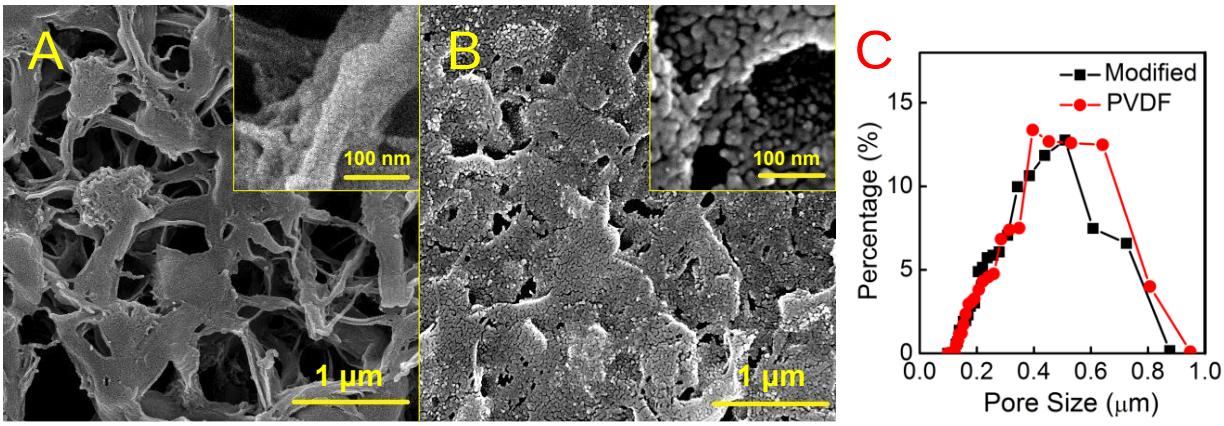


Figure 0.1 SEM images featuring the morphology of (A) a commercial PVDF membrane and (B) a composite membrane modified by coating the commercial PVDF membrane with a CTS-PFO/SiNPs nanocomposite layer. The inset images in (A) and (B) show the local morphology of the PVDF membrane and composite membrane, respectively. (C). Pore size distributions of the pristine and modified PVDF membrane.

The pristine PVDF membrane and the fabricated composite membrane showed drastically different surface wetting properties. After briefly soaking in water, the modified surface of the composite membrane was fully wetted (Figure 2.2A), with a clearly observable film of bounded water; while the unmodified surface of the composite membrane and both surfaces of the pristine PVDF membrane remained non-wetted in air with water droplets beading up on the surfaces (Figure 2.2B and 2.2C). More quantitatively, the in-air sessile drop CA with water were 106.6±0.2° for the pristine PVDF membrane (Figure 2.2F) and 104.1±0.5° for the unmodified surface of the composite membrane (Figure 2.2E), which indicate that both surfaces were reasonably hydrophobic in air. In contrast, the sessile drop CA was zero for the modified surface of the composite membrane (Figure 2.2D), which suggests that the modified surface of the composite membrane was in-air superhydrophilic.

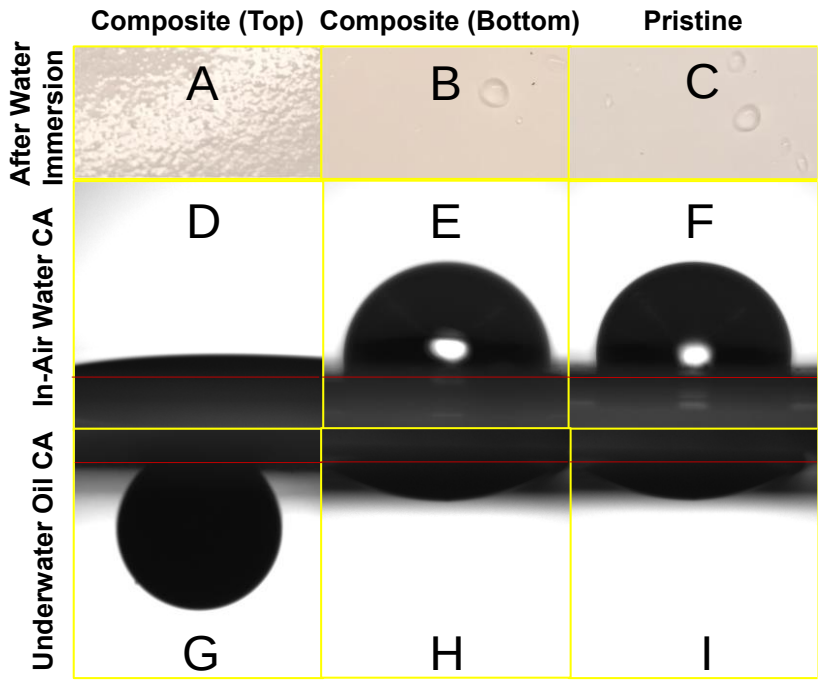


Figure 0.2 Photographic images of water wetting on (A) the modified surface of the composite membrane, (B) the unmodified surface of the composite membrane, and (C) the pristine PVDF membrane. These images were taken right after the membranes were removed from water after being soaked for 2 minutes. In-air water CA of (D) the modified surface of the composite membrane, (E) the unmodified surface of the composite membrane, and (F) the pristine PVDF membrane. These CA were measured with membranes pre-conditioned by soaking in water. Underwater oil CA of (G) the modified surface of the composite membrane, (H) the unmodified surface of the composite membrane, and (I) the pristine PVDF membrane. Crude oil, which served as the foulant in subsequent MD experiments, was the oil phase for these underwater oil CA measurements.

To acquire information of membrane wetting properties that are directly relevant to oil fouling, we also measured the CA with crude oil underwater. The unmodified surface of the composite membrane and both surfaces of the pristine PVDF membrane were wetted by crude oil, resulting in very small CA (Figure 2.2H and 2.2I). In comparison, the modified surface of the composite membrane showed underwater oleophobicity with a very high oil CA (149.5±0.5°, Figure 2.2G). Such underwater oleophobicity resulted from the favorable interactions between water and the highly hydrophilic surface coating[128,129]. As a hydrogel, chitosan has a wide variety of surface functional groups that can form hydrogen bonds with water molecules. These hydrogen forming functional groups, including alcohol, amine, amide and ether, strongly interact with the surrounding water, resulting in an interfacial hydration layer[130–132]. Wetting such a

highly hydrophilic layer underwater by an oil droplet requires the destruction of the hydration layer at the membrane surface, which is energetically highly unfavorable due to the relatively large energy associated with hydrogen bonding.

Despite the drastic change in surface wetting property, the LEP of the membrane was barely influenced. The LEP for the pristine and the modified membranes were both 3.26±0.2 bar. Considering the significantly different CA between the modified and the pristine membranes, the conventional equation for quantifying LEP based on CA and pore size apparently cannot directly apply to explain their almost identical LEP[133]. This can be readily explained by the fact that the LEP is not determined by the properties (e.g. pore size, wetting property) of the membrane top surface but rather by those of the hydrophobic layer. The hydrophilic coating layer is immediately wetted by water and thus does not contribute to any resistance against pressurized water from breaking through. Because the spray coating technique employed allowed modification of only the top surface, the presence of the coating did not affect the LEP.

### *2.3.2. Properties of Oily Feed Solution*

The crude oil emulsion with 1,000 ppm oil prepared using physical emulsification was highly turbid and stable for at least 24 hours without observable phase separation (Figure 2.3A). The kinetic stability of the crude oil emulsion is attributable to the presence of naturally occurring emulsifiers such as asphaltenes, naphthenic acid, carboxylic acid, and other oil-soluble acids and bases[134,135]. Optical microscopic images suggest that the size (diameter) of the oil droplets was in the range of a few micrometers (Figure 2.3B). More quantitative size distribution of oil droplets in the aqueous suspension was measured using dynamic light scattering, which yielded a distribution of hydrodynamic diameter with $5.4 \pm 0.6$ μm (Figure 2.3C). The overall size of the oil droplet in the emulsion was significantly larger than the nominal pore size of the pristine PVDF membrane (0.45 μm) and even more so than the coated surface of the composite membrane. Therefore, if the oil droplets have a strong affinity toward the membrane surface, they will readily block the membrane pores and lead to significant membrane fouling.

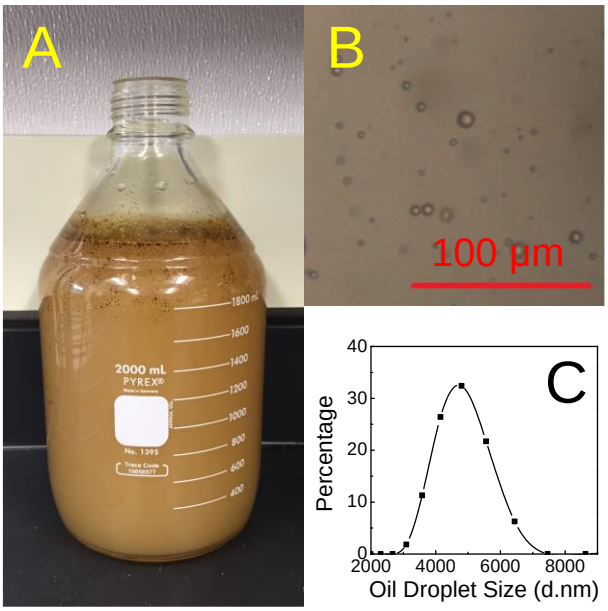


Figure 0.3 (A) A photographic image of the crude oil (in water) emulsion prepared using vigorous physical emulsification. The emulsion has a high kinetic stability with no observable phase separation for at least 24 hours. (B) A microscopic image of crude oil droplets in the emulsion shown in Figure 2.3A, taken by an optical microscope. (C) The distribution of hydrodynamic diameters of crude oil droplets measured using dynamic light scattering with a ZetaSizer.

*2.3.3. Membrane Performance in Direct Contact Membrane Distillation*

DCMD experiments with feed solution containing crude oil, using the fabricated composite membrane and pristine PVDF membrane, demonstrated drastically different fouling behaviors between the two membranes (Figure 2.4). Significant fouling was observed in DCMD experiments with the pristine PVDF membrane, as indicated by an appreciable decline of water vapor flux in a short period of time (red circles in Figure 2.4). Since the pristine PVDF membrane was underwater hydrophobic and oleophilic (Figure 2.2I), the oil droplets would tend to attach onto the surface of the pristine PVDF membrane via the long-range hydrophobic-hydrophobic interaction.

The attachment and accumulation of the oil droplets on the membrane surface resulted in blockage of membrane pores that served as the pathways for water vapor, and consequently led to the decline of water vapor flux. In addition, because the oil droplet sizes were significantly larger than the membrane pore size, the fouling occurred almost immediately when the MD operation started.

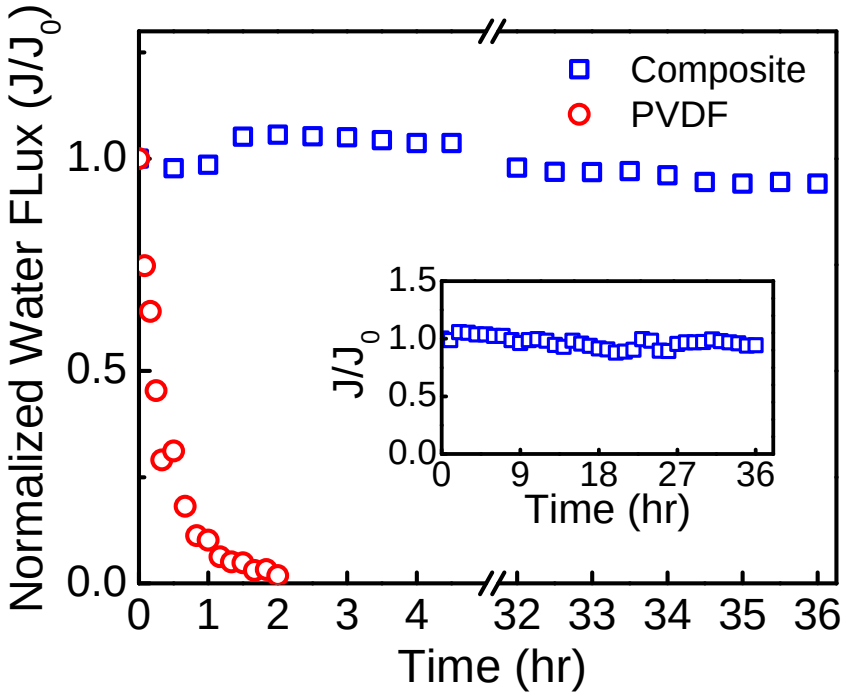


Figure 0.4 Normalized water (vapor) flux for the fabricated composite membrane (blue squares) and pristine PVDF membrane (red circles) with feed solution containing 1,000 ppm crude oil in the DCMD experiments. The time-dependent water fluxes were normalized by the initial water fluxes. The cross flow velocities of the streams in the membrane cell of all DCMD experiments were 9.6 cm/s and 4.3 cm/s in the feed stream and distillate stream, respectively. The feed and distillate temperatures were 60°C and 20°C, respectively. The initial water fluxes for PVDF membrane and composite membrane were 30.96 L $m^{-2}$ $h^{-1}$, and 26.15 L $m^{-2}$ $h^{-1}$, respectively.

In comparison, the DCMD performance of the composite membrane with asymmetric wettability was significantly more stable. When challenged by the oily feed solution that markedly fouled the pristine PVDF membrane, the fabricated composite membrane maintained a stable water vapor flux without significant flux decline in the 36-hour operation (blue squares). In addition, the salt rejection rate of the composite membrane always remained ~100%.

The anti-oil-fouling property of the composite membrane is attributable to the in-air hydrophilic and underwater oelophobic CTS-PFO/SiNPs nanocomposite coating on the membrane surface. The hydrophilic moieties on the chitosan strongly interact with water and keep the membrane surface hydrated, providing a hydration layer that deters the oil droplet from attaching[128,129]. Such anti-fouling mechanism for the composite membrane is similar to the mechanism for its underwater oleophobicity suggested by the underwater oil CA measurements.

The low surface tension fluoro- functional groups on PFO, on the other hand, may further contribute to fouling mitigation due to its weak interaction with the oil foulants. The comparative advantage of the membranes with both hydrophilic and oleophobic functional groups, over those with only hydrophilic functional groups, in the effectiveness of fouling control, has been reported in literature for microfiltration membranes[86].

The fact that the composite membrane maintained a perfect salt rejection throughout the experiment suggests that the PVDF substrate of the composite membrane remained hydrophobic and functioned as a barrier for liquid transport as expected. The prevention of undesired wetting of the hydrophobic substrate was achieved by carefully coating only the membrane surface with the CTS-PFO/SiNPs nanocomposite by maintaining a low spraying rate, a small spraying angle, and a high degree of nebulization. Other common surface modification approaches, such as dip-coating or spin-coating[106,108,110,111], may result in membranes that are partially or entirely wetted when immersed in water. Furthermore, even in the presence of naturally occurring surfactants that wetted the pristine PVDF membrane, the highly hydrophilic coating on the composite membrane helped alleviate surfactant-induced wetting and maintained an uncompromised salt rejection. A similar phenomenon has been observed in other studies in which composite membranes were challenged with alternative wetting agents[52]. However, the exact mechanism behind this anti-wetting property of the highly hydrophilic coating remains unclear.

It is worth noting that the initial water vapor flux with the fabricated composite membrane (26.15 L $m^{-2}$ $h^{-1}$) was lower than that with the pristine PVDF membrane (30.96 L $m^{-2}$ $h^{-1}$). The reduction of the initial water flux might be attributable to the blocking of the membrane pores by the CTS-PFO/SiNPs nanocomposite as suggested by the SEM image presented in Figure 1B. However, the detrimental impact of the nanocomposite coating on the vapor permeability of the membrane might not be as significant as the portion of the pore blockage suggests, because CTS-PFO/SiNPs coating was a porous and superhydrophilic hydrogel network that liquid water might freely penetrate.

On the other hand, the hydrodynamic condition in such a hydrogel network was stagnant compared to that in the cross-flow feed stream as a result of both the absence of hydrodynamic mixing and strong interaction between water and hydrophilic functional groups in such a network. The relatively ineffective mass and heat transfer of liquid water in the coating layer enhanced temperature polarization[16,136,137], curtailing the driving force for vapor transfer and

consequently reducing the water vapor flux. This effect of enhanced temperature polarization is a very important, if not the dominant, contribution to the reduction of initial vapor flux.

### *2.3.4. Underwater Oil-Membrane Interaction*

To further understand the anti-oil-fouling behavior of the composite membrane in DCMD experiments, underwater dynamic oil adhesion measurements with the modified surface of the composite membrane and the pristine PVDF membrane were conducted. A mineral oil droplet was employed as the force probe interacting with membrane surfaces. The force curves, which quantify the position dependent interaction force between the oil droplet and the membrane surfaces, are presented in Figure 2.5A for both membranes tested. The "adhesion force" reported in Figure 2.5A was in essence the force experienced by the micro-electro-mechanical sensor (MEMS) due to the pulling of the adhesion force probe.

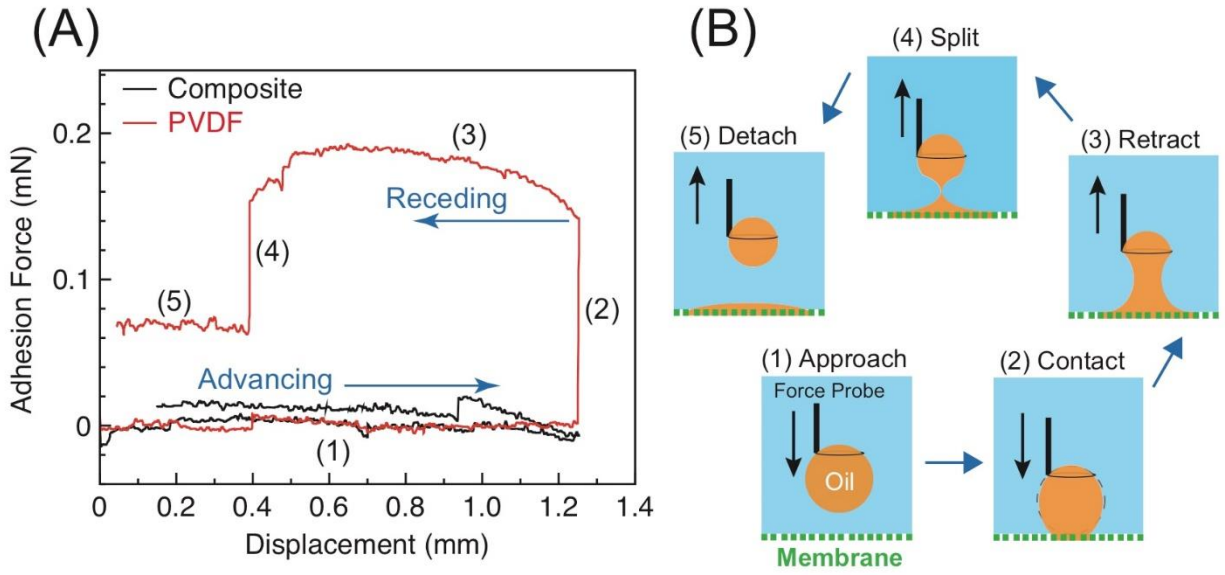


Figure 0.5 (a) Force-displacement curves (or force curves) recorded in experiments where a mineral oil droplet interacted with the composite membrane (black curve) and the pristine PVDF membrane (red curve) underwater. The advancing parts of the force curves represent the approaching of the oil droplet toward the membrane surface before any interaction occurred and are therefore mostly flat (event 1). For the interaction with the pristine PVDF membrane, the oil droplet experienced a strong attraction to the membrane immediately upon the initial physical contact, as reflected by a sudden increase in adhesion force (event 2). The adhesion force continued to increase as the oil droplet moved away from the PVDF membrane surface (event 3) until the oil droplet split into two smaller parts (event 4), one remaining on the force probe and the other retained by the hydrophobic membrane surface. The residual "adhesion force" measured after droplet breakage in the receding stage (event 5) was an artifact that stemmed from the change of

oil droplet volume that affected the flotation force of the oil droplet and thus the pulling force on the MEMS. For the interaction with the underwater oleophobic surface of the composite membrane, the overall pattern of the advancing and receding curves resembled that measured with the hydrophobic PVDF membrane, except for the absence of event 2 and significantly lower magnitude of interactions in all events.

To facilitate understanding the force curves on Figure 2.5A, Figure 2.5B illustrates the five distinct events (denoted in Figure 2.5A) that occurred in different stages of the interaction between the oil droplet and the pristine PVDF membrane (red curve in Figure 2.5A). In event 1, the oil droplet approached the membrane at a constant speed (0.3 mm/min). Because the force initially sensed by the MEMS was set as the baseline and the movement of oil droplet reached a steady state, the adhesion force for event 1 was zero by default. In event 2, the bottom tip of the oil droplet was in its first contact with PVDF membrane. Due to the strong hydrophobic-hydrophobic interaction, the oil droplet experienced a sudden attraction from the membrane, resulting in a significant and abrupt increase of adhesion force as shown in Figure 2.5A.

The retraction started upon the oil-membrane contact and the adhesion force gradually increased as the oil droplet continued to be stretched (event 3). Further retracting the force probe from the membrane eventually split the remaining oil droplet from the oil attached on the membrane, which was indicated by an abrupt decrease in the adhesion force (event 4). Finally, the force probe assumed a steady-state upward movement that again yielded a flat force curve similar to the baseline (event 5). Even though there was no interaction between oil and membrane in event 5, an artifact of "positive adhesion force" was measured by the MEMS. Such an artifact can be explained by the fact that the floating force on a smaller remaining oil droplet was lower than that on the larger original oil droplet, and that the so called "adhesion force" was factually the pulling force experienced by the MEMS. Consequently, the artificial "adhesion force" in event 5 can also be applied for quasi-quantification of the amount of oil retained by the membrane.

In strong contrast, the interaction between the oil droplet and the fabricated composite membrane was very weak, which was supported by several features of the corresponding force curve (black curve on Figure 5A). Most prominently, the abrupt increase of adhesion (event 2) observed with pristine PVDF membrane did not occur for the composite membrane. Instead, zero or even slightly negative adhesion force (which suggests possible repulsion) was observed upon the initial contact between the oil droplet and the composite membrane. Oil-membrane adhesion did occur after extended and forced contact, as evidenced by the presence of the gradual growth,

and, more clearly, a precipitous drop of the adhesion force (event 3 and 4, respectively). However, the strength of the adhesion was significantly lower than that for the pristine PVDF membrane. Last but not least, the artificial "adhesion force" measured in event 5 was appreciably smaller than that for the pristine PVDF membrane, which implies that considerably less oil was retained by the composite membrane than by the pristine PVDF membrane. These evidences collectively demonstrate that the oil droplet has significantly lower affinity toward the underwater oleophobic surface of the composite membrane than the pristine hydrophobic PVDF membrane, which convincingly explained the markedly enhanced anti-oil-fouling performance of the composite membrane observed in DCMD experiments.

### 2.4. Implications

As a membrane-based technology that can harness low-grade heat to desalinate hypersaline waters, MD has the potential to become a highly promising technology for desalinating challenging saline wastewaters such as shale oil/gas wastewater and industrial wastewater. However, while MD excels for desalinating relatively clean water such as seawater, the intrinsic incompatibility between the hydrophobic membranes required for MD operation and saline feedwater with an abundance of hydrophobic contaminants results in significant fouling that hinders MD from achieving its full potential in other more challenging applications. The composite MD membrane with asymmetric surface wetting properties developed in this study unlocks the potential of MD for treating highly challenging wastewaters that are rich in hydrophobic foulants. Beyond its anti-oil-fouling capability, the composite membrane also seemed to resist wetting by naturally occurring surfactants in crude oil.

Even for feed waters with lower concentrations of foulants, membrane fouling is still a long-term concern for practical MD operation[17,28,32]. Although this study only demonstrates the excellent fouling resistance of the composite membrane using relatively short experiments with a high concentration of a very potent foulant (i.e. oil), it is likely that the observed improvement in anti-fouling performance of the composite membrane over the conventional hydrophobic membrane will also apply to longer-term MD operations with foulants of other types, such as organic, colloidal and biological fouling, and at lower concentrations. However, whether a composite oleophobic membrane can offer appreciable enhancement in fouling control over a broader range of foulant types and concentrations remains to be experimentally confirmed. Lastly,

the specific modification technique employed in this study, and the general surface modification strategy to yield underwater oleophobicity, may have the potential to mitigate organic and biological fouling in other pressurized membrane processes.

**Supporting Information**

See Appendix A. Details on the methodology of measuring membrane porosity, pore size distribution, and liquid entry pressure; infrared adsorption spectra for both the pristine membrane and the modified surface of the composite membrane acquired using polarization modulation-infrared reflection-adsorption spectroscopy (Figure A1).

**Acknowledgement**

We acknowledge the financial support from Bureau of Reclamation, Department of Interior, via DWPR Agreement R15AC00088. We also acknowledge the support received by Dr. Deyin Hou from the Chinese Scholarship Council.

CHAPTER 3

# INFLUENCE OF SURFACE CHARGE ON FOULING RESISTANCE OF MD MEMBRANES

This chapter has been published in the journal Journal of Membrane Science as the following peer-reviewed manuscript: Wang Z., Jin J., and Lin S., Tailoring Surface Charge and Wetting Property for Robust Oil-fouling Mitigation in Membrane Distillation. Journal of Membrane Science. **516** (2016). p. 113-122. doi:10.1016/j.memsci.2016.06.011.

## 3.1. Introduction

Membrane distillation (MD) is an emerging thermal desalination process capable of utilizing low-grade heat. In an MD process, a microporous hydrophobic membrane is employed as the barrier for liquid water transport and the medium for water vapor transport. The temperature difference between hot salty water (the feed solution) and cold deionized water (the distillate) results in a partial vapor pressure difference which drives the vapor to transport from the feed stream to the distillate stream, thereby desalinating the feed water [16,87,138]. Research interests in MD have recently grown significantly due to the increasing demand for desalination and the potential of MD to become a competitive technology in certain challenging desalination applications. For example, a distinct advantage of MD is the ability to harness low-grade thermal energy such as waste heat, geothermal energy, and solar thermal energy for desalination [21,139,140]. Such an advantage, together with the small system footprint and low capital cost, render MD an appealing process for sustainable and off-grid desalination[88–92]. On the other hand, MD has also been identified as one of the only few promising technological candidates for desalinating shale gas produced water, which, in certain cases, is too saline for reverse osmosis to treat[13,44,93].

Most existing MD membranes are only applicable to desalinate relatively ‘clean’ water (e.g. seawater) with a very low concentration of hydrophobic contaminants. This is because the commercially available hydrophobic membranes are inherently susceptible to fouling by hydrophobic contaminants due to the strong and long-range hydrophobic-hydrophobic interactions[29–31]. The direct consequence of MD membrane fouling is flux decline attributed to

the blocking of membrane pores by the accumulated foulants. This problem of membrane fouling by hydrophobic contaminants is particularly conspicuous when MD is employed to desalinate saline industrial wastewaters enriched in hydrophobes. One prominent example is shale gas produced water, which is not only hyper-saline but in many cases abundant with hydrocarbons. Previous MD studies using a hydrophobic polyvinylidene fluoride (PVDF) membrane to treat a feed solution with oil reported rapid flux decline that led to process failure in a relatively short time [100,141]. Another example is the application of MD to treat anaerobic digestate which, though not as potent as oil emulsion as a foulant, still led to considerable flux decline in a long term operation[142].

An effective approach to mitigate oil fouling in MD is to develop membranes with an underwater oleophobic surface that resists oil adhesion when submerged in water. The underwater oleophobicity is to be distinguished from the in-air oleophobicity which stands for resistance to oil adhesion in air. Inspired by biological surfaces such as sharkskin and clamshells that are resistant to biological or organic adhesion underwater, the materials science community has developed a plethora of interfacial materials with underwater superoleophobicity for different applications such as marine biofouling control [143,144] and oil-water separations [102–109,111,112,145]. In general, there are two requirements for constructing an underwater superoleophobic surface: rough (textured) surface morphology and hydrophilic surface chemistry. Following this principle, composite MD membranes with a hydrophobic substrate and an underwater oleophobic top surface have been developed using hydrogel-nanoparticle composites for oil fouling mitigation[100,141]. The presence of highly hydrophilic surface coating renders the feed-facing surface of the MD membrane in-air superhydrophilic and underwater superoleophobic, enabling MD to desalinate oily feed water with robust anti-fouling performance.

It is well known in surface science that a hydrogen-bond forming, superhydrophilic surface can resist the adhesion of hydrophobic substances underwater due to the formation of a surface hydration layer that serves as an energetic barrier for hydrophobic foulants to attach onto substrate surface[130–132,146,147]. This mechanism, namely the hydration force, has been a pivotal guiding principle for developing fouling resistant membranes and anti-oil-adhesion surfaces[148,149]. Although the effect of hydration force is indeed prominent, there is another important factor that plays a critical role in oil-membrane interaction but is nonetheless often

neglected in developing underwater oleophobic surfaces[107,150–152]. This factor is surface charge, which plays a significant role in controlling both electrical double layer (EDL) interaction and interfacial tension[153,154].

In a recent study where a PVDF MD membrane was coated with titanium dioxide ($TiO_2$) nanoparticles and polyethylene glycol (PEG) to acquire resistance to mineral oil fouling, it has been observed that varying the pH around the isoelectric point of the modified PVDF slightly affected the fouling kinetics[100]. However, such an effect was not appreciable, which may be explained by the fact that both the modified PVDF membrane and the mineral oil emulsion had similar isoelectric points and their interaction was thus always repulsive regardless of the solution pH. On the other hand, many studies conducted to develop underwater superoleophobic meshes or membranes for oil-water separation only focused on engineering the surface wetting properties but largely overlooked the impact of the surface charge. Because both the electrostatic interaction and the hydration force may be important as suggested by the extended Derjaguin Landau Verwey Overbeek (x-DVLO) theory[155], it is our objective in this study to systematically assess the impacts of these two interactions on the oil-membrane interaction and consequently on the propensity of an MD membrane to be fouled by an oil-in-water emulsion.

In this study, we compare the performance of three membranes with different surface wetting and charge properties in direct contact membrane distillation (DCMD) experiments with feed water containing crude oil. A hydrophobic and negatively charged PVDF membrane is used as the reference. The other two membranes are composite membranes prepared by modifying the hydrophobic PVDF membranes with nanocomposite coating comprising silica nanoparticles and hydrophilic polymers with different surface charges. We characterize these membranes to acquire information regarding their morphological and wetting properties and conduct DCMD experiments with these membranes to compare their fouling kinetics. We also conduct the force spectroscopy using a force tensiometer to probe the underwater interactions between a crude oil droplet and different membranes, and apply these force curves to elucidate the difference of these membranes in their fouling propensity.

## 3.2. Materials and Methods

### *3.2.1. Materials and Chemicals*

The hydrophobic microporous membranes, used as the reference in fouling experiments and as the substrates for surface modification, were made of PVDF with a nominal pore size of 0.45 μm (GE Healthcare Life Sciences, Pittsburg, PA). Dopamine hydrochloride, Trizma hydrochloride buffer, poly(diallyldimethylammonium chloride) solution (PDDA, 20% in $H_2O$), acetone, sodium chloride (NaCl), potassium chloride (KCl), sodium hydroxide (NaOH), and hydroochloric acid (HCl) were all procured from Sigma Aldrich (St. Louis, MO). Silica nanoparticles (SiNPs) with diameters ranging between 20 and 60 nm were purchased from SkySpring Nanomaterials (Houston, TX). The crude oil as the fouling agent was acquired from Texas Raw Crude Oil (Midland, TX).

### *3.2.2. Fabrication of the Underwater Oleophobic Membranes*

We prepared two different composite membranes by modifying the PVDF substrate membrane. Both membranes were underwater oleophobic due to the presence of the highly hydrophilic coating. However, due to the different hydrophilic surface modifiers used, the two membranes were of opposite charges at environmentally relevant pH. This subsection describes the experimental details of fabricating the two composite membranes.

#### *3.2.2.1. Composite membrane coated with polydopamine (PDA) and SiNPs*

The first composite membrane was prepared by coating a PVDF membrane with a layer of negatively charged nanocomposite of PDA and SiNPs (PDA/SiNPs). We prepared such a composite membrane by first spray-coating the substrate membrane with SiNPs and then dip-coating the SiNPs coated membrane with PDA[156,157]. The SiNPs, which are inexpensive and chemically inert, were used to increase the surface roughness and create hierarchical morphology that are essential for in-air superhydrophilicity and underwater superoleophobicity. For spray coating, 0.5 g SiNPs were dispersed in 100 mL acetone under sonication for 5 min to obtain a 5 g/L SiNPs suspension. 20 mL of SiNPs suspension were spray-coated onto a PVDF membrane substrate with an area of 20 cm × 10 cm using a spray gun with 0.2 MPa air.

After briefly dried in air, the SiNPs coated membrane was submerged in a dopamine solution prepared by dissolving 0.1 g dopamine powder in 100 mL of a 15 mM Trizma hydrochloride buffer solution with the pH adjusted to 8.5. A layer of PDA formed as a result of self-polymerization of dopamine, covering the SiNPs and the top surface of the PVDF membrane. During the dip-coating process, the PVDF membrane was taped around on a glass substrate to ensure that only the SiNPs coated surface of the membrane was exposed to the dopamine suspension. Because the hydrophilic PDA solution could not wet the hydrophobic pores of the PVDF membrane, the hydrophobicity of the inner pore structure of the PVDF substrate was not compromised, i.e., only the wetting property of the membrane surface, not that of the entire membrane, was altered by this membrane modification approach. After 24-hour self-polymerization of dopamine, the PDA/SiNPs coated PVDF (PDA/SiNPs-PVDF) membrane was washed with DI water and dried at room temperature.

#### *3.2.2.2. Composite membrane coated with PDDA and SiNPs*

The second composite membrane with PDDA and SiNPs nanocomposite (PDDA/SiNPs) was fabricated via layer-by-layer spray coating[158]. All the spray coating steps were conducted using a spray gun with 0.2 MPa pressurized air. First, a PVDF membrane substrate with an area of 20 cm × 10 cm was spray coated with a layer of PDDA with 5 mL aqueous PDDA solution (52 g/L) and then dried at room temperature. Second, 10 mL SiNPs suspension (5 g/L in acetone) was sprayed onto the PDDA coated membrane to form a SiNPs layer. The function of first PDDA layer was to impart positive charge to the PVDF substrate so that the SiNPs can attach onto the PDDA coated membrane via electrostatic interaction. Lastly, the air-dried SiNPs decorated membrane was spray coated with another layer of PDDA solution (1 ml, 52 g/L). The resulting membrane was heated at 100 °C for 1 hour. The coating applied using this approach has been tested to be mechanically robust[158].

### *3.2.3. Characterizations of Morphology and Wetting Property*

The surface morphology of the pristine PVDF membrane and the two fabricated composite membranes was observed using scanning electron microscopy, or SEM (Merlin, Zeiss, Thornwood, NY) and atomic force spectroscopy, or AFM (Dimension Icon, Bruker, Billerica, MA). The pore size distribution and liquid entry pressure, LEP, of each membrane were determined with a capillary flow porometer (Poroflux 1000, IB-GT GmbH, Germany)[121,122].

In addition, the chemical composition of each membrane surface was confirmed via polarization modulation-infrared reflection-adsorption spectroscopy, or PM-IRRAS (PMA 50, Bruker, Billerica, MA).

To compare the wetting properties of the three membranes, the static contact angle (CA) was measured using an optical tensiometer (TL100, Attension, Finland). For each membrane, both the in-air sessile drop CA with water and underwater CA with crude oil were measured. The measurements of underwater CA with crude oil were similar to measuring captive bubble CA but with the bubble replaced by a floating crude oil droplet. Each contact angle was measured at five different locations on the membrane sample[159,160].

### *3.2.4. Preparation and Characterization of Oily Feed Solution*

The saline crude oil emulsion (1000 ppm wt%) was prepared by mixing 2 g of crude oil with 2 L of NaCl aqueous solution (0.6 M) at 16,000 rpm for 15 min using a homogenizer (Fisher Scientific, Waltham, MA). The morphology of the oil droplets in the prepared solution was observed using an optical microscope (Nikon LV100, Japan). The size distribution and zeta potential of the oil droplets in the emulsion were determined by dynamic light scattering (DLS) and electrophoresis, respectively, both with a Zetasizer (Malvern Nano ZS, UK). The pH of the prepared feed solution was also measured.

### *3.2.5. Streaming Potential Measurement of the Membranes*

We measured the zeta potential of the pristine PVDF membranes and the composite membranes using a streaming potential analyzer (SurPASS, Anton Paar, Ashland, VA). In these measurements, the membrane coupons were taped onto two parallel and opposing planar surfaces across a slit with adjustable width. The electrolyte flowed, in alternating directions, along the slit composed of the two parallel surfaces covered by the membrane samples. This flow of electrolyte solution generated streaming potentials from which the zeta potential of the membrane surface was calculated using the Helmholtz–Smoluchowski equation[161,162]. The electrolyte solution was 1 mM KCl and the pH was automatically adjusted by the addition of KOH and HCl.

*3.2.6. Membrane Fouling Tests*

DCMD experiments were conducted with the saline crude oil emulsion to compare the fouling behaviors of the pristine PVDF membrane and the fabricated composite membranes. In these experiments, membrane coupons with an area of 2.5 cm × 8 cm were used in a cross-flow test cell using a co-current flow configuration. In the experiments with composite membranes, the modified, underwater oleophobic surfaces of the membrane were in contact with the feed solution, whereas the unmodified sides faced the distillate. The influent temperatures of the oily feed solution and deionized distillate were 60 °C and 20 °C, respectively.

To facilitate the detection of membrane wetting, the flowrates of feed and distillate streams were controlled to be 0.45 L/min and 0.2 L/min (9.6 cm/s and 4.3 cm/s in our test cell), respectively [44,141]. These operation conditions resulted in a slightly higher hydraulic pressure in the feed stream than in the distillate stream in this specific test cell, so that the liquid flow through any potentially wetted pores would always be driven from the feed stream to the distillate stream and thereby increase the salinity of the distillate stream. The mass and conductivity of the solution in the distillate reservoir were constantly measured and recorded. The water vapor flux and salt rejection were calculated from the temporal change of mass and conductivity of the distillate.

*3.2.7. Underwater Oil-Adhesion Force Measurements*

To mechanistically understand the fouling behaviors of the pristine PVDF membrane and the fabricated composite membranes, force spectroscopy was conducted with a force tensiometer (Sigma701, Attention, Finland) to probe the underwater interaction between a crude oil droplet and the membrane surfaces[104,123–125]. In these force spectroscopic experiments, the membrane samples were fixed at the bottom of a transparent test cell filled with electrolyte solution. A small droplet (~6 μL) of crude oil was carefully hung on to a submerged force probe (T114, Attention, Finland) using a syringe. For collecting the force curves, the force probe with the attached oil droplet approached the membrane sample surface at a constant speed of 0.3 mm/min until the oil droplet contacted with the membrane surface. Once physical contact between the oil droplet and the membrane sample occurred, the force probe retracted from the membrane surface at the same speed as approaching. Compressing the oil droplet against the sample surface was deliberately avoided, because the force probe was an open ring that can be readily forced into the crude oil phase and generate data that is not directly relevant to the oil-membrane interaction.

The results from the force spectroscopy were force curves that quantify force, measured by the micro-electro-mechanical sensor, as a function of the force probe position.

## 3.3. Results and discussions

### *3.3.1. Membrane Surface Properties*

#### *3.3.1.1. Membrane Surface Morphology*

The SEM and AFM images of the pristine PVDF membrane (Figure 3.1 A, D and G), the PDA/SiNPs-PVDF membrane (Figure 1B, E and H), and the PDDA/SiNPs-PVDF (Figure 3.1 C, F and I), show that surface modifications drastically affected the morphology of the PVDF membranes. Specifically, both the top view (Figure 3.1 B and C) and the cross-section view (Figure 3.1E and F) of the SEM images suggest that the nanocomposite coatings thoroughly cover the surface of the PVDF substrate and block most of the membrane pores on the surface. However, the modifications did not significantly affect the pore size distribution (Figure B.1) of the membrane because the thickness of coating layer is very small compared to the thickness of the PVDF membrane which was 176.4±7.3 μm.

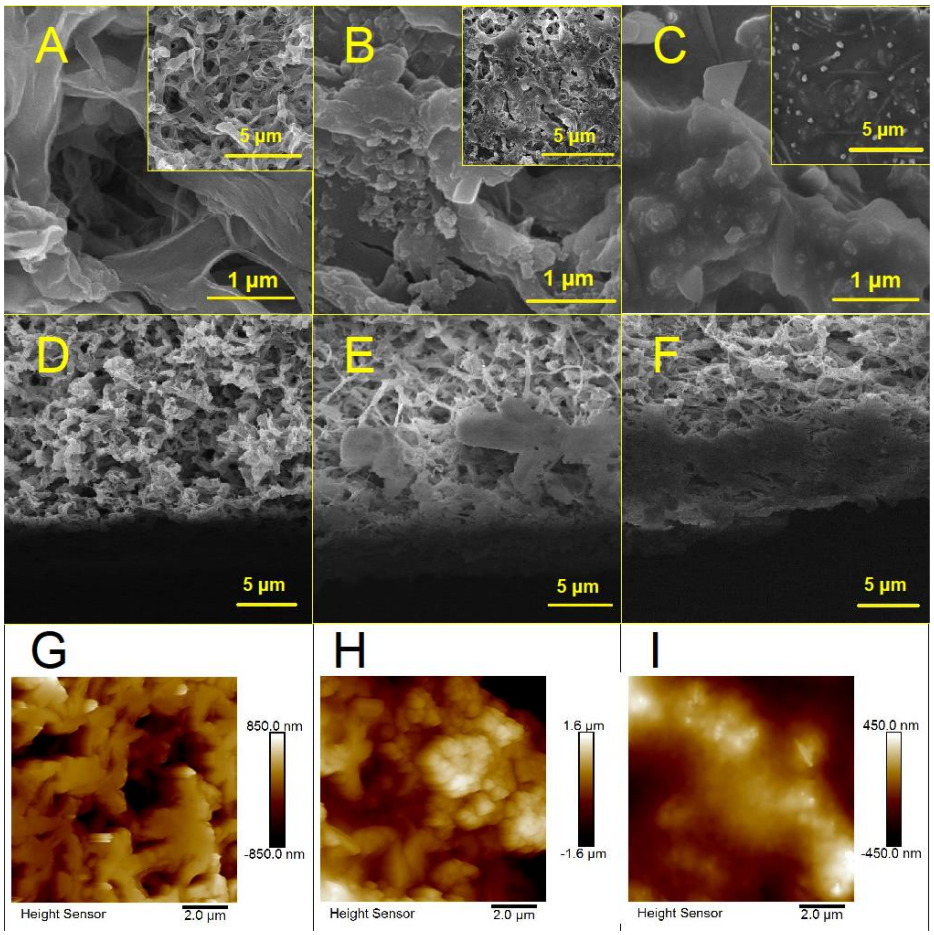


Figure 0.1 SEM images featuring the local morphology of (A) the commercial PVDF membrane, (B) the PDA/SiNPs-PVDF composite membrane, and (C) the PDDA/SiNPs-PVDF composite membrane. The inset images show the membranes surface at a larger scale. The PDA/SiNPs and PDDA/SiNPs coatings covered most of the membrane pores. Cross-section SEM images of (D) the commercial PVDF membrane, (E) the PDA/SiNPs-PVDF composite membrane, and (F) the PDDA/SiNPs-PVDF composite membrane. Surface AFM images of (G) the commercial PVDF membrane, (H) the PDA/SiNPs-PVDF composite membrane, and (I) the PDDA/SiNPs-PVDF composite membrane.

The surface modifications did not lead to any appreciable change in LEP either. Compared to the PVDF membrane with an LEP of 2.93 bar, the LEP of the PDDA/SiNPs and PDA/SiNPs modified PVDF membranes were 2.98 and 3.01 bar, respectively. Although the surface modification significantly reduced the size of the membrane surface pores, the strong hydrophilicity of the coating layer facilitated the permeation of water with little extra resistance. Consequently, the LEP should still be primarily determined by the wetting property and pore size of the hydrophobic substrate which in all three cases were the same PVDF membrane. For the similar reason, the coated membranes still maintained significant water vapor permeability, which

will be further discussed in Section 3.3.3. The hydrophilic nanocomposite PDA/SiNPs and PDDA/SiNPs coatings exhibited hierarchical roughness which, according to Wenzel theory, enhances the hydrophilicity of the surface[126,127]. The results from PM-IRRAS spectra confirmed the chemical compositions of the surface coatings on the modified composite membranes (Figure B.2).

*3.3.1.2. Membrane Surface Potential*

Surface potential is an important membrane property affecting the electrostatic interaction between membranes and oil droplets. In this study, we measured the zeta potentials of each membrane at different pH (Figure 3.2). The zeta potential varied with pH due to protonation or deprotonation of surface functional groups[163,164]. Throughout the entire pH range tested, the pristine PVDF membrane was negatively charged (green triangles in Figure 3.2) and the PDDA/SiNPs-PVDF composite membrane was positively charged (red circles in Figure 3.2). The point of zero charge (PZC) for the PDA/SiNPs-PVDF membrane was slightly below 4, significantly lower than the pH of the saline crude oil emulsion, which was between 5-6.

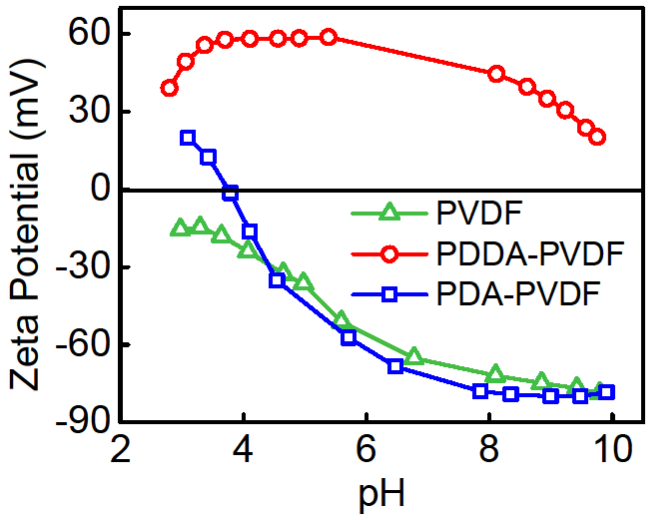


Figure 0.2 Zeta potentials of the unmodified PVDF membrane (green triangles) and the PDDA/SiNPs-PVDF composite membrane (red circles) and PDA/SiNPs composite membrane (blue squares) as a function of pH. The background electrolyte concentration was 1 mM KCl.

*3.3.1.3. Membrane Surface Wetting Property*

The wetting properties of the composite membranes were drastically different from that of the pristine PVDF membrane. The in-air water CA (blue bars in Figure 3.3) of the pristine PVDF, the PDA/SiNPs-PVDF composite membrane, and the PDDA/SiNPs-PVDF composite membrane were 106.7±3.7°, 35.1±5° and 17.9±2°, respectively. Both nanocomposite coatings imparted strong hydrophilicity to the PVDF membrane that was originally hydrophobic, which can be explained by the strong attractive interaction between water and the hydrophilic polymer on the modified membrane surfaces.

To obtain the membrane wettability information directly relevant to oil fouling in MD, we also measured the underwater CA with crude oil for the three membranes (orange bars in Figure 3.3). The unmodified PVDF membrane was instantly wetted by the crude oil with a negligibly small oil CA, indicating that the membrane was underwater superoleophilic. In comparison, the PDA/SiNPs-PVDF composite membrane exhibited underwater superoleophobicity with a very high oil CA (162.8±2.4°). Such underwater superoleophobicity is attributable to the strong interaction between the water and the hydrophilic surface coating (i.e., the hydration force). As a highly hydrophilic polymer, PDA has a variety of amide and alcohol functional groups that can form hydrogen bonds with water and create an interfacial hydration layer on the membrane surface[128–132]. Wetting the hydrogel coated membrane by the crude oil requires surface dehydration, which is energetically highly unfavorable.

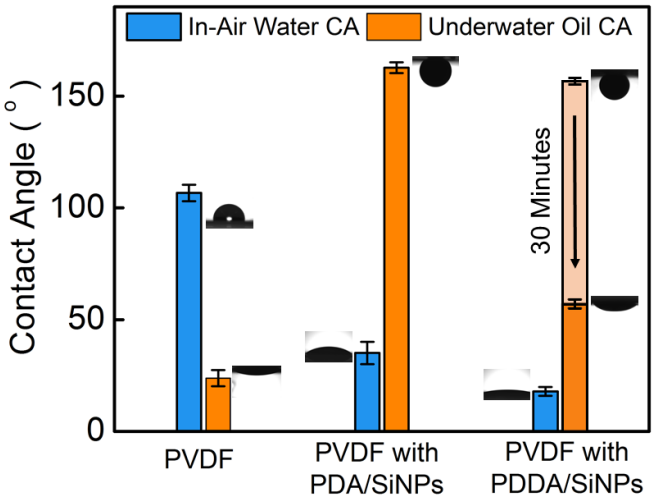


Figure 0.3 Comparison of in-air water CA (blue bars) and underwater oil CA (orange bars) between the pristine PVDF membrane and the fabricated composite membranes. The images for the sessile water drop and captive oil drop are juxtaposed with the corresponding CA. The underwater oil CA for the PDDA/SiNPs-PVDF composite membrane decreased with time (shown in the bar chart) and eventually became zero as the crude oil wicked the membrane.

With a similar principle, underwater superoleophobicity was also expected for the PDDA/SiNPs-PVDF composite membrane, because PDDA is also a highly hydrophilic polymer that forms abundant hydrogen bonds with water. Indeed, the initial underwater oil CA for PDDA/SiNPs-PVDF membrane was also very high (157.7±1.5°), indicating the composite membrane was superoleophobic upon immediate contact with water. However, the oil CA decreased over time to 57.1±2° in about 30 min, which implies that the PDDA/SiNPs-PVDF composite membrane became oleophilic if sufficient time was given for the oil-membrane interaction to reach equilibrium. In comparison, the underwater oil CA for the PDA/SiNPs-PVDF membrane was stable with no observable change over 1 h.

Such a difference between the two composite membranes in their dynamic wetting behavior is most likely attributable to the difference in their surface charges and hence the electrostatic interaction with the crude oil. In fact, the x-DLVO theory accounts for the electrical double layer, van der Waals, and the Lewis acid-based (AB) interactions, two of which depend on surface charge [153,155]. The x-DLVO theory can in part explain the observed difference in the wetting behaviors between the two composite membranes, as the electrostatic interaction between the PDA/SiNPs-PVDF membrane and the oil droplet was repulsive and that for between the PDDA/SiNPs-PVDF

membrane and the oil droplet was attractive. More detailed discussion will be given in section 3.4.1 and 3.4.2 regarding the applicability of the x-DLVO theory in explaining the oil-membrane interaction.

### *3.3.2. Properties of Saline Crude Oil Emulsion*

The crude oil emulsion (1000 ppm wt%), prepared as oil feed solution, was highly turbid (Figure 3.4A inset). The emulsion was stable without observable phase separation for at least 24 hours. Such kinetic stability of the emulsion can be attributed to the presence of naturally occurring emulsifier such as asphaltenes, naphthenic acid, carboxylic acid, and other oil-soluble acids and bases in crude oil[134,135].

Observation using optical microscopy suggested that the diameters of the oil droplets in the emulsion were in the range of few microns (Figure 3.4A), which was confirmed by DLS measurements that yielded a distribution of hydrodynamic diameter of 4.9±0.8 μm (Figure 3.4B). Since the nominal pore size of the PVDF membrane substrate was only 0.45 μm, the oil droplets are expected to effectively block the membrane pores once they attach onto the membrane surfaces. The zeta potential of the oil droplets in the emulsion was -16.4±0.8 mV derived from the measured particle electrophoretic mobility. The pH of the prepared feed solution was measured to be between 5 and 6, probably due to the various amphiphilic acids present at the water-oil interface.

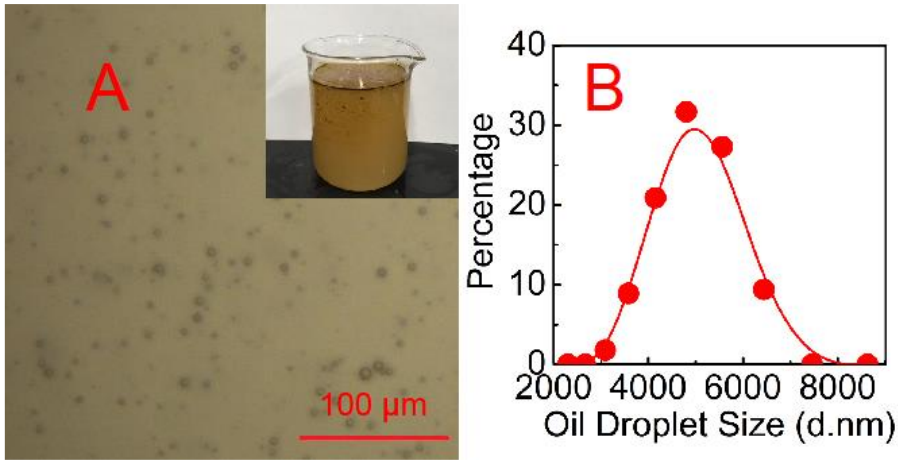


Figure 0.4 (A) A microscopic image of crude oil droplets in the crude oil (in water) emulsion prepared via vigorous physical emulsification. The inset showed a photographic image of the

emulsion. The emulsion was kinetically stable with no observable phase separation for at least 24 hours. (B) The hydrodynamic size (diameter) distribution of the crude oil droplets measured using dynamic light scattering.

### *3.3.3. Membrane Performances in MD Experiments*

DCMD experiments with the saline crude oil emulsion using the pristine PVDF membrane and the two composite membranes showed drastically different fouling behaviors (Figure 3.5). In each experiment, the monitored conductivity of the distillate was observed to be decreasing with the more feed water recovered, yielding a salt rejection rate of over 99.9% for every membrane tested. The fouling of the pristine PVDF membrane was very fast as indicated by drastic decline of water vapor flux in a short period of time (green triangles in Figure 3.5). In fact, the water flux dropped to almost zero in only about two hours. Since the PVDF membrane was in-air hydrophobic and underwater oleophilic as suggested by the CA measurements, the very strong long-range hydrophobic-hydrophobic interaction between the crude oil droplets and the membrane surface promoted the retention of oil droplets on the membrane surface and resulted in blockage of membrane pores that served as the pathways for water vapor flux.

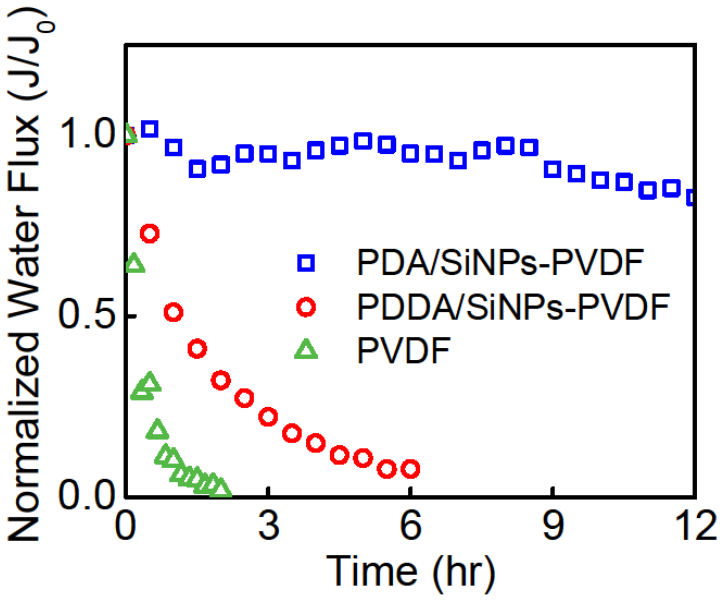


Figure 0.5 Normalized water (vapor) flux for PDA/SiNPs-PVDF composite membranes (blue squares), PDDA/SiNPs-PVDF composite membrane (red circles), and pristine PVDF membrane (green triangles) with a saline feed solution containing 1000 ppm (% wt) crude oil in the DCMD experiments. The time-dependent water fluxes were normalized by the initial water fluxes of the respective membranes. The cross flow velocities in the feed stream and distillate stream were 9.6 cm/s and 4.3 cm/s, respectively. The feed and distillate temperatures were 60 °C and 20 °C,

respectively. The initial water fluxes for PVDF membrane and composite membranes with PDA/SiNPs and PDDA/SiNPs were 30.96 L $m^{-2}$ $h^{-1}$, and 24.29 L $m^{-2}$ $h^{-1}$ and 23.6 L $m^{-2}$ $h^{-1}$, respectively.

In comparison, the DCMD performance of the PDA/SiNPs-PVDF composite membrane was appreciably more stable. With the same crude oil emulsion that severely fouled the pristine PVDF membrane, the PDA/SiNPs-PVDF composite membrane was able to maintain a nearly constant water vapor flux along the 12 h MD operation (blue squares in Figure 3.5). The more robust MD performance of the PDA/SiNPs-PVDF composite membrane can be explained by the underwater superoleophobicity of the composite membrane as suggested by its underwater oil CA. The strong hydration force due to the presence of the highly hydrophilic PDA polymer, and the electrostatic repulsion between the nanocomposite and the oil droplets, both contributed to mitigating the adhesion of the oil droplets to the membrane surface.

The PDDA/SiNPs nanocomposite coating slowed down the membrane fouling as reflected by the appreciably slower flux decline of the water vapor flux (red circles in Figure 3.5) as compared to that with the pristine PVDF membrane. However, the fouling control was significantly less effective with the PDDA/SiNPs nanocomposite than with the PDA/SiNPs nanocomposite. The difference in anti-fouling performance between these two nanocomposite membranes is in good accordance with the results observed in underwater oil CA measurements. The initial underwater superoleophobicity of the PDDA/SiNPs-PVDF membrane, which was a result of the repulsive hydration force, contributed to the slower flux decline as compared to the pristine PVDF membrane. However, the PDDA/SiNPs-PVDF membrane gradually lost its oleophobicity possibly due to electrostatic attraction, which eventually led to significant membrane fouling within a relatively short time. In comparison, the PDA/SiNPs-PVDF was able to sustain a much more robust MD performance due to the presence of both hydration force and electrostatic repulsion.

The initial fluxes of the PDDA/SiNPs-PVDF composite membrane (23.6 LMH) and PDA/SiNPs-PVDF composite membrane (24.3 LMH) were lower than that of the pristine PVDF membrane (31.0 LMH). The flux reduction was obviously consequent of the surface modification that blocked a significant portion of the membrane. On the other hand, the percentages of flux reduction were clearly not in proportion to the fraction of pore blockage shown in the SEM images. Because the nanocomposite layers were porous hydrophilic networks, the liquid feed water should be able to permeate through layer with limited resistance. We therefore speculate that the reduction

of vapor flux was mostly attributable to the enhanced temperature polarization in the coating layer. The hydrated nanocomposite coating is a hydraulically stagnant layer insusceptible to the cross-flow induced mixing in the feed channel[16,136,137]. Similar to the internal concentration polarization in forward osmosis which has a detrimental impact on mass transfer[165], the temperature polarization across the hydrated nanocomposite layer was also "internal" in the sense that it occurred within the membrane structure. This additional temperature polarization served to reduce the driving force for vapor transfer across the MD membranes.

### *3.3.4. Force Spectroscopy with Oil Droplet Probe*

To acquire more fundamental understanding about the interaction between the oil droplet and the membrane surface and to explain the different fouling behaviors with different membranes, we conducted force spectroscopy with an oil droplet as the force probe and water as the medium. The position dependent interaction forces between an oil droplet and different membrane surfaces are presented in Figure 3.6 for comparison. A complete interaction curve includes two stages, the advancing and receding stages, and five distinct events, including "approach", "contact", "retract", "split" and "detach". The details for general interpretation of the force curves were given in our previous publication[141].

Before the oil droplet force probe contacted the surface, the "adhesion force" was set to zero by default, as there was no physical interaction between the oil droplet and the membrane. Upon contact between the oil droplet force probe and the pristine PVDF membrane, a strong and sudden attraction was detected. This strong attraction can be attributed to the hydrophobic interaction between the oil droplet and the PVDF membrane[29,30,166]. As the force probe retracted, it experienced an attractive force until the split of the oil droplet. The oil droplet split was reflected on the force curve as a precipitous drop in the "adhesion force". A finite "adhesion force" was measured after the split of the oil droplet, which was an artifact resulting from a smaller oil droplet remaining on the force probe. The new "baseline" was non-zero because the difference between buoyancy and gravity for the remaining oil droplet was smaller than that of the original oil droplet[141]. However, there was no physical oil-membrane interaction or "adhesion" corresponding to the finite "adhesion force", because the oil droplet had already detached from the surface. Although such an "adhesion force" measured by the tensiometer was an artifact in essence, its magnitude positively correlates with the size of the oil droplet remaining on the force probe,

which still yields a useful piece of information regarding the affinity between oil droplet and the membrane surface.

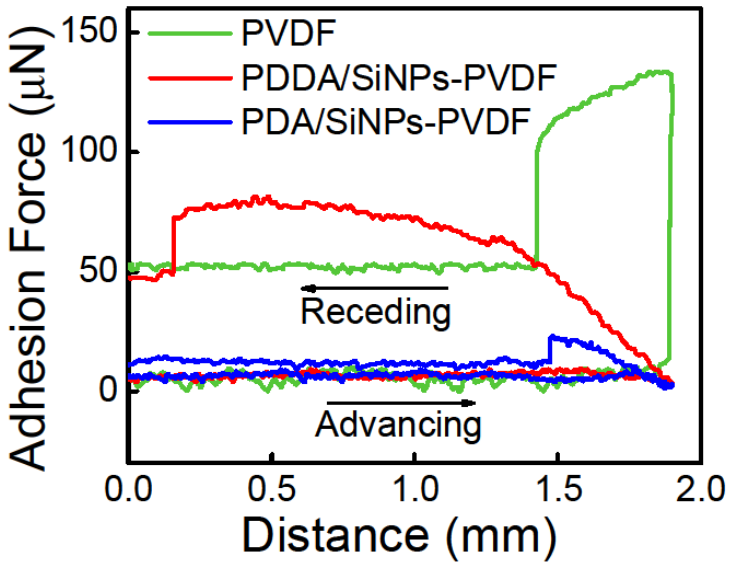


Figure 0.6 Force curves for the interactions of a crude oil droplet with the pristine PVDF membrane (green curve), the PDA/SiNPs-PVDF membrane (blue curve) and the PDDA/SiNPs-PVDF membrane (red curve). The advancing stage was represented by the flat baselines with close-to-zero adhesion force measured when the oil droplet probe approached the membrane surface (the bottom parts on the force curves, proceeding from left to right). There was no difference between the three tested membranes in the force curves during the advancing stage since no interaction with the membrane had occurred. The remaining parts of the force curves were obtained from the receding stage in which the oil droplet probe was pulled away from the surface (proceeding from right to left on the figure). This part of the force curve was distinctive for each membrane as it was strongly dependent on the oil-membrane interaction. A precipitous drop in adhesion force was present in every single force curve, representing the split of the oil droplet probe into two parts with one remaining on the probe and the other staying on the membrane surface. A constant "adhesion force" was measured, without exception, in the end of the each force curve because the oil droplet probe no long interacted with the membrane after the split. The non-zero and constant "adhesion forces" at the end of all force curves were nothing but an artifacts (i.e. they do not represent actual adhesion), resulting from the change of oil droplet volume and thus the forces measured by the tensiometer.

For the PDA/SiNPs-PVDF composite membrane, no strong and sudden attraction between the oil droplet and the membrane was observed. On the contrary, a slight repulsive interaction was detected as suggested by a negative "adhesion force" measured upon the contact between the oil droplet and the composite membrane. We did not attempt to quantify such a repulsive force by further pressing the oil probe against the membrane, as the ring-shaped force probe could be forced

into the compressed oil droplet and generates irrelevant interaction information. Therefore, the force probe was retracted almost instantly after the oil droplet contacted the membrane. Nonetheless, the repulsion between the oil droplet and the PDA/SiNPs-PVDF composite membrane upon their first contact was conspicuous from the recorded force curve. The retraction of the force probe resulted in attractive interaction between the oil droplet and the membrane as evidenced by the increasing adhesion force during the receding stage, before the oil droplet split. However, such an adhesion force was very small for the PDA/SiNPs-PVDF composite membrane, as revealed by the force curve (blue curve in Figure 3.6). Furthermore, the remaining part of the force curve after oil droplet split only shifted slightly from the original baseline, indicating that only a small proportion of the oil droplet remained on the membrane surface.

The shape of the force curve for the interaction of an oil droplet with the PDDA/SiNPs-PVDF composite membrane resembled that for the interaction with the PDA/SiNPs-PVDF membrane. For instance, repulsion was also observed upon the initial contact between the oil droplet and the composite membrane. However, the attractive interaction between the oil droplet and the PDDA/SiNPs-PVDF was significantly stronger than that between the oil droplet and the PDA/SiNPs-PVDF membrane during the force probe retraction. Since the primary difference between the two composite membranes was the surface zeta potential, it is likely that electrostatic interaction played an important role that differentiated two composite membranes in their interactions with the oil droplet probe.

### *3.3.5. Implications of Electrostatic Interaction*

The results from the force spectroscopy can be employed to explain the different fouling behaviors observed with different MD membranes. The pristine PVDF membrane was most susceptible to fouling as evidenced by the fastest flux decline among three membranes. This can be explained by the instant and very strong attraction between the oil droplets and the PVDF membrane via the strong hydrophobic-hydrophobic interaction.

On the other hand, the other two underwater oleophobic membranes both mitigated membrane fouling due to the presence of the repulsive hydration force. However, the extents to which membrane fouling was alleviated by the two composite membranes were very different due to the different surface charges and consequently different electrostatic interactions. The attractive electrostatic interaction between the positively charged PDDA/SiNPs-PVDF membrane and the

negatively charged crude oil particles offset the repulsive hydration force, leading to a membrane fouling rate between that with the hydrophobic and underwater oleophilic PVDF membrane and that with the underwater oleophobic and negatively charged PDA/SiNPs-PVDF membrane.

The response for the wettability-based interaction seemed to be much faster than that for the electrostatic interaction. This phenomenon was observed in both the underwater oil CA measurements and the oil droplet probe force spectroscopy. In the underwater oil CA measurement using the PDDA/SiNPs-PVDF membrane, the initial underwater oil CA was very high due to the in-air hydrophilic surface coating of the PDDA/SiNPs. The gradual transition of the membrane surface from being underwater superoleophobic to underwater oleophilic can be attributed to electrostatic interaction which did not take effect immediately after the initial oil-membrane contact.

Different responses based on the interaction mechanisms were also observed in force spectroscopy. For example, the precipitous attraction upon the first contact between the membrane and the oil droplet was manifest for PVDF membrane but absent for the PDDA/SiNPs-PVDF membrane, which can be explained by their different surface wetting properties. The relatively significant electrostatic interaction between the positively charged PDDA/SiNPs-PVDF membrane and the negatively charged oil droplet did not become effective until the oil droplet force probe was being retracted from the membrane surface.

The experimental evidences from CA measurements, force spectroscopy, and fouling experiments consistently lead to a cogent conclusion that surface potentials (charges) played a critical role, in addition to wettability, in determining the oil-membrane interaction in water. However, electrostatic interaction is a rather broad concept with many manifestations. For example, ionic bonding, electrical double layer interaction, or even the Keesom type of vdW interaction (e.g. hydrogen bond) can all be considered as electrostatic interaction[166]. The exact mechanism of electrostatic interaction relevant to our experimental observations in this study still needs to be explicated. In the following subsections, we will discuss the impact of the surface potentials on the oil-membrane interaction from both the DLVO and the interfacial tension perspectives.

*3.3.6. The relative Irrelevance of the DLVO Approach*

When particle-membrane interaction (colloidal deposition) is involved, the DLVO theory has been often cited for theoretical explanation[167–169]. The DLVO theory states that the affinity between a particle and a surface is primarily determined by the electrical double layer (EDL) interaction and the van der Waals (vdW) interaction. The attachment efficiency, defined as the probability for successful attachment per collision, has been employed to quantify such an affinity.

However, the applicability of the DLVO theory, for explaining the experimental results of membrane fouling in our study, is questionable. One major problem is that the EDL interaction, which comprises both osmotic and Coulombic contributions[166,170], should theoretically have negligible impact on the overall interaction due to the very short Debye length (calculated to be ~0.4 nm for the feed solution used). Within such a short Debye length, the vdW force should dominate the overall interaction and eclipse any difference in the EDL interaction. Therefore, the EDL interaction was unlikely the manifestation of the differential electrostatic interactions between the PDA/SiNPs-PVDF and PDDA/SiNPs-PVDF membranes that led to drastically different fouling behaviors.

To account for the impact of surface wetting properties, the extended DLVO (*x*-DLVO) theory has often been cited to quantify the affinity between a particle and a membrane surface[171]. The x-DLVO theory incorporate the Lewis acid-base (AB) interaction that accounts for the wetting property based short-range interactions such as hydration force. The short range vdW and AB interactions contribute to the interfacial tension and the free energy of adhesion that not only determine how easy a particle can attach onto the membrane surface (i.e. the attachment efficiency) but also how readily a particle can detach from the membrane surface upon local perturbation.

According to van Oss, the AB component of the interfacial tension involves interaction between electron acceptors and electron donors and only takes effect when the two interacting surfaces are both polar[82,171,172]. The surface charges of the membranes and the oil droplets have significant impact on the electron donor and electron acceptor parameters, which can explain the drastically different wetting, adhesion, and fouling behaviors between the positively charged PDDA/SiNPs-PVDF membrane and the negatively charged PDA/SiNPs-PVDF membrane. In other words, the electrostatic interaction most likely exerted its impact via the polar interaction component in surface adhesion, rather than the EDL interaction.

However, as free energy of adhesion is a thermodynamic property, it still cannot explain the dynamic behaviors of the PDA/SiNPs-PVDF membrane in the CA measurement and force spectroscopy. We speculate that such dynamic wetting behavior involves the redistribution of natural anionic surfactants at the interface between crude oil and water. These anionic surfactants have lateral mobility along the interface and thus can migrate under the influence of electric field. When the oil droplet was in contact with a positively charged surface, these anionic surfactants gradually concentrated toward the contact area and thereby increased the local electronegativity, which resulted in a higher electron donor parameter of the oil surface and thus a stronger attractive AB interaction between the oil droplet and the membrane.

### 3.4. Conclusion

In this study, we tested a hydrophobic PVDF membrane, a PDA/SiNPs-PVDF composite membrane with a hydrophilic and negatively charged surface, and a PDDA/SiNPs-PVDF composite membrane with a hydrophilic and positively charged surface in membrane distillation experiments with a saline crude oil emulsion. While the fouling resistance of the PVDF membrane was expectably poor, both composite membranes were effective in fouling control, but to different extents. The negatively charged PDA/SiNPs-PVDF membrane was highly effective and robust in mitigating the fouling of the negatively charged crude oil emulsion; whereas the positively charged PDDA/SiNPs-PVDF membrane only offered limited improvement over the hydrophobic PVDF membrane. The difference in the fouling behaviors between the three membranes was, to a high degree, corroborated by results obtained from underwater oil CA measurement and from oil droplet probe force spectroscopy.

Dynamic behaviors of the wetting and adhesion were observed when the negatively charged crude oil droplet interacted with the hydrophilic but positively charge PDDA/SiNPs-PVDF membrane. The fundamental mechanism underlying this dynamic behavior remains uncertain. We also demonstrated the relative irrelevance of the colloidal deposition approach and the strong relevance of the adhesion energy approach for elucidating the impact of electrostatic interaction on oil-membrane interaction. One possible explanation for the dynamic wetting and adhesion behaviors was the redistribution of charge baring surfactants at the oil water interface under the electrostatic influence of the oppositely charged membrane, which led to increasing attractive interaction between the crude oil droplet and the PDDA/SiNPs-PVDF membrane.

## Supporting Information

See Appendix B. Details about pore size distribution and FTIR spectra of each membrane can be found in Figure B.1 and B.2, respectively.


## Acknowledgement

The author acknowledge the financial support from Bureau of Reclamation, Department of Interior, via DWPR Agreement R15AC00088.

# CHAPTER 4

# MECHANISM OF MEMBRANE PORE WETTING IN MEMBRANE DISTILLATION

This chapter has been published as two peer-reviewed manuscripts: the first one is on Environmental Science & Technology Letters as "Chen Y.[1], Wang Z.[1], Jennings G. K., and Lin S., Probing Pore Wetting in Membrane Distillation Using Impedance: Early Detection and Mechanism of Surfactant-Induced Wetting, Environmental Science & Technology Letters **4** (2017), p. 505-510. ([1]equal contributions) doi:10.1021/acs.estlett.7b00372.", and the other one is on Journal of Membrane Science as "Wang Z.[1], Chen Y.[1], Sun X., Duddu R., and Lin S., Mechanism of Pore Wetting in Membrane Distillation with Achohol vs. Surfactant, Journal of Membrane Science **559** (2018). p. 183-195. ([1]equal contributions) doi: 10.1016/j.memsci.2018.04.045.".

## 4.1. Introduction

Membrane distillation (MD) is a thermal desalination technology capable of using low-temperature heat to desalinate hypersaline water[16,19,138,173–175]. In an MD process, a microporous hydrophobic membrane is applied to separate a hot salty stream, known as feed solution, and a cold distillate stream. Air pockets are trapped within such a membrane because the membrane hydrophobicity prevents the feed solution and distillate from intruding into the membrane pores. Driven by the partial water vapor pressure difference resulting from the temperature difference of the two streams, water evaporates from the feed solution, transports across the air pockets, and condenses to become part of the distillate. The hydrophobic membrane thereby serves as a barrier to prevent the salty feed stream from passing through the membrane in its liquid form and mixing with the distillate. MD has several major technological advantages, including the capability of utilizing low-grade energy, the ability to treat hypersaline wastewaters, small system foot print, and low capital cost due to the absence of high pressure and high temperature components[1,13,20,88,90,91,176–178].

In spite of all its advantages, MD has not been widely applied in industry, likely due to several major technical challenges. One of the major technical challenges that limit the application of MD is membrane pore wetting[42,179,180]. Membrane pore wetting refers to the penetration of feed

water through the membrane pores and the consequent failure of MD operation due to the compromised salt rejection rate. Previous studies have shown that the presence of low-surface-tension (LST) or amphiphilic agents in the feed solution induces pore wetting in MD with hydrophobic membranes[40,43,44,94]. Recent studies have explored both material and operational solutions to this technical challenge. Specifically, the development of omniphobic membranes has been shown to be a promising material solution[44,48,50,51]. Alternatively, composite membranes with a hydrophilic coating have been shown to enhance wetting resistance[52,53]. On the other hand, a combined material and operational approach using a superhydrophobic membrane with air-layer recharging has also proven to be a viable solution[43,54].

Despite all these efforts in addressing the challenge of pore wetting in MD, the exact mechanism of pore wetting has yet to be thoroughly elucidated. It is generally believed that wetting occurs if the transmembrane hydraulic pressure difference exceeds the liquid entry pressure (LEP) that depends on membrane material, pore structure, and the surface tension of the feed solution. This theoretical framework can explain pore wetting induced by lowering the surface tension of the feed solution via addition of LST and water miscible liquid, such as alcohol, into the aqueous feed solution. However, when surfactants are used to promote pore wetting, it is unclear if wetting occurs simply because surfactants reduce the surface tension of the feed solution, or because the pore surface becomes hydrophilic due to surfactant adsorption. While the first mechanism is certainly important, the second mechanism also sounds probable and has been suggested by several studies to be a possible contribution[40,181]. However, if the first mechanism is the sole contribution to pore wetting, a testable hypothesis is that feed solutions containing LST liquid and surfactants should behave similarly in inducing pore wetting, as long as their surface tension is adjusted to be the same. Differentiating these mechanisms requires more advanced techniques for probing wetting dynamics which is inaccessible by simply monitoring salt rejection.

The conventional approach of wetting detection is by monitoring the electrical conductivity of the distillate[182,183]. Despite its simplicity and prevalent use, this conductivity-based approach can detect wetting only when certain pores have been penetrated and the MD membrane has already failed. Recently, an alternative wetting detection technique based on measuring the direct current across a conductive MD membrane was proposed[184]. While this approach appears to be more sensitive than measuring distillate conductivity for monitoring the onset of membrane wetting, it still cannot detect imminent wetting of membrane pores that have not yet been wicked

through. A novel monitoring approach that can provide effective early detection of imminent membrane wetting is highly desirable, as it may potentially enable the implementation of timely measures to prevent process failure due to wetting.

Electrochemical impedance spectroscopy (EIS) is a versatile characterization technique that probes the magnitude and phase of the electrochemical impedance of a system. It works by measuring the electrical response of a system upon application of alternating potentials with a wide spectrum of frequencies[185,186]. Recently, EIS has been utilized to determine the wetting state of textured surfaces, taking advantage of the fact that the impedance varies depending on whether the grooves (or pores) of a rough (or porous) surface are filled with an electrolyte solution or air[187–189]. Similarly, EIS has also recently been utilized to construct a novel porometry for characterizing pore size distribution of microporous membranes[190]. In addition, several studies about the successful implementations of EIS to monitor fouling in membrane systems such as RO, microfiltration, and forward osmosis (FO) haven been reported[185,191–197]. Through the use of EIS, early detection of RO membrane fouling has been achieved[185,198]. The mechanisms of various types of membrane fouling have also been investigated using EIS[185,192,193,199,200]. MD differs from all these membrane processes in that pores in a functional MD membrane should always be filled with air. These air-filled pores, sandwiched by the feed solution and distillate, comprise an equivalent capacitor for which impedance-based characterization is strongly relevant. Surprisingly, however, no impedance-based study of MD pore wetting has been reported.

In this study, we explore the use of an impedance-based technique to monitor pore wetting in MD. Here, we construct a direct contact MD (DCMD) system with the capability of in-situ impedance measurement and use such a system to investigate the dynamics of surfactant-induced pore wetting. Specifically, we perform DCMD experiments with a commercial hydrophobic polyvinylidene fluoride (PVDF) membrane and induce pore wetting by adding surfactants into the feed solution. Two real-time monitoring techniques, one based on cross-membrane impedance and the other based on distillate conductivity, are employed and compared in probing membrane pore wetting. Exploiting this impedance-based technique, we comparatively investigate the behaviors of pore wetting in direct contact membrane distillation (DCMD) with feed solutions containing two different types of wetting agents. The first wetting agent, ethanol, is a LST and non-adsorbing liquid miscible with water. The second wetting agent, Triton X-100, is a charge-neutral surfactant. Using the wetting monitoring technique based on single-frequency impedance measurement, we

study the dynamic wetting of PVDF membranes in DCMD experiments to elucidate the fundamental difference between wetting induced by ethanol and by surfactant. We also develop a novel theoretical model to describe the dynamics of surfactant-induced pore wetting, and use DCMD experiments to verify several key predictions from such a model regarding the impacts of surfactant concentration, feed temperature, and transmembrane hydraulic pressure on wetting kinetics.

## 4.2. Theory and Model Development

### *4.2.1. General criterion of pore wetting*

The minimum transmembrane pressure difference required for liquid to intrude into a membrane pore is the liquid entry pressure (LEP) as given by equation 4.1:

$$LEP = -\frac{2B\gamma_L cos\theta}{r} \tag{4.1}$$

where $\gamma_L$ is the liquid surface tension, $\theta$ is the intrinsic liquid contact angle between the liquid and the solid membrane material, $r$ is the equivalent pore radius, and $B$ is the geometric factor accounting for the non-cylindrical pore geometry and is unity for perfect cylindrical pores. The addition of wetting agents, regardless of chemical compositions, reduces $\gamma_L$ of the feed solution, thereby decreasing LEP and facilitating pore wetting[19,40,50,201,202]. We note that the change of $\gamma_L$ also affects $\theta$, as the intrinsic contact angle depends on both $\gamma_L$ and the surface energy of the solid material. In this sense, $\gamma_L$ and $cos\theta$ can be grouped into one single parameter, $\gamma_L cos\theta$, because they cannot vary independently as $\gamma_L$ changes.

Both alcohol and surfactants can reduce $\gamma_L$, $cos\theta$, and consequently, $\gamma_L cos\theta$. However, the fundamental difference between these two wetting agents is that the surface energy of the solid pore surface can be modified by surfactants via surface adsorption (Figure 4.1b) but not by simple alcohols which is hardly surface active (Figure 4.1a). Is it possible, then, that surface adsorption is one of the reasons for pore wetting induced by surfactants, because the membrane pores are rendered hydrophilic by the adsorbed surfactants? This mechanism of pore wetting induced by surfactant adsorption has indeed been suggested in literature[40,181,203]. However, we contend here with two arguments that surface adsorption of surfactants unlikely has positive contribution to pore wetting.

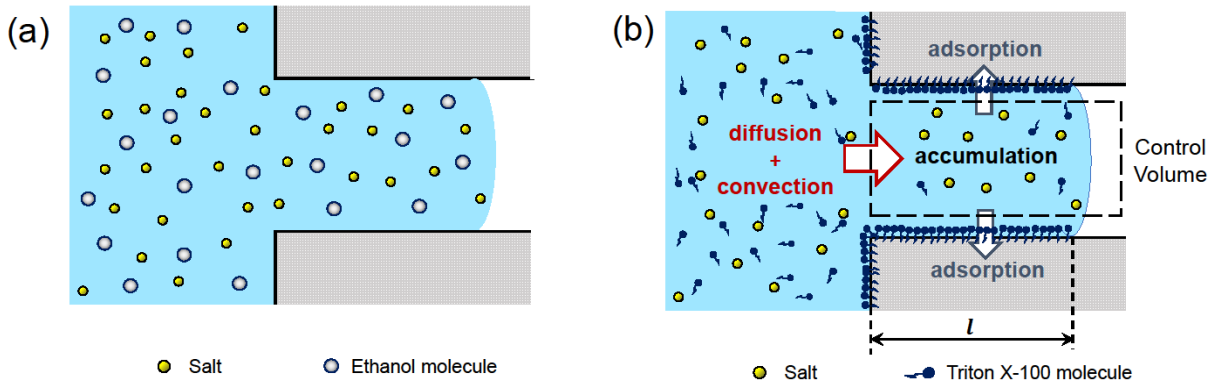


Figure 4.1 Illustration of wetting of a cylindrical pore by saline feed solutions containing (A) ethanol and (B) Triton X-100. For pore wetting induced by ethanol, the solution enters the membrane pore when the transmembrane pressure exceeds the LEP. Adsorption of ethanol molecules onto the pore surface is negligible. For pore wetting by Triton X-100 solution, the liquid-air interface (i.e. the wetting frontier) propagates forward toward the distillate when the transmembrane pressure exceeds the LEP corresponding to the Triton X-100 concentration at the liquid-air interface. Triton X-100 in the feed solution inside the pores are constantly removed by the pore surface via adsorption, which tends to reduce the surfactant concentration and increase the LEP at the liquid-air interface. The kinetics of interface propagation is therefore controlled by the kinetics of surfactant adsorption.

First, surface adsorption of surfactants is possible only when the surfactant-containing feed solution is already in contact with the solid surface, in which case the solid surface has already been wetted by definition. In other words, it is improbable that surfactants can adsorb onto the non-wetted area of the solid surface and render it hydrophilic. Altering the surface energy of the already-wetted region of a solid surface has little relevance to whether the non-wetted portion of a surface can be wetted by the surfactant solution or not, i.e. the relevant surface energy that should be used in equation 4.1 is the intrinsic surface energy of the membrane material, not that of the surfactant-modified surface. The second argument regards the ability of omniphobic membrane to resist wetting by surfactant solution[44,48,50,51]. According to well-established theory, omniphobicity is attainable only if the surface has both low surface energy and reentrant structure[204–206]. If surface hydrophilization were indeed a mechanism for surfactant-induced pore wetting, omniphobic membrane should not have wetting resistance to surfactant solutions, which is inconsistent with experimental observations[44,49,50]. Therefore, surfactant adsorption

should not contribute positively to pore wetting. On the contrary, surfactant adsorption deters pore wetting by surfactant-containing solutions in MD, as we will explain below.

Now we assume that surface hydrophilization by surfactant adsorption is not a positive contribution to membrane pore wetting, the general criterion of pore wetting is simply that $\Delta P$ is higher than LEP according to the general criterion of wetting[19,40]:

$$\Delta P > LEP \tag{4.2}$$

The reason of using $\Delta P$ instead of just the feed hydraulic pressure when comparing with LEP has been elucidated in literature [207] and summarized in Appendix C.

This general criterion should apply to wetting induced by both alcohols and surfactants. However, we note that the LEP should be calculated based on the solution properties of the wetting frontier but not those of the bulk solution. This is of particular importance for surfactant-induced wetting, as adsorption of surfactants reduces the surfactant concentration at the wetting frontier and leads to a frontier LEP that may be much higher than that of the bulk solution.

### *4.2.2. Membrane Wetting by Alcohol Solution*

For wetting of an ideal cylindrical pore by feed solution containing ethanol, which is non surface active, the kinetics of propagation of the wetting frontier toward the distillate can be modeled by treating the solution within a pore as an expanding Poiseuille flow[208,209]. In this case, the wetting kinetics is described by equation 4.3 (detailed derivation shown in Appendix C):

$$l(t) = \sqrt{\frac{r^2}{4\mu}(\Delta P - LEP)t} \tag{4.3}$$

where $l$ is the intrusion depth defined as the distance between the wetting frontier and the pore entrance, $r$ is the pore radius, $\mu$ is the dynamic viscosity of the feed solution, and $t$ is the time since feed solution enters the pore. The function $l(t)$ describes the time-dependent position of the wetting frontier, which can be semi-quantitatively probed by measuring the transmembrane impedance[181].

*4.2.3. Membrane wetting by surfactants*

Albeit pore wetting by surfactant solution should follow the same general criterion given by equation 4.2, its wetting dynamics differs drastically from that of alcohol-induced wetting due to the strong adsorption of surfactant onto the pore surface (Figure 4.2b). The relevant LEP for the propagation of the wetting frontier (i.e. the liquid-air interface) depends on the interfacial concentration of surfactants, which is in turn controlled by the transport of surfactants to the wetting frontier. On the one hand, adsorption of surfactants onto the pore surface surrounding the wetting frontier tends to reduce the surfactant concentration, which in turn tends to increase $\gamma_L$ at the wetting frontier and retards further wetting. On the other hand, diffusion of surfactants down concentration gradient and convection induced by transmembrane vapor flux, both in the axial direction of the pore, replenish the surfactants at the wetting frontier, which in turn tend to decrease $\gamma_L$ and further promote wetting.

Theoretically, we can solve a partial differential equation (PDE) regarding the diffusion-convection-adsorption of surfactants to obtain the spatiotemporal distribution of surfactant concentration in the water column within a partially wetted pore (Appendix C). One key boundary condition is that the surfactant concentration at the wetting frontier is such that the corresponding LEP equals $\Delta P$. In addition, the spatial boundary for the PDE, which is the position of the wetting frontier, constantly changes as interface continuously propagates toward the distillate. The goal of solving the PDE is to quantify the position of the shifting boundary as a function of time, i.e., $l(t)$. The numerical solution of such a PDE of a time-dependent boundary condition is challenging to obtain, and more importantly, provides limited intuitive insight to understanding the dynamics of surfactant-induced pore wetting. Here, we present a simplified quasi-equilibrium-adsorption model with which we can derive a simple analytical approximation of $l(t)$ that captures the most important features of surfactant-induced dynamic wetting.

Two primary simplifying assumptions are applied in our derivation. First, it can be shown that the longitudinal diffusive contribution to surfactant transport is negligible compared to the convective contribution (Appendix C). Second, we assume that adsorption is very fast compared to longitudinal surfactant transport so that local adsorption equilibrium is reached at any moment, i.e., the local surface concentration of surfactants, $\tau(x)$, can be determined by the local aqueous surfactant concentration, $c(x)$, following an adsorption isotherm. This assumption of quasi-equilibrium-adsorption is a reasonable approximation because (1) the mean radial diffusion

distance, i.e., the mean distance for which surfactant molecules travel radially before they adsorb onto the pore surface, is roughly the membrane pore size and thus very small compared to $l(t)$ except at the beginning of wetting; and (2) physical adsorption of surfactants via hydrophobic interaction involves no specific chemical interaction that requires activation energy, and is therefore not rate-limiting.

To describe the adsorption equilibrium, we first consider the Langmuir isotherm which is widely applied for monolayer adsorption as in the case of surfactant adsorption. The Langmuir isotherm is given by

$$\tau(x) = \tau_{max} \frac{Kc(x)}{1 + Kc(x)} \tag{4.4}$$

where $\tau_{max}$ is the maximum area density of Triton X-100 (surfactant to be used in this study) on pore surface and $K$ is an equilibrium constant that governs the partition of Triton X-100 between the membrane surface and the solution phase. Here, we consider an MD membrane made of polyvinyldine fluoride (PVDF) for obtaining the parameters in equation 4.4. With the Triton X-100 concentration used in this study and the relevant $K$ value reported in literature for PVDF[210], it can be shown that $Kc(x) \gg 1$, which reduces the Langmuir isotherm to a stepwise adsorption isotherm employed in the previous literature[209]:

$$\tau(x) = \begin{cases} \tau_{max}, c(x) > 0 \\ 0, c(x) = 0 \end{cases} \tag{4.5}$$

Equation 4.5 implies that, as long as the PVDF surface is in equilibrium with a Triton X-100 solution of a non-trivial concentration, the surface will always be fully saturated by the Triton X-100 molecules. Consequently, if the PVDF surface has not yet been fully saturated, which is the case for the differential portion of the pore surface surrounding the wetting frontier, the aqueous concentration of Triton X-100 in equilibrium with such an unsaturated part of the surface should approach zero. In other words, the wetting frontier is depleted of surfactants due to the continuous and fast removal of surfactants from the solution via adsorption onto the pore surface near the frontier. As a result, the $\gamma_L$ of the wetting frontier is close to the $\gamma_L$ of surfactant-free water due to the very low interfacial surfactant concentration. Therefore, wetting frontier does not proceed toward the distillate until its surrounding pore surface is fully saturated with surfactant molecules that are constantly replenished to the wetting frontier by axial convection. In other words, the

wetting kinetics is mostly controlled by the kinetics of convective transport of Triton X-100 molecules to the wetting frontier.

The mass balance for surfactants in a partially wetted pore, including both the feed solution and the wetted PVDF surface, is expressed by equation 4.6.

$$vc_0 t\pi R^2 = \int_0^{l(t)} [\tau_{max} 2\pi R(1-\varepsilon) + c(x)\pi R^2] dx \tag{4.6}$$

where $c_0$ is the concentration of Triton X-100 in the bulk solution outside the membrane pore, and $v$ is the convective flow velocity, which is approximately equal to vapor flux, $J$, divided by porosity, $\varepsilon$ (i.e. $v = J/\varepsilon$). Specifically, the term on the left-hand-side represents the total amount of Triton X-100 entering the pore from time zero to $t$, considering only convection. The first part of the integral on the right-hand-side quantifies the amount of Triton X-100 adsorbed onto the pore surface that has been already wetted, with the factor $1-\varepsilon$ accounting for the fact that a typical pore wall (except for those in a track-etched membrane) is fragmented in the axial direction and membrane porosity is assumed to be isotropic. The second part of the integral represents the amount of Triton X-100 in the aqueous solution in the partially wetted pore. According to previous literature[211,212], $\tau_{max}$ is estimated to be $3\times10^{-6}$ mole $m^{-2}$ for Triton X-100 adsorption on PVDF, rendering the second term in the integral negligible compared to the first term. Therefore, equation 4.6 can be simplified as

$$l(t) \approx \frac{r}{2\varepsilon(1-\varepsilon)\tau_{max}} J c_0 t \tag{4.7}$$

Equation 4.7 suggests that for given membrane and surfactant, in which case $r$, $\varepsilon$, and $\tau_{max}$ are constant, the kinetic rate of wetting frontier propagation is proportional to the feed surfactant concentration, $c_0$, and to vapor flux, $J$. Remarkably, equation 4.7 also implies that the kinetics of wetting does not depend on $\Delta P$, except when $\Delta P$ is too high that it exceeds the LEP of surfactant-free feed solution. These unique dependences of wetting kinetics on $c_0$, $J$, and $\Delta P$ can be readily and reliably tested using MD experiments.

## 4.3. Materials and Methods

### *4.3.1. Materials*

The hydrophobic PVDF membrane with a nominal pores size of 0.45 µm was purchased from GE Healthcare (Pittsburg, PA). Sodium chloride (NaCl), Triton X-100, and ethanol (200 proof) were all procured from Sigma Aldrich (St. Louis, MO) and used without further purification.

### *4.3.2. Surface tension Measurements*

The surface tensions of aqueous NaCl solution (0.6 M) with different concentrations of ethanol and Triton X-100 were measured at 60 °C by analyzing the shape of a submerged air bubble in a given solution using an optical tensiometer (TL100, Attension, Finland) with drop shape analysis software[213–215]. Additionally, the surface tensions of 50 ppm Triton X-100 in NaCl aqueous solutions at temperatures of 50, 60, and 70 °C were also measured.

### *4.3.3. Principle and experimental setup of impedance-based wetting monitoring*

In an MD process, the pores in the microporous membrane have three possible wetting states: the non-wetted state, the transition state, and the wetted state (Figure 4.2a). In the non-wetted state, the membrane pores are fully filled with air[23]. According to literature[187,188], the air-filled microporous membrane can be modeled as a parallel circuit of a resistor and a capacitor when considering its impedance. Specifically, the polymeric membrane material and the air-filled pores between the two liquid –air interfaces constitute the resistor and the capacitor, respectively.

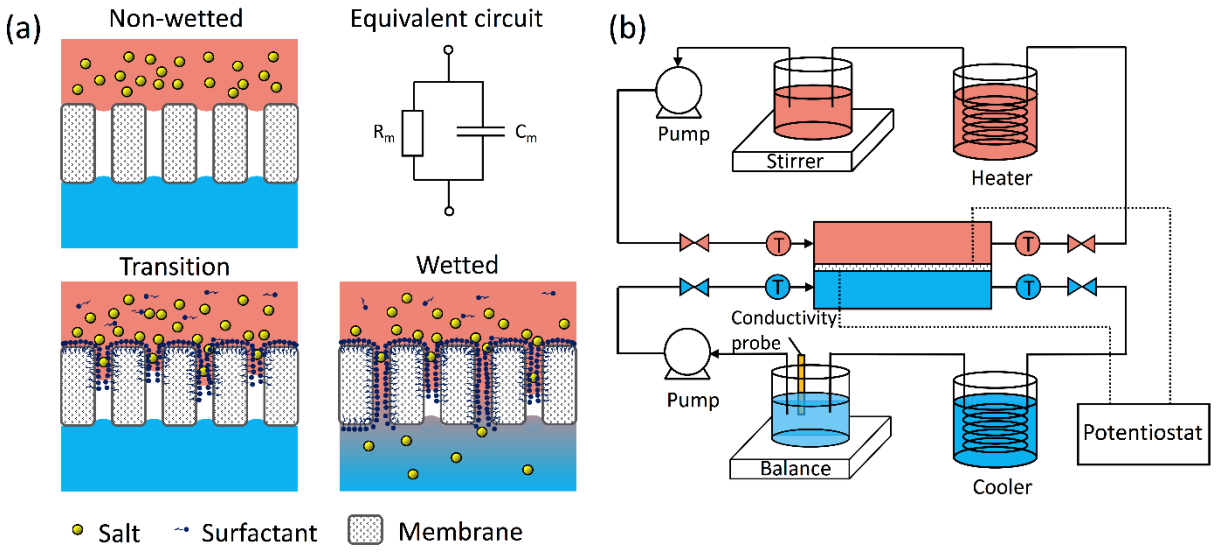


Figure 4.2 (a) Illustration of the possible membrane pore wetting mechanism and corresponding working principle for impedance-based monitoring. The equivalent circuit only captures the region of the MD membrane with air pockets and does not consider contributions to impedance at and outside the membrane-solution interfaces. (b) A schematic of a DCMD system equipped in-situ impedance measurements capability.

In the presence of surfactant molecules in the feed solution, the feed solution can partially penetrate the air-filled pores (i.e. the transition state). This partial penetration of the feed solution decreases the average distance between the two liquid-air interfaces, or the thickness of the air-gap within the pores, which consequently increases the capacitance of the air pocket and reduces the resistance of the polymeric membrane, both leading to a reduction of the overall system impedance (at a given frequency). If such a picture of partial wetting without pore breakthrough is true, one should expect the observation of reduced impedance but no change in distillate salinity, as the pores have not yet been penetrated to become available channels for direct liquid permeation of the feed solution.

As surfactant-induced wetting proceeds further, some membrane pores are eventually fully penetrated (i.e. the wetted state)[23], in which case the salt in the feed solution can freely move through the wetted pores and thereby significantly undermine the salt rejection of the MD process. In this wetted state, the equivalent capacitor is short-circuited by the wicked-through pores, leading to a drastic decrease in the overall impedance. The final system impedance in the wetted state is

expected to be negligible compared to the initial impedance as the resistance due to the wetted pores is negligible compared to the capacitive contribution to the overall impedance.

Following this principle, a DCMD system with the capability of measuring impedance in the wetting experiments is shown in Figure 4.2b. A commercial hydrophobic PVDF membrane coupon of 8 cm × 2.5 cm (GE Health Life Sciences, Pittsburg, PA) was used in this study. The nominal pore size and average thickness of the membrane are 0.45 and 170 μm, respectively. In all DCMD experiments, a 0.6 M NaCl solution was used as the feed solution and deionized water was used as the distillate. The influent temperatures of feed and distillate streams were maintained at 60℃ and 20℃, respectively. The hydraulic pressure of the feed stream was kept higher than that of the distillate stream to facilitate unequivocal detection of membrane pore wetting that will be reflected by the increased salinity of the distillate[44,49,50,216].

A potentiostat (SP-150, BioLogic Science) was coupled with the DCMD system to conduct in-situ measurement of the impedance across the membrane during MD. Two titanium electrodes (1cm × 0.5 cm) were placed in direct contact with the two sides of the MD membrane. To identify a suitable operational frequency for time-resolved impedance measurement, a frequency scan was first conducted in an operating DCMD system. On the basis of the results of the frequency scan, we chose 100 kHz as the operational frequency for measuring time-resolved impedance. (justifications given in Appendix C).

### *4.3.4. MD Wetting Experiments*

For each membrane wetting experiment, the time-resolved impedance and the salt rejection rate of the membrane were both monitored. Cross-membrane impedance at a single-frequency of 100 kHz was measured over time to probe the dynamics of membrane wetting. Real-time salt rejection of the membrane was obtained from real-time water flux and distillate conductivity. Prior to the addition of wetting agent (ethanol or Triton X-100), the system was operated with feed solution (0.6 M NaCl aqueous solution) free of wetting agent for half an hour to establish baselines of flux and impedance. Five different sets of DCMD wetting experiments were conducted. The first set of experiments compared wetting induced by ethanol solution and by Triton X-100 solution with the same surface tension. The second set of experiments was designed to study the impact of transmembrane hydraulic pressure in wetting induced by ethanol. The third and fourth

sets of experiments were performed to investigate the influences of surfactant concentration and vapor flux in membrane wetting induced by Triton X-100, respectively. The last set of experiments was conducted to show the effect of transmembrane hydraulic pressure on surfactant-induced wetting.

When interpreting the measured impedance, the MD membrane can be considered as equivalent to a parallel circuit of a capacitor and a resistor[181,187,188]. At high frequencies, the capacitive contribution dominates the transmembrane admittance (i.e. reciprocal of impedance). Therefore, the impedance is roughly proportional to the thickness of the remaining air gap. The time-resolved transmembrane impedance normalized by the initial transmembrane impedance can thus provide a semi-quantification of the wetting frontier position following equation 4.8 (Appendix C):

$$\frac{Z(t)}{Z_0} = \frac{d_0 - l(t)}{d_0} \tag{4.8}$$

Where, $Z_0$ is the initial transmembrane impedance, $Z(t)$ is the transmembrane impedance at time $t$, $d_0$ is the thickness of the membrane which was 180 μm for the membrane used in this study.

## 4.4. Results and Discussion

### *4.4.1. Triton X-100 vs. ethanol as a wetting agent: drastically different wetting behaviors*

Representative data of transmembrane impedance (red squares) and salt rejection (blue circles) in DCMD wetting experiments with Triton X-100 or ethanol as wetting agent are shown in Figure 4.3.

Before the addition of Triton X-100, both constant impedance and perfect salt rejection were observed (Figure 4.3a), indicating that the PVDF membrane was in a nonwetted state (Figure 4.2a). Soon after the addition of surfactants, the impedance began to decrease, whereas the salt rejection remained almost perfect until the impedance became negligibly small. This stage marked by decreasing impedance suggests the system to be in a transition state of membrane wetting (Figure 4.2a). In this state, the impedance was constantly reduced as the feed solution–air interface gradually propagated toward the distillate. However, because the membrane pores were

not yet wicked through by the feed solution in this transition state, the partially air-filled membrane pores still served as a barrier for direct liquid permeation and maintained a near-perfect salt rejection. In addition, the normalized water flux remained at unity during this transition stage (Figure C.5), again supporting the argument that none of the pores were fully penetrated. Eventually, the feed solution penetrated through some membrane pores, resulting in a noticeable drop in the salt rejection rate. Such a drop in the salt rejection rate, however, was not observed until the impedance became negligibly small. The time difference between the onsets of impedance reduction and salt rejection rate reduction represents the duration of the transition state in a membrane pore wetting process. Even with these surfactant-containing feed solutions of a relatively strong wetting propensity, such a delay was still quite significant (Figure 4.3a). Therefore, this impedance-based technique, capable of capturing the transition state, can be utilized for monitoring the membrane pore wetting kinetics and the membrane pore wetting induced by Triton X-100 was progressive after the addition of Triton X-100 (Figure 4.3a).

For membrane wetting caused by ethanol, the transmembrane impedance and salt rejection rate responded almost simultaneously and the wetting was instantaneous (Figure 4.3b). The wetting occurred so fast that it required almost no time, after the addition of ethanol, for the feed solution to fully wick through the pores.

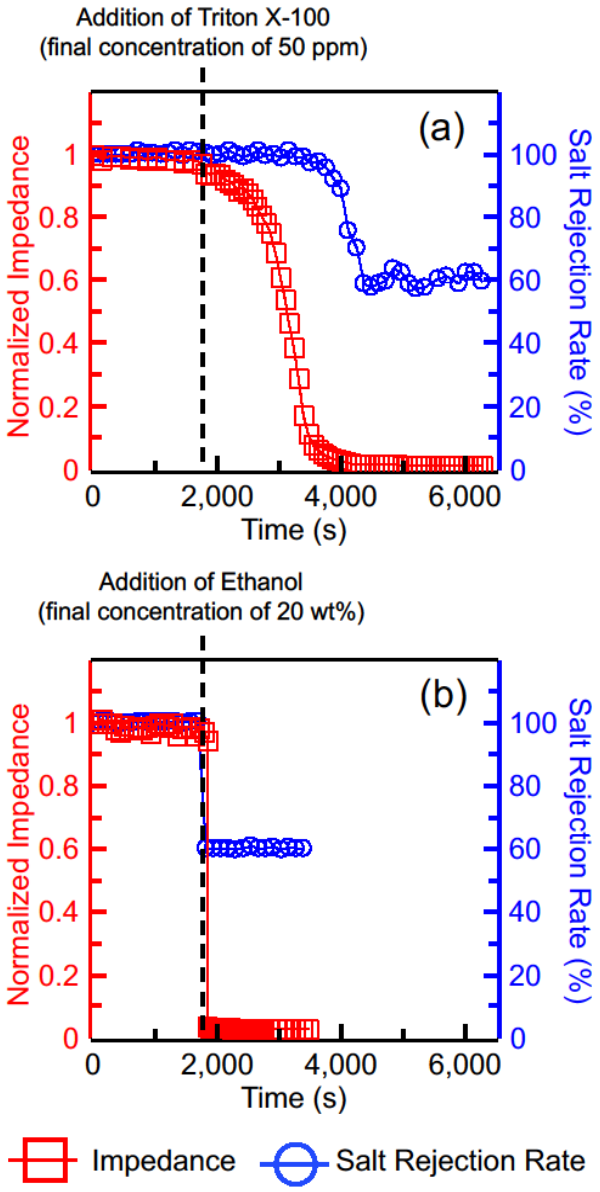


Figure 4.3 Impedance (red squares, left Y-axis) across the PVDF membrane and salt rejection (blue circles, right Y-axis) in DCMD experiments in the presence of (a) 50 ppm Triton X-100 and (b) 20 wt% ethanol solution. The impedances are normalized by the initial impedance (4299 Ohms in panel a, and 4439 Ohms in panel b). In both DCMD experiments, 0.6 M NaCl solution and DI water were used as the feed and distillate streams, respectively. The temperatures of the feed and distillate streams were kept at 60 and 20 °C, respectively. The transmembrane hydraulic pressure was set at 5 kPa. The black dashed line indicates the addition of wetting agent (Triton X-100 in panel a, and ethanol in panel b) to the feed solution, which resulted in a feed solution with surface tension of around 35 mN/m according to the surface tension measurements data (Figure C4 in Appendix C). The water flux data corresponding to the experiments are shown in Figure C5 in Appendix C.

For the two experiments shown in Figure 4.3, the surface tension of the feed solutions after adding Triton X-100 or ethanol were controlled to be approximately the same (~35 mN/m, Appendix C), despite the drastically different wetting behaviors observed. Whereas wetting induced by ethanol was instantaneous, wetting induced by Triton X-100 was gradual and dynamic. The dynamic behavior of surfactant-induced wetting is attributable to the adsorption of Triton X-100 to the membrane pore surface which constantly removes the amphiphilic wetting agent from the wetting frontier and thereby slows down the wetting process. In contrast, because ethanol does not adsorb onto the membrane pore surface (even if it does, adsorption would barely change bulk ethanol concentration which is very large), as long as $\Delta P$ exceeds LEP, pore wetting occurs at a kinetic rate following the Poiseuille flow. Using equation 4.3 with the experimental conditions, the time for complete wetting is estimated to be less than 1 s (Appendix C), which is in accordance with the experimentally observed instantaneity of ethanol-induced wetting.

*4.4.2. Ethanol-induced wetting: a simple application of the general wetting criterion*

When ethanol was employed as the wetting agent, we can simply apply the general wetting criterion given by equation 4.2 using the LEP of the bulk solution: if $\Delta P$ is lower than LEP, membrane wetting does not occur; if $\Delta P$ is higher than LEP, wetting occurs instantly. The experiment shown in Figure 4.3b is an example of inducing wetting via lowering the LEP by reducing the surface tension of the feed solution via adding ethanol. When the surface tension of the feed solution was low enough, LEP became lower than $\Delta P$, which led to instant and complete pore wetting. Alternatively, one can also induce wetting by increasing $\Delta P$ to an extent that it surpasses the LEP of all pores. For example, we conducted an MD wetting experiment with a saline feed solution containing 15 wt% ethanol using different transmembrane hydraulic pressures (Figure 4.4). The results suggest that an MD membrane that was not wetted with $\Delta P = 1$ kPa was immediately fully wetted as soon as $\Delta P$ was raised to 11 kPa. The results on Figure 4.3b and Figure 4.4 both demonstrate that, for ethanol-induced wetting, one can simply determine if wetting can occur using equation 4.2 with the LEP of bulk solution.

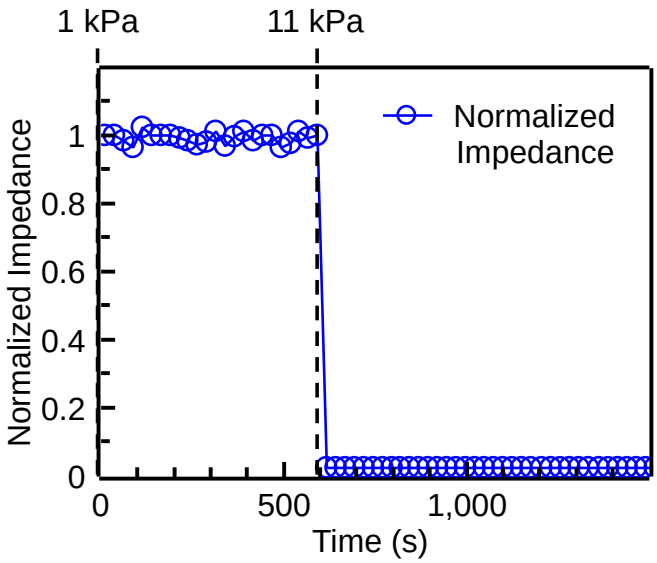


Figure 4.4 Experimentally measured transmembrane impedance with feed solution containing ethanol. The transmembrane hydraulic pressure was changed from 1 kPa (before the dash line) to 11 kPa (at and after the dash line). The impedances are normalized by the initial impedance which was 4854 Ohms. The ethanol concentration of the feed solution was 15 wt%. The temperatures of feed and distillate streams were set at 60 and 20 °C, respectively. The water flux and salt rejection are shown in Figure C.6 in Appendix C.

*4.4.3. Surfactant-induced wetting: a dynamic process limited by surfactant transport*

When surfactants are employed to induce wetting in MD, more complex dynamic wetting occur due to the adsorption of surfactants onto the pore surface. By treating surfactant transport and adsorption as a pseudo-steady-state processes, we have developed a simplified model that describes the kinetics of wetting frontier propagation (equation 4.7) which predicts several key features of surfactant-induced wetting. Here, using Triton X-100 as the model surfactant, we experimentally assess these key features and verify their consistence with the equation 4.7. Specifically, we want to evaluate whether the model summarized in equation 4.7 can, at least qualitatively, predict the impacts of several key factors on the kinetics of surfactant-induced wetting. The kinetics of wetting frontier propagation can be semi-quantitatively approximated by the transmembrane impedance using the following obtained simply by combining equations 4.7 and 4.8:

$$\frac{Z(t)}{Z_0} = 1 - \frac{R}{2\varepsilon(1-\varepsilon)\tau_{max}d_0} J c_0 t \tag{4.9}$$

Equation 4.9 suggests that the rate of impedance decline is proportional to vapor flux, $J$, and the feed concentration of surfactants, $c_0$. It also implies, rather surprisingly, that $\Delta P$, does not have a direct impact on wetting kinetics, which we will elaborate later. While equation 4.9 suggests a linear decline of normalized transmembrane impedance, we note that such linearity results from a highly simplified model with the ideal assumptions that the membrane pores are perfectly cylindrical and of a uniform size and that diffusive contribution to overall surfactant transport is negligible. Because these ideal assumptions, which are required to derive equation 4.9, are most certainly not satiated with any realistic MD membrane, we do not expect to apply equation 4.9 for accurate quantitative prediction of experimental results. Rather, we want to experimentally assess the semi-quatitative dependence of impedance decline rate on critical operating parameters such as $c_0$, $J$ and $\Delta P$.

For wetting experiments with different Triton X-100 concentrations in feed solutions (Figure 4.5a), it was observed that the impedance decline was significantly faster with a feed solution of a higher Triton X-100 concentration (100 ppm, blue squares) than with a feed solution of a lower surfactant concentration (50 ppm, red circles), which is semi-quantitatively consistent with equation 4.9. Based on the developed model, the wetting frontier does not proceed unless its surrounding pore surface has been fully saturated with the adsorbed surfactants. For multiple factors that have been discussed in the model development section, the kinetics of Triton X-100 adsorption around the wetting frontier is limited by how fast the surfactants are replenished via convection from the bulk solution to the wetting frontier. Since the rate of convective transport is primarily determined by $c_0$ and $J$, a higher bulk concentration of surfactants leads to a faster wetting process.

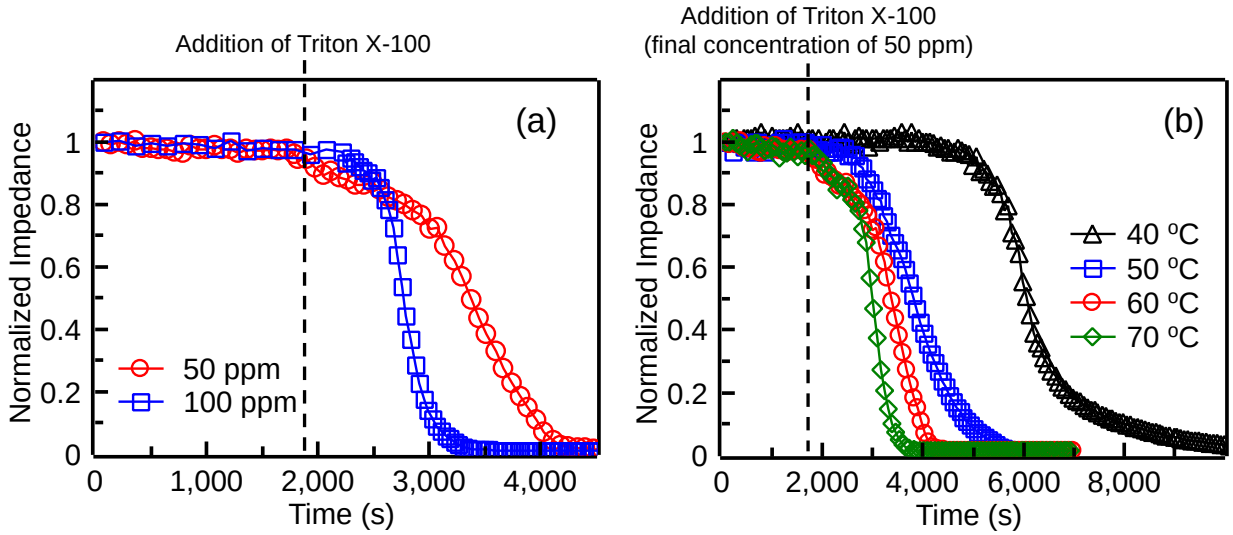


Figure 4.5 (a) Experimentally measured impedances across the PVDF membrane in DCMD experiments in the presence of 50 ppm Triton X-100 (red circles) and 100 ppm Triton X-100 (blue rectangles) in the feed solutions. The impedances are normalized by the initial impedances which were 4299 and 4199 Ohms for experiments with feed solutions containing 50 ppm ethanol and 100 ppm Triton X-100, respectively. The temperatures of feed and distillate streams were kept 60 and 20 °C, respectively. (b) Experimentally measured impedances across the PVDF membrane in DCMD experiments with different fluxes resulting from different feed temperatures. With a constant distillate temperature of 20 °C, the feed temperatures were set at 40°C (black triangles), 50 °C (blue rectangles), 60 °C (red circles) and 70 °C (green diamonds) to yield vapor fluxes of 14.97, 29.95, and 47.13 L $m^{2-}$ $h^{-1}$, respectively. The measured impedances are normalized by the initial impedances which were 5007, 4480, and 3329 Ohms for experiments with feed temperatures of 40°C, 50 °C, 60 °C and 70 °C, respectively. In all panels, the black dash lines indicate the additions of Triton X-100 to the feed solutions. The resulting Triton X-100 concentration was 50 ppm. The transmembrane hydraulic pressure was kept at 5 kPa in all experiments. The water fluxes and salt rejections corresponding to the experiments are shown in Figure C.7 and C.8 in Appendix C.

For the similar reason, the wetting kinetics also positively correlates with vapor flux, $J$ (Fig. 4.5b). To show this, a set of MD wetting experiments were conducted to achieve different vapor fluxes by adjusting feed temperature. Specifically, the measured vapor fluxes with a constant distillate temperature of 20 ºC but different feed temperatures at 40, 50, 60, and 70 °C were 8.60, 14.97, 29.97, and 47.13 L $m^{-2}$ $h^{-1}$, respectively. The experimental results (Fig. 4.5b) shows a positive correlation between vapor flux and wetting kinetics. It is worth noting that changing the temperature from 50 to 70 °C does not significantly affect the surface tension of the feed solution with 50 ppm Triton X-100: the measured surface tensions of the solution are 32.5 ± 0.5, 32.4 ± 0.4, 32.9 ± 0.8, and 32.2 ± 0.9 mN/m at 40 °C, 50 °C, 60 °C, and 70 °C, respectively. Therefore,

the primary impact of feed temperature on the wetting kinetics was realized mostly via the enhanced vapor flux.

One counterintuitive prediction from equation 4.9 is that the rate of surfactant-induced pore wetting is independent of the $\Delta P$. This theoretical prediction is particularly surprising especially considering that the general wetting criterion solely compares the $\Delta P$ with LEP regardless of the chemical nature of the wetting agent. Nonetheless, controlled wetting experiments with all other parameters maintained the same except for different $\Delta P$ yielded results that support the theoretical prediction (Figure 4.6). Pore wetting in experiments with two very different transmembrane pressures (5 and 11 kPa) was both progressive instead of instantaneous, which is characteristic of surfactant-induced wetting, and has remarkably similar kinetics of impedance decline.

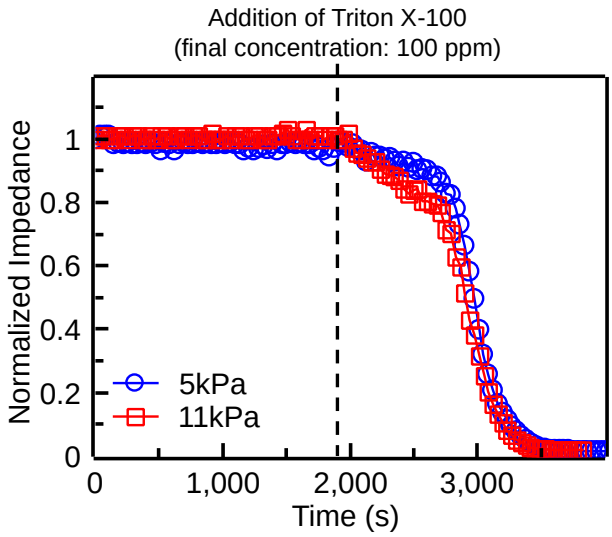


Figure 4.6 Experimentally measured impedances across the PVDF membrane in DCMD experiments with transmembrane hydraulic pressures of 5 kPa (blue circles) and 11 kPa (red rectangles). The impedances are normalized by the initial impedances which were 4270 and 4377 Ohms for experiments with transmembrane pressures of 5 kPa and 11 kPa, respectively. The black dash line indicates the addition of Triton X-100 to the feed solution which yielded a Triton X-100 concentration of 100 ppm. The vapor flux was controlled to be around 30 LMH by adjusting the feed temperatures to account for the different hydrodynamic impacts resulting from having different feed pressures. The vapor flux and salt rejection in these experiments are shown in Figure C.9 in Appendix C.

The insensitivity of wetting kinetics to $\Delta P$ can be interpreted in the following way. Let us apply the general wetting criterion stipulated by equation 4.2 and assume a critical condition that wetting frontier moves forward as long as $\Delta P = LEP$. Here, LEP is defined not based on the property of the bulk feed solution, but rather on the property of the solution at the wetting frontier

which has a surfactant concentration significantly lower than the bulk concentration. Due to the dependence of $\gamma_L$ on surfactant concentration and the dependence of LEP on $\gamma_L$, there exists a specific surfactant concentration at the wetting frontier that corresponds to a specific LEP. Let us define the critical surfactant concentrations at the wetting frontier with which wetting occurs with an $\Delta P$ of 5 kPa and 11 kPa as $c_A'$ and $c_B'$, respectively, with the superscript emphasizing the concentrations are the defined for the wetting frontier but not the bulk solution. From equations 4.1 and 4.2, together with the dependence of $\gamma_L$ on Triton X-100 concentration (Figure C.4b), it can be readily shown that $c_A'$ is significantly lower than $c_B'$. However, the adsorption isotherm given by equation 4.4 suggests that, regardless of the aqueous Triton X-100 concentration (except when it is very close to zero), the equilibrium surface concentration of the adsorbed Triton X-100 should always be roughly equal to the maximum surface concentration, $\tau_{max}$, which can also be mathematically written as

$$\tau(c_A') \approx \tau(c_B') \approx \tau_{max} \tag{4.10}$$

In other words, a lower critical concentration of surfactants at the wetting frontier does not lead to a lower equilibrium surface concentration of the adsorbed surfactants on the pore surface near the wetting frontier. In any case, the aqueous surfactant concentration at the wetting frontier cannot increase to the critical concentration required for forward propagation of the frontier until the surrounding pore surface is almost fully saturated with the adsorbed surfactants. Therefore, the wetting kinetics is eventually controlled by the rate at which pore surface is saturated by the adsorbed surfactants, which is in turn controlled by the rate at which surfactants are transported to wetting frontier via convection. Transmembrane hydraulic pressure has relatively little significance in determining wetting kinetics because it has no impact on neither the convective transport nor the adsorption of surfactants.

The only exceptional scenario in which $\Delta P$ will play a role is when it becomes higher than the LEP of a surfactant-free feed solution (significantly higher than 100 kPa). In this case, $\Delta P$ is always higher than the LEP of the feed solution, regardless of the surfactant concentration at the wetting frontier. Wetting will become instantaneous, similar to ethanol-induced wetting. However, this is a rather trivial scenario in the current context because wetting of such kind is not really induced by surfactants.

## 4.5. Conclusion

Pore wetting is a failure mechanism unique to MD, and at the same time, a technical challenge that limits the applications of MD. Unlike membrane fouling, which is a common failure mechanism across different membrane processes, pore wetting in MD has been understood to a significantly lesser extent. In this study, we develop a novel impedance-based monitoring technique that is able to capture the dynamic membrane pore wetting processes. Furthermore, by implementing this impedance-based technique in DCMD wetting experiments with different wetting agents, we acquire new fundamental insights to understanding MD pore wetting and elucidates the mechanism of surfactant-induced wetting. Specifically, we demonstrate the fundamental difference between wetting induced by surfactants and by alcohols, and show that the two drastically different phenomena share the same simple underlying wetting principle.

Ethanol wetting is instant as long as $\Delta P$ exceeds the LEP. In comparison, surfactant-induced wetting is dynamic, with its kinetic rate strongly dependent on several factors that affect the kinetics of surfactant adsorption to pore surface. Both theoretical model and experimental results suggest that bulk concentration of surfactants and water vapor flux in MD have strong impacts on the wetting kinetics. Notably, a surprising yet justifiable feature of surfactant-induced wetting is that its kinetics are mostly independent of transmembrane hydraulic pressure.

While the current study provides new and mechanistic insights to understanding MD pore wetting, the conclusions from this study may not be universally applicable to all pore wetting phenomena in MD. In particular, compared to pore wetting induced by highly effective wetting agents, pore wetting in many practical MD processes involving mineral scaling or fouling by natural organic matter occurs in much lower rates and may involve different mechanisms. Future work is needed to further elucidate wetting in those more complicated and longer-term scenarios before we can arrive in a comprehensive understanding of pore wetting in MD.

## Supporting Information

See Appendix C.


## Acknowledgement

The authors are grateful to the National Science Foundation for its support via Grants CBET 1705048 and CBET 1739884.

# CHAPTER 5

# KINETIC MODEL FOR SURFACTANT-INDUCED PORE WETTING IN MEMBRANE DISTILLATION

This chapter has been divided into two peer-reviewed manuscripts: the first one has been published on Journal of Membrane Science as "Wang Z., Chen Y., and Lin S., Kinetic Model for Surfactant-Induced Pore Wetting in Membrane Distillation, Journal of Membrane Science **564** (2018), p. 275-288. doi:10. 1016/j.memsci.2018.07.010.", and the other one has been submitted to Desalination as "Wang Z.[1], Chen Y.[1], and Lin S., Surface Excess Concentration of Surfactants Controls the Wetting Kinetics in Membrane Distillation".

## 5.1. Introduction

Membrane distillation (MD) is a membrane-based thermal desalination technology [16,19,87]. In a typical MD process, a microporous hydrophobic membrane is employed to separate a hot salty stream (the feed solution) and a cold salt-free distillate stream. Driven by the partial vapor pressure difference resulting from the temperature difference between the feed and distillate streams, water vapor transports through the membrane pores from the feed stream to the distillate stream. Any non-volatile solute (e.g. salt) is rejected by the hydrophobic membrane. Compared to reverse osmosis (RO), the state-of-the-art desalination technology, MD has several advantages including the capability of treating hypersaline brines, the ability to utilize low grade thermal energy, relatively low capital cost due to the absence of high pressure and high temperature components, and small system footprint that is important to mobile desalination applications[1,13,20,88–92,177,178].

However, large scale practical applications of MD are still limited due to a variety of technical challenges, several of which are related to the use of conventional hydrophobic membranes. In particular, membrane pore wetting is an important technical challenge that is unique to MD (i.e. it does not exist in other membrane processes)[42,180,217,218]. Membrane pore wetting refers to the penetration of feed solution through membrane pores, which in most cases leads to unacceptable salt rejection. Membrane pore wetting can be induced by low-surface-tension liquids (e.g. alcohol), amphiphilic molecules (e.g. surfactants), or other natural surface active agents[40,43–45]. Much effort has been made on developing novel membrane materials and

operating strategies to prevent or mitigate pore wetting in MD, which includes the development of omniphobic membranes[44,48,50,51], composite membranes with a hydrophilic surface layer[52,53], and superhydrophobic membrane coupled with air-layer recharging during operation[43,54].

Interestingly, despite the technological successes in developing wetting prevention measures, the exact mechanism of pore wetting in MD has not been fully understood. Most past studies applied the very simple wetting criterion based on comparing transmembrane pressure and liquid entry pressure[19,133,201]. Some recent studies suggested amphiphilic contaminants can render the membrane surface hydrophilic and thereby induce wetting[181,203]. In a recent study, we showed the fundamental difference between pore wetting induced by alcohol, with which the impact of surface adsorption is negligible, and by surfactants, with which the impact of surface adsorption is significant[219]. It was shown that alcohol-induced wetting was instantaneous whereas surfactant-induced wetting was progressive[208,209]. Our study also suggests that, while the presence of surfactants in feed solution promotes wetting, the adsorption of surfactants onto pore surface does not promote wetting by rendering the pores hydrophilic, but instead deters pore wetting by reducing the surface tension of the feed solution at the liquid-air interface[219]. To accurately describe the kinetics of surfactant-induced wetting, we need to develop a model that accounts for all major mechanisms for mass transport of surfactants into the membrane pores, which has never been reported in literature.

In addition, it has been reported in literature that different types of surfactants have very different wetting behaviors in MD[203,220]. Specifically, different surfactants at the same molar concentration can result in very different wetting kinetics. Such difference in wetting behavior was attributed to the different hydrophilic-lipophilic balance (HLB) which is one of the most important parameters for a surfactant. HLB quantifies to what degree a surfactant is hydrophilic or lipophilic and thus dictates its partition between water and oil. However, the adsorption of amphiphilic molecules onto a hydrophobic surface is energetically highly favorable and should thus be controlled by the rate of surfactant transport. In other words, even though strength of the interaction between surfactants and hydrophobic pore surface may vary depending on HLB, it should have negligible impact on the adsorption kinetics, because the adsorption is limited by transport in the absence of energy barrier. An analogous scenario can be found in colloidal aggregation or deposition, whereas the strength of particle-particle or particle-surface interaction is relevant only

if an energy barrier exists[221]. When the energy barrier is eliminated, the aggregation or deposition kinetics become diffusion limited. Based on this argument, the kinetics of wetting should have little direct correlation with HLB.

In this study, we investigate the kinetics of pore wetting in MD with feed solutions containing surfactants. We first develop a theoretical model to predict the kinetic rate of wetting frontier propagation in a progressively wetted membrane pore. This model is based on three major assumptions including force equilibrium at the liquid-air interface, pseudo-steady state transport of surfactants, and pseudo-equilibrium surfactant adsorption. This kinetic model accounts for the major transport mechanisms of convection, diffusion, and adsorption of surfactants in a slowly expanding volume of feed solution in a partially wetted pore. We use sodium dodecyl sulfate (SDS) as a model surfactant to validate several key characteristics predicted by the model, and then study the membrane pore wetting induced by different surfactant species with the model.

## 5.2. Theory and Model Development

The widely accepted wetting criterion in an MD process is that the transmembrane hydraulic pressure (ΔP) exceeds the liquid entry pressure, LEP, of the membrane pore (Eq. 5.1)[22,207,222].

$$\Delta P \geq LEP \tag{5.1}$$

By definition, LEP is the minimum pressure for a liquid to enter a pore and can be calculated using with Eq. 5.2.

$$LEP = -\frac{2B\gamma_L \cos\theta}{R} \tag{5.2}$$

where $\gamma_L$ is the surface tension of the feed solution, $\theta$ is the intrinsic contact angle between the feed solution and the membrane surface, $R$ is the equivalent radius of the membrane pore, B is the geometric factor accounting for the non-cylindrical pore geometry ($B = 1$ for cylindrical pore). The presence of surfactants (e.g. SDS) in an aqueous solution reduces both $\gamma_L$ and $\cos\theta$ in Eq. 5.2 and thereby results in a decreased LEP[40,50,202,223]. The LEP decreases as the surfactant concentration increases. We note that transmembrane hydraulic pressure, instead of just the hydraulic pressure of the feed stream, should be used in Eq. 5.1. This is rather counter-intuitive but has been thoroughly explained by Zmievskii[207].

If the SDS concentration in the feed solution is sufficiently high (Fig. 5.1(a)), the corresponding LEP would be lower than ΔP, and the feed solution would enter the membrane pore according to the wetting criterion. As the feed solution intrudes into the membrane pore, the SDS in the feed solution would adsorb onto the hydrophobic surface in the membrane pore. The adsorption causes a decrease of SDS concentration at the wetting frontier and consequently leads to an increased LEP (calculated based on the reduced frontier SDS concentration), which impedes the further progression of wetting frontier in the membrane pore. With the supplement of SDS to the wetting frontier by convection induced by vapor flux and diffusion induced by concentration gradient, the SDS concentration in the wetting frontier could be maintained at a critical concentration ($c^*$) if force balance at the liquid-air interface (i.e. LEP=ΔP at the wetting frontier) is assumed. This force balance assumption is reasonable because a hypothetic Hagan-Poiseuille flow of a force unbalanced water column would take only a fraction of a second to penetrate the pores, which is significantly faster than what have been observed. The force equilibrium at the wetting frontier can be maintained until the SDS concentration at the wetting frontier has to increase beyond $c^*$ when SDS can no longer adsorb onto the pore surface near the wetting frontier due to surface saturation. Because the surface tension of the feed solution at the wetting frontier, which is dependent on $c^*$, and the surface tension of the unwetted pore surface, which is relevant to LEP calculation, are both constant, the static contact angle at the triple phase boundary at the wetting frontier can also be approximated to be constant.

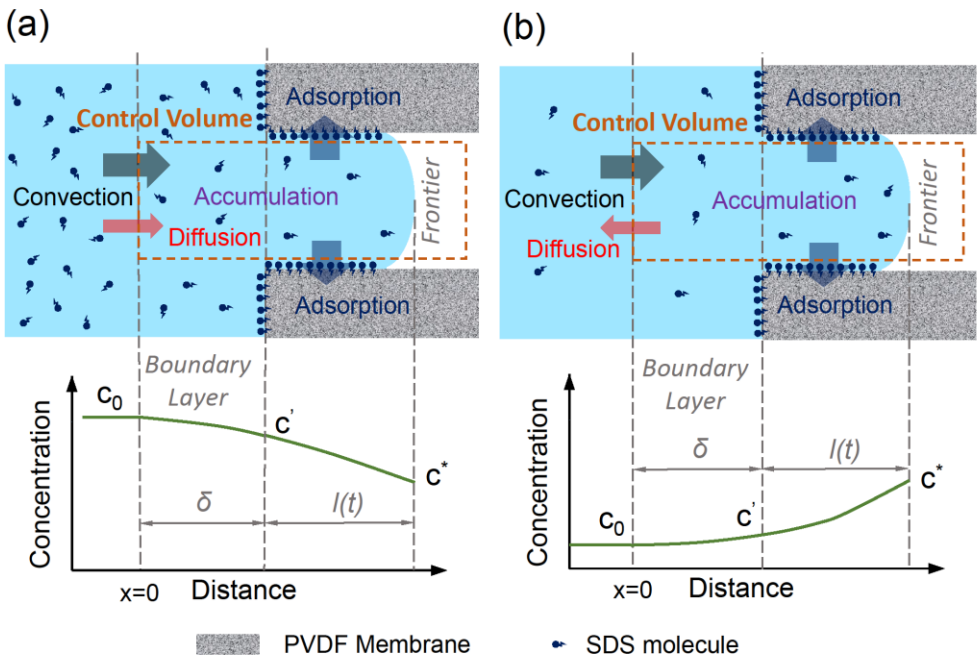


Figure 5.1 Schematics of a cylindrical pore wetting by SDS at (a) a high concentration and (b) low concentration, respectively. In both scenarios, for the SDS solution to enter the membrane pore, the SDS concentration in the solution frontier must reach the critical concentration $c^*$ (corresponding to LEP=ΔP). Once the SDS solution enters the membrane pore, within a control volume (orange dash rectangle) consisting of the solution inside the membrane pore and the boundary layer outside the membrane pore, the mass balance of SDS can be performed considering SDS transports via convection, diffusion, accumulation (in the solution) and adsorption. The distinction between (a) and (b) is the concentration profile of SDS in the control volume (green lines). SDS diffuses into and out of the control volume in (a) and (b), respectively.

For the feed solution with SDS at a low concentration, the LEP corresponding to the bulk SDS concentration may be higher than ΔP, which may suggest that pore intrusion should not occur. However, the SDS concentration at the pore entrance (i.e. the feed/membrane interface) can be significantly higher than the bulk concentration due to concentration polarization (CP)[136,224]. If the elevated SDS concentration reaches the critical concentration ($c^*$), the feed solution is able to enter the membrane pore. Once in the pore, the SDS can adsorb onto the pore surface. The sole effect of adsorption is to reduce the SDS concentration and thus the liquid surface tension at the wetting frontier, not to change the pore surface tension used in LEP calculation. On the other hand, convective transport of SDS tends to increase the SDS concentration at the wetting frontier. These two effects of convective transport and surface adsorption are exactly the same as in the case with high bulk concentration of SDS described in the last paragraph. However, with low bulk

concentration of SDS, the direction of diffusion along the pore is opposite to that when the bulk concentration of SDS is high. In another word, diffusion tends to reduce the SDS concentration at the wetting frontier when the bulk SDS concentration is low. The concentration profile of SDS in the case of low bulk SDS concentration is illustrated in Fig. 5.1b.

Regardless of the SDS concentration in the feed solution, the transport of SDS within an ideal cylindrical pore can be described by Eq. 5.3 that is derived based on the mass balance of SDS in a control volume including the solution in the boundary layer and the partially wetted membrane pore (Fig. 5.1):

$$\begin{aligned}\left(\mathrm{J_w c_0} - \mathrm{D}\frac{\partial \mathrm{c(x,t)}}{\partial \mathrm{x}}_{\mathrm{x=0}}\right)\mathrm{dt} \\ = \int_0^{\delta_b}[\mathrm{c(x,t+dt)} - \mathrm{c(x,t)}]\mathrm{dx} \\ + \varepsilon\left\{\int_{\delta_b}^{\delta_b+\mathrm{l(t+dt)}}\left[\frac{2}{R}\tau(\mathrm{x,t+dt})(1-\varepsilon) + \mathrm{c(x,t+dt)}\right]\mathrm{dx}\right. \\ \left. - \int_{\delta_b}^{\delta_b+\mathrm{l(t)}}\left[\frac{2}{R}\tau(\mathrm{x,t})(1-\varepsilon) + \mathrm{c(x,t)}\right]\mathrm{dx}\right\}\end{aligned} \tag{5.3}$$

where $\mathrm{J_w}$ is the vapor flux in MD, $\varepsilon$ is the porosity of the membrane ($\varepsilon = 0.6$ in our simulation), $\mathrm{c_0}$ is the SDS concentration in bulk solution, t is time, R is the radius of the ideal cylindrical pore, D is the diffusion coefficient of the SDS ($\mathrm{D} = 7.3\times10^{-10}\ \mathrm{m^2/s}$ according to literatures[225]), x is the position of a certain point from the starting point of the boundary layer (x=0, see Fig.1) in the direction pointing from the feed solution to the distillate, $\mathrm{c(x,t)}$ is the SDS concentration at position "x" and time "t", $\delta_b$ is the thickness of the boundary layer (estimated to be 15 μm based on Sherwood correlation and the flow conditions [136,224,226]), $\mathrm{l(t)}$ is distance between the pore entrance and the wetting frontier, $\tau(\mathrm{x,t})$ is the surface density of SDS adsorbed on the pore surface at position x, and time t. The left-hand-side of Eq. 5.3 represents the amount of SDS entering the control volume in the period from time $t$ to $t + dt$, with the first and second terms representing the convective and diffusive components to the flux at the entrance of the membrane pores, respectively. The right-hand-side of Eq. 5.3 represents increase of the total amount of SDS in the

control volume within that time period. More detailed explanation of the development of Eq. 5.3 is given in Appendix D. We note that the control volume as defined is expanding over time as the wetting frontier moves deeper into the pore.

Our ultimate goal of solving Eq. 5.3 is to identify $l(t)$, which quantifies the kinetics of wetting frontier propagation. Solving Eq. 5.3 requires the relationship between $\tau(x,t)$ and $c(x,t)$ which is described by the adsorption isotherm. The simplest adsorption isotherm is the stepwise adsorption isotherm:

$$\tau(x,t) = \begin{cases} \tau_{max}, & c(x,t) > 0 \\ 0, & c(x,t) = 0 \end{cases} \tag{5.4}$$

where $\tau_{max}$ is the maximum surface adsorption density of SDS on polyvinylidene fluoride (PVDF) surface (~$10 \times 10^{-6}$ mole $m^{-2}$ according to literature[227]). The stepwise adsorption isotherm is a valid approximation of Langmuir adsorption isotherm for SDS adsorption onto PVDF membrane surface as justified in Appendix D. With the assumption of stepwise adsorption isotherm, the surface of the wetted pores has $\tau_{max}$ everywhere except for the negligibly small differential area at the wetting frontier.

Finding $l(t)$ from Eq. 5.3 also requires the knowledge of $c(x,t)$, which is described by the convection-diffusion equation in the boundary layer (Eq. 5.5) and by the convection-diffusion-adsorption equation within the pore (Eq. 5.6):

$$\frac{\partial c(x,t)}{\partial t} = -J_w \frac{\partial c(x,t)}{\partial x} + D \frac{\partial^2 c(x,t)}{\partial x^2} \text{ (for } 0 \le x \le \delta_b) \tag{5.5}$$

$$\frac{\partial c(x,t)}{\partial t} = -\frac{J_w}{\varepsilon} \frac{\partial c(x,t)}{\partial x} + D \frac{\partial^2 c(x,t)}{\partial x^2} - \frac{2}{R} \frac{\partial \tau}{\partial t} \text{ (for } \delta \le x \le \delta_b + l(t)) \tag{5.6}$$

The initial condition of these two equations is $c(x,0) = 0$ except for $c(0,0) = c_0$. The two boundary conditions are $c(0,t) = c_0$, and $c(\delta_b + l(t), t) = c^*$, respectively.

The challenge for solving Eqs. 5.5 and 5.6 is the moving boundary of the feed solution with in the pore (i.e. $l(t)$ is a function of t). To overcome this problem, we assume a pseudo-steady state for SDS transport at any moment (i.e. $\partial c/\partial t \approx 0$). This is a reasonable approximation because the time scale for wetting frontier propagation is significantly larger than the relevant time scale for surfactant transport. With the pseudo-steady assumption, Eqs. 5.5 and 5.6 can now be rewritten as:

$$0 = -J_w \frac{dc}{dx} + D\frac{d^2c}{dx^2} \text{ (for } 0 \le x \le \delta_b) \tag{5.7}$$

$$0 = -\frac{J_w}{\varepsilon}\frac{dc}{dx} + D\frac{d^2c}{dx^2} \text{ (for } \delta_b \le x \le \delta_b + l(t)) \tag{5.8}$$

with the boundary conditions being $c(0) = c_0$, and $c(\delta_b + l(t)) = c^*$, respectively.

We note that Eqs. 5.7 and 5.8 are similar to the equations describing the concentration polarization (CP) phenomenon in forward osmosis, FO[228–230]. Specifically, Eq. 5.7 accounts for CP in the boundary layer, which is the analogous to external concentration polarization (ECP) in FO; whereas Eq. 5.8 accounts for CP within the membrane pore, which is equivalent to internal concentration polarization (ICP) in FO. Analytical solutions of Eqs. 5.7 and 5.8 are available and presented as Eqs. 5.9 and 5.10 for the boundary layer and the wetted region within the pore, respectively:

$$c(x) = \frac{(1-\varepsilon)\exp\left(\frac{J_w\delta_b}{D}\right)c_0 + \varepsilon\exp\left[\frac{J_w}{D}\left(\delta_b + \frac{l(t)}{\varepsilon}\right)\right]c_0 - c^*}{(1-\varepsilon)\exp\left(\frac{J_w\delta_b}{D}\right) + \varepsilon\exp\left[\frac{J_w}{D}\left(\delta_b + \frac{l(t)}{\varepsilon}\right)\right] - 1} + \frac{c^* - c_0}{(1-\varepsilon)\exp\left(\frac{J_w\delta_b}{D}\right) + \varepsilon\exp\left[\frac{J_w}{D}\left(\delta_b + \frac{l(t)}{\varepsilon}\right)\right] - 1}\exp\left(\frac{J_w x}{D}\right) \tag{5.9}$$

$$\text{(for } 0 \le x \le \delta_b)$$

$$c(x) = \frac{c^*\left[(1-\varepsilon)\exp\left(\frac{J_w\delta_b}{D}\right)-1\right]+\varepsilon c_0\exp\left[\frac{J_w}{D}\left(\delta_b+\frac{l(t)}{\varepsilon}\right)\right]}{(1-\varepsilon)\exp\left(\frac{J_w\delta_b}{D}\right)+\varepsilon\exp\left[\frac{J_w}{D}\left(\delta_b+\frac{l(t)}{\varepsilon}\right)\right]-1} + \frac{\varepsilon\exp\left(\frac{J_w\delta_b}{D}\right)(c^*-c_0)}{(1-\varepsilon)\exp\left(\frac{J_w\delta_b}{D}\right)+\varepsilon\exp\left[\frac{J_w}{D}\left(\delta_b+\frac{l(t)}{\varepsilon}\right)\right]-1}\exp\left(J_w\frac{x-\delta_b}{D\varepsilon}\right) \quad (5.10)$$

$$(\text{for } \delta_b \le x \le \delta_b + l(t))$$

Given the position of wetting frontier as quantified by $l(t)$, the SDS concentration profile can be obtained using Eqs. 5.9 and 5.10. Inserting the spatial distributions of solution concentration of SDS, $c(x)$, at time $t$ and $t + dt$, into Eq. 5.3 allows us to perform a numerical evaluation of the differential time, $dt$, that is required for the wetting frontier to move forward by a differential distance, $dl$. Numerical integration of $dl$ from 0 to $\delta_m$, with $\delta_m$ being the membrane thickness (180 μm for the membrane tested), yields the time required for the feed solution to fully penetrate a cylindrical pore after the introduction of surfactants into the feed solution. We define this as the wetting breakthrough time, $t_{\text{wetting}}$.

## 5.3. Materials and Methods

Direct contact membrane distillation (DCMD) experiments were performed to validate the results simulated using the model presented in Section 5.2. Here, we provide relevant information regarding these experiments.

### *5.3.1. Materials and Chemicals*

The hydrophobic PVDF membrane with a nominal pore size of 0.45 μm and a thickness of 180 μm was procured from GE Healthcare (Pittsburgh, PA). Sodium chloride (NaCl), SDS, and Triton X-100 were all purchased from Sigma Aldrich (St. Louis, MO) and used without further purification. Sodium chloride (NaCl) and different types of surfactants, including SDS, sodium dodecylbenzenesulfonate (SDBS), Triton X-100, Cetrimonium bromide (CTAB), Tween 20,

Tween 85, and Span 20 were all purchased from Sigma Aldrich and used without further purification.

### *5.3.2. Surface tension measurements*

The surface tensions of aqueous NaCl solutions (0.6 M) containing different concentrations of SDS were measured at 60 °C using drop shape analysis of air bubbles in respective solutions by an optical tensiometer (TL100, Attension Finland). The surface tensions of NaCl solution (0.6 M) with 0.5 mM SDS at different temperatures from 35 to 70 °C were also measured using the same method. For each solution, the reported surface tension is the average of five different measurements.

The surface tension of NaCl aqueous solutions with different types of surfactants at different concentrations were evaluated by analyzing the shape of reverse pendant drops using an optical tensiometer (TL100, Attention, Finland). Specifically, an air bubble was extruded into the solution using a submerged micro-syringe and stayed attached to the micro-syringe tip. The shape of the air bubble was analyzed using the built-in software of the instrument to obtain the surface tension of the solutions. All measurements were conducted at 60 °C which was the feed temperature for the MD experiments. In almost all cases, the NaCl concentration was maintained at 0.6 M which was the feed concentration in the MD experiments. An additional concentration of 0.3 M was also used for measuring the surface tensions of SDBS for investigating the impact of ionic strength which also has a strong impact on surface tension. Five measurements were performed for each set of conditions and the mean values were reported with standard deviations.

### *5.3.3. Intrinsic contact angle measurements*

The direct measurements of contact angle (CA) using PVDF membranes cannot yield relevant information that can be used for calculating LEP based on Eq. 5.2. This is because the CA in Eq. 5.2 is the intrinsic CA which can only be measured using a smooth and non-porous surface, as otherwise the system would be in a Cassie-Baxter state and yield a CA that is significantly higher than the intrinsic CA. Therefore, a smooth and non-porous PVDF film was fabricated by first melting the PVDF membrane at 200 °C and then cooling it at room temperature. The roughness of the reconstructed PVDF film was measured by atomic force microscopy (AFM, Dimension ICON,

Bruker, Billerica, MA). With the reconstructed PVDF film, the intrinsic CA between the PVDF membrane and the given solutions were measured using captive bubble method. For each SDS concentration, CA measurements were conducted at 5 different positions on the reconstructed PVDF film and the average and standard deviation of the measurements are reported.

*5.3.4. Determination of LEP*

With the surface tension of the feed solution and intrinsic CA of the feed solution on the reconstructed PVDF film, we use Eq. 5.2 to calculate the LEP for each feed solution assuming perfect cylindrical pores (B=1) with a pore radius of $R = 0.225$ μm. We note that due to fast adsorption of surfactants in membrane pores, LEP cannot be accurately determined using conventional experimental protocol[97,122] because the properties of the wetting frontier differ significantly from those of the bulk solution. We also note that the calculated LEP based on measured parameters and Eq. 5.2 is merely an estimation due to the simplifying assumption of ideal cylindrical pore.

*5.3.5. Surface excess concentration*

The accurate experimental determination of $\tau_{max}$ for a given surfactant on PVDF surface, or on any other solid surface, is practically rather challenging. However, there is another readily assessible parameters that can be used as a proxy of $\tau_{max}$, which is the surface excess concentration, $\Gamma$ [231,232]. By definition, $\Gamma$ is the areal concentration of a surfactant at the air-water interface. Surface excess concentration is numerically similar to $\tau_{max}$ for PVDF given that both air and PVDF are sufficiently hydrophobic so that adsorption of surfactants onto the liquid-air interface and the liquid-solid interface is energetically highly favorable in both cases. The accurate estimation of $\Gamma$ can be readily performed by measuring the surface tension of the solutions with different concentrations of surfactant and applying the Gibbs adsorption equation [233,234]:

$$\Gamma = -\frac{1}{RT}\frac{\partial \gamma}{\partial lnC} \qquad (5.11)$$

where $\gamma$ is the surface tension of the liquid, $C$ is the molar concentration of the surfactant, $R$ is the ideal gas constant, $T$ is the temperature (333K in our experiments).

*5.3.6. DCMD wetting experiments*

The membrane wetting experiments were conducted with a standard DCMD experimental setup that was described in detail in our previous studies[235,236]. The feed solution was 0.6 M NaCl aqueous solution with SDS, whereas deionized water was utilized as permeate stream. Both the vapor flux and the conductivity of the permeate stream were continually monitored and recorded with a time interval of 1 min. The real-time salt rejection of the membrane was calculated using the monitored vapor flux and conductivity data. Without wetting, the salt rejection of the PVDF membrane is always above 99.9%. In this study, we quantify the kinetic rate of pore wetting by measuring the breakthrough time, $t_{\text{wetting}}$. The breakthrough moment is defined as the point at which a small portion of membrane pores have already been fully penetrated by the feed solution. To be consistent between experiments, we arbitrarily set the time when salt rejection dropped to 99% as the breakthrough moment.

In each experiment, prior to the addition of SDS to induce membrane wetting, the system was operated for half an hour to establish a stable baseline of vapor flux. Three different sets of wetting experiments were performed for the purposes of studying the impacts of three parameters on membrane wetting process. These three parameters include bulk concentration of SDS in feed solution, vapor flux, and transmembrane hydraulic pressure, respectively. In each set of experiments, only the target parameter under investigation was varied, while the other two parameters were maintained constant. The detailed experimental conditions are given in the following discussion section and also summarized in Table D1 in Appendix D. The experimental results shown in the figures from section 5.4.1 to 5.4.3 are marked with an experimental number that can be referred to Table D1.

Comparative DCMD wetting experiments with different surfactant species were carried out using commercial PVDF membrane with a dimension of 8 cm × 2.5 cm. For each surfactant species, 0.6 M NaCl solution and deionized water were used as feed solution and distillate, respectively. For SDBS, an additional set of experiments were performed with a NaCl concentration of 0.3 M. The temperatures of the feed solution and distillate were maintained at 60 and 20 °C, respectively, which resulted in vapor fluxes in a range of 30.5±1.2 L $m^{-2}$ $hr^{-1}$. Before the addition of surfactants, the system was operated for 10 minutes to develop a stable baseline for vapor flux. The dosing of surfactants resulted in a surfactant concentration of 0.3 mM in the feed

solution. During the entire experiment, the mass and conductivity of permeate solution were constantly monitored to determine the water (vapor) flux and salt rejection. To quantify the kinetics of pore wetting, we measured the breakthrough time defined as the time from the addition of surfactant to the point when the salt rejection dropped to 99%. Three replicate experiments were performed for each set of experimental conditions and the experimental results were reported as average values with error bars.

## 5.4. Results and Discussion

### *5.4.1. The impact of SDS concentration*

The model predictions for DCMD membrane wetting with different bulk concentrations of SDS, $c_0$, are remarkably consistent with the experimental data (Fig. 5.2). In general, a higher $c_0$ results in a shorter $t_{\text{wetting}}$. Based on the mass transfer model elaborated in section 5.2, the kinetics of forward propagation of wetting frontier largely depends on how fast the pore surface is saturated by SDS adsorption, which in turn depends on how fast the SDS molecules are transported from the bulk solution to the wetting frontier. When water flux, $J_w$, is constant, a higher $c_0$ enhances both the convective and diffusive transport of SDS to the wetting frontier (when $c_0 < c^*$, a higher $c_0$ deters the back diffusion), which leads to faster pore wetting as indicated by Fig. 5.2.

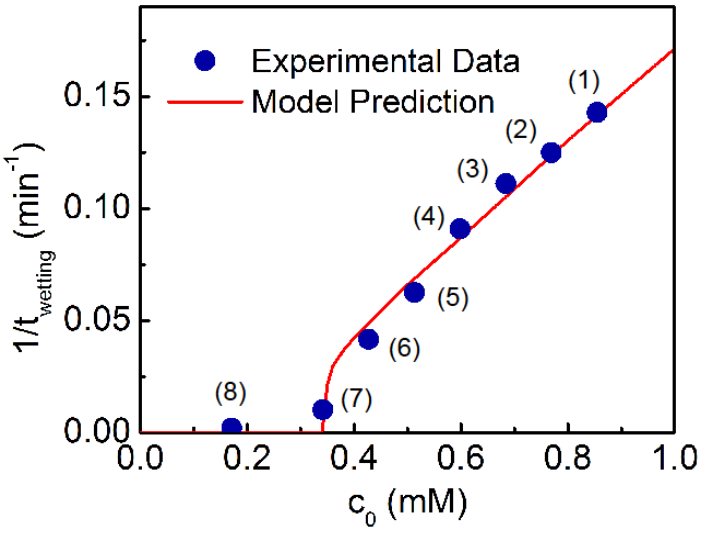


Figure 5.2 Experimental results (blue circles) and model prediction (red line) of MD membrane wetting time with different SDS concentrations in feed solution. For the DCMD wetting

experiments, different SDS concentrations $c_0$ ranging from 0.17 to 0.85 mM were evaluated. All other experimental conditions are maintained constant except for $c_0$. Specifically, the feed and permeate solution temperatures were maintained at 60 and 20 °C, respectively, which resulted in a constant vapor water flux $J_w$ at 32.3 ± 0.9 L $m^{-2}$ $h^{-1}$ prior to the addition of SDS. The transmembrane hydraulic pressure ΔP was maintained at 6 kPa. The time series of water flux and salt rejection for DCMD wetting experiments are given in Fig. A1 in Appendix D. For the simulation, the $c_0$ and $J_w$ are based the experimental conditions, and the critical SDS concentration $c^*$ in the wetting frontier is assumed to be 0.42 mM which corresponds to an LEP of 6 kPa.

Fig. 5.2 also suggests that when $c_0$ was lower than a critical bulk concentration $c_0'$ (~0.35 mM), the membrane was not wetted by the feed solution, which can also be explained by the wetting model. For the feed solution to enter the membrane pore, the SDS concentration at the pore entrance must at least equal the critical SDS concentration $c^*$ (0.42 mM for $\Delta P = 6$ kPa) so that ΔP is higher than LEP calculated using the concentration at the pore entrance. If the bulk concentration, $c_0$, is too low, the concentration at the pore entrance cannot exceed $c^*$ even considering the effect of external concentration polarization (ECP), in which case the feed solution cannot even enter the pores. This critical bulk concentration $c_0'$ below which feed solution cannot enter membrane pore can be determined based on the equation that describes ECP:

$$c_0' = c^* \exp\left(-\frac{J_w \delta_b}{D}\right) \tag{5.12}$$

*5.4.2. The impact of vapor flux*

When flux is increased, convective transport of SDS to the wetting frontier is faster, which in turn accelerates the saturation of the pore surface by SDS and thus the forward propagation of the wetting frontier. Such an effect of vapor flux on wetting kinetics is consistently observed from both experimental data and model simulation (Fig. 5.3). Specifically, Fig. 5.3 suggests that $1/t_{wetting}$ is a linear function of vapor flux, i.e., the wetting time is roughly inversely proportional to vapor flux. We note that the surface tension of the feed solution did not change much with temperature varying from 35 to 70 °C as indicated by experimental measured surface tensions (in this temperature window) that all fall into the range of 32.4±3.5 mN/m.

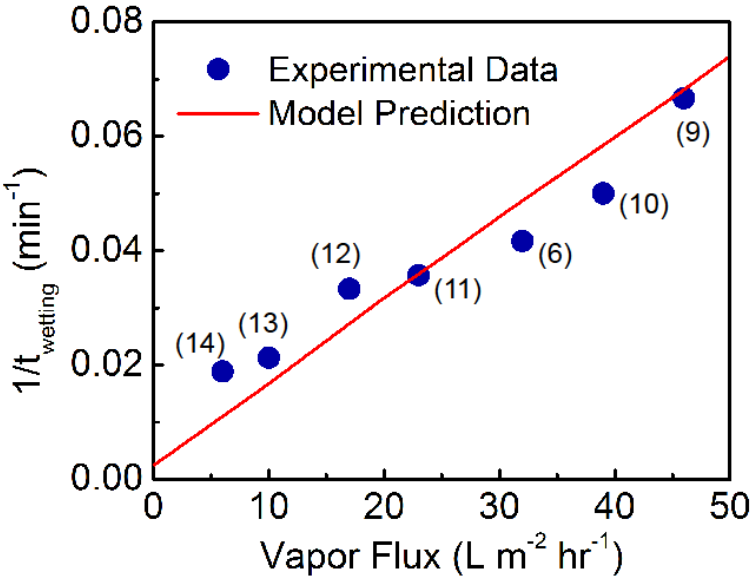


Figure 5.3 Experimental results (blue circles) and model prediction (red line) of MD membrane wetting at different vapor fluxes. In the DCMD wetting experiments, the permeate solution temperature was maintained at 20 °C, whereas the feed solution temperatures varied from 35 to 70 °C, which resulted in varied vapor water flux $J_w$ from 6.0 to 45.8 L $m^{-2}$ $h^{-1}$. Except for the feed solution temperature, all experimental conditions are maintained the same. Specifically, the SDS concentration $c_0$ of the feed solution was 0.43 mM, and the transmembrane hydraulic pressure ΔP was 6 kPa. The detailed water flux and salt rejection rate data for DCMD wetting experiments were shown in Figure D.2 in Appendix D. For model simulation, $c_0$ and $J_w$ are based on the experimental conditions, and the critical SDS concentration $c^*$ in the wetting frontier is assumed to be 0.42 mM which corresponds to an LEP of 6 kPa.

The simulated the "$1/t_{wetting}$ vs. flux" line does not pass the origin, which suggests that wetting can still occur with zero vapor flux, although it takes a very long breakthrough time. Wetting can occur in the absence of vapor flux due to transport of SDS to the wetting frontier via diffusion, if the bulk surfactant concentration is sufficiently high. However, in the case described by Fig. 5.3, we can conclude that vapor flux induced convective transport has a dominant effect on the overall SDS transport as long as the flux is not too low.

### *5.4.3. The impact of transmembrane hydraulic pressure*

In addition to the influences of surfactant concentration and vapor flux, the impact of transmembrane hydraulic pressure, ΔP, was also investigated. As described in section 5.2, the system is considered to be always in a force balance described by the continuous equality between

$\Delta P$ and $LEP$. Because $LEP$ is a function of $\gamma_L \cos\theta$ (we do not separate $\gamma_L$ and $\cos\theta$, because $\theta$ is dependent on $\gamma_L$, anyway) which is in turn a function of surfactant concentration, each $\Delta P$ corresponds to a critical surfactant concentration, $c^*$, at the wetting frontier. With the force balance condition ($LEP = \Delta P$), the impact of $\Delta P$ is eventually exerted via the corresponding $c^*$ that serves as the boundary condition for solving the pseudo-steady state surfactant transport equation (Eq. 5.8).

We note that for a given $\Delta P$, $c^*$ is dependent on the surfactant species, salt composition, and surface tension of the pore surface, which all have significant influence on $\gamma_L \cos\theta$ (as a function of surfactant concentration), and on pore geometry, which also has a strong impact on LEP. However, the dependence of $c^*$ on temperature is weak due to the weak dependence of $\gamma_L$ on temperature. Due to the complex relation between $c^*$ and $\Delta P$ the establishment of which requires the knowledge of other parameters and relation (e.g. $\gamma_L \cos\theta$ as a function of surfactant concentration), in the following analysis, we will use $c^*$ as a proxy variable of $\Delta P$ when we systematically study the impact of $\Delta P$ on the wetting kinetics. For a given system with known surfactant species, salt composition, material and morphological properties of the membrane, there exists a one-to-one relation between $\Delta P$ and its proxy variable $c^*$. Although not particularly straightforward, this treatment using $c^*$ as a proxy variable allows us to focus on the wetting mechanism itself without having to arbitrate several unknown parameters and relations. In the following analysis, all simulations will be carried out using $c^*$ as the variable to generate the wetting time. In the few experimental measurements, however, we will estimate the $c^*$ based on $\Delta P$ and other estimated properties and relations.

Fig. 5.4 shows the simulation results of $1/t_{wetting}$ as a function of $c^*$ with different $c_0$ at the same vapor flux. The relative positions of the different $1/t_{wetting}$ vs. $c^*$ curves with different $c_0$ suggest that increasing the bulk concentration of SDS in the feed solution accelerates the wetting process, which is consistent with the results in Fig. 5.2. Within each curve, increasing $c^*$, which is equivalent to decreasing $\Delta P$, slows down pore wetting. While $\Delta P$ itself does not have direct impact on SDS transport, a lower $\Delta P$ leads to a higher $c^*$ based on the force equilibrium assumption. Regardless of $c_0$, a higher $c^*$ always contributes negatively to the transport of SDS to the wetting frontier. In particular, when $c^*$ is sufficiently high, the forward convection is offset by the back

diffusion, resulting in no net transport of SDS to the wetting frontier. This maximum $c^*$, $c^*_{max}$, beyond which wetting does not occur is given by

$$c^*_{max} = c_0 \exp\left(\frac{J_w \delta_b}{D}\right) \tag{5.13}$$

This $c^*_{max}$ correspond to a critical ΔP below which wetting would not occur. Such ΔP is essentially the LEP calculated using Eq. 5.2 with the $\gamma_L \cos\theta$ the surfactant concentration of the $c^*_{max}$. We note that LEP can even become negative when the surfactant concentration is sufficiently high, in which the force balance condition requires that distillate hydraulic pressure be higher than the feed hydraulic pressure.

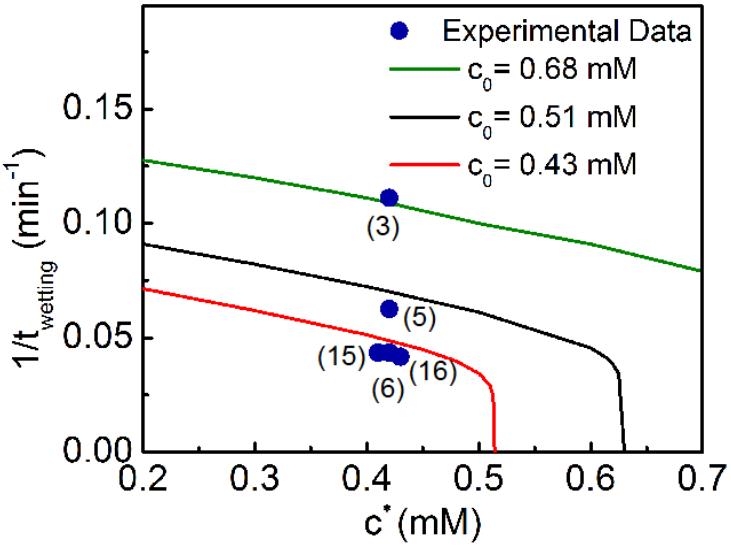


Figure 5.4 Experimental results (blue circles) and model predictions (red line for $c_0$ = 0.43 mM, black line for $c_0$ = 0.51 mM, and green line for $c_0$ = 0.68 mM) of DCMD membrane wetting experiments with different critical concentrations $c^*$ that depends on the transmembrane hydraulic pressure ΔP and is thus employed to serve as a proxy variable to ΔP without the detailed knowledge of solution and membrane properties. For DCMD wetting experiments with $c_0$ = 0.43 mM, three different ΔP were employed (0, 6, and 12 kPa), and the critical concentrations $c^*$ were estimated by LEP calculation results in Appendix D. For DCMD wetting experiments with $c_0$ = 0.51 and 0.68 mM, ΔP was controlled to be 6 kPa. In all wetting experiments, the feed and permeate solution temperatures were maintained at 60 and 20 °C, respectively, which resulted in a constant vapor water flux $J_w$ at 32.1 ± 0.8 L $m^{-2}$ $h^{-1}$ prior to the addition of SDS. The detailed water flux and salt rejection rate data for DCMD wetting experiments were shown in Fig. D.3 in Appendix D. For the model simulations, three different $c_0$ (0.43, 0.51, 0.68 mM) were investigated with the same $J_w$ at 32 L $m^{-2}$ $h^{-1}$, respectively. For the experimental results, with $c_0$ = 0.43 mM,

$t_{wetting}$ is 25, 24, and 24 min for $\Delta P = 0$, 6, and 13 kPa, respectively; with $c_0$ = 0.51 mM, $t_{wetting} = 17$ min for $\Delta P = 6$ kPa; with $c_0$ = 0.68 mM, $t_{wetting} = 9$ min for $\Delta P = 6$ kPa.

To compare the model prediction with the experimental data from MD wetting experiments using different $\Delta P$, the quantitative relationship between $\Delta P$ and $c^*$ is required. However, accurate measurement of LEP using conventional approach is not applicable for solution with surfactants due to the rapid adsorption of surfactants onto the pore surface which leads to a significant difference of surfactant concentration between the bulk solution and the wetting frontier. Therefore, we have estimated the LEP using Eq. 5.2 with measured surface tension and the intrinsic CA of the solution on a smooth, reconstructed PVDF surface (detailed results are shown in Fig. D.4, D.5 and D.6). The intrinsic CA cannot be measured using the PVDF membrane due to the presence of the pores, as a sessile drop on a porous PVDF membrane surface is in a Cassie-Baxter state that yields a CA significantly higher than the intrinsic CA[112,237].

As shown in Fig. 5.4, LEP decreases with the increasing $c^*$. It can be observed from Fig. D.3 and D.7 (Appendix D) that the range of $\Delta P$ investigated in our experiments only corresponds to very small change in $c^*$. Using linear interpolation, we estimate the $c^*$ corresponding to the tested $\Delta P$ of 0, 6, and 12 kPa to be 0.43, 0.42, and 0.41 mM, respectively. Within such a small range of $c^*$, the kinetic model predicts that breakthrough time should be very similar, which is indeed observed from experiments. While the range of $c^*$ of the three investigated cases seems small, the corresponding range of $\Delta P$ is actually significant in the context of MD, because (1) MD is not a pressurized membrane process and only requires relatively small hydraulic pressures to circulate the feed and distillate streams, and more importantly, (2) $\Delta P$ represents the transmembrane hydraulic pressure which is typically zero when the feed and distillate stream have the same hydraulic pressures. Therefore, the experimental data was not collected to validate a full simulated curve on Fig. 5.4 because $\Delta P$ for the lower range of $c^*$ is too high in the context of MD and is thus practically irrelevant.

The "clustering" of the three data points for $\Delta P$=0, 6, and 12 kPa (when $c_0$ = 0.43 mM) suggests that wetting kinetics in MD is virtually independent of $\Delta P$, which is quite counter-intuitive because the very criterion of wetting is $\Delta P > LEP$. The key to resolve this counter-intuition is to understand the pseudo steady-state and force balance assumption in the wetting model, that, $\Delta P$ does not exert its impact directly by inducing force unbalance, but rather by

affecting the SDS concentration at the wetting frontier required to maintain the force balance, which in turn impacts the mass transfer rate of SDS to the wetting frontier.

*5.4.4. Membrane wetting kinetics for different surfactant species*

The surface tension of each surfactant solution decreases as the surfactant concentration increases (Fig. 5.5a). Following the Gibbs adsorption equation (Eq. 5.11), $\Gamma$ can be estimated using the slope of "$\gamma$ vs. $\ln(C)$" before the surfactant concentration reaches the critical micelle concentration, CMC. A more negative slope represents a larger $\Gamma$ which suggests that the surfactants occupy less surface area and that it requires more such surfactants to saturate a given surface area. Likewise, a less negative slope indicates that the surfactants are "larger" and fewer of such surfactants are needed to saturate a given surface area (Fig. 5.5b).

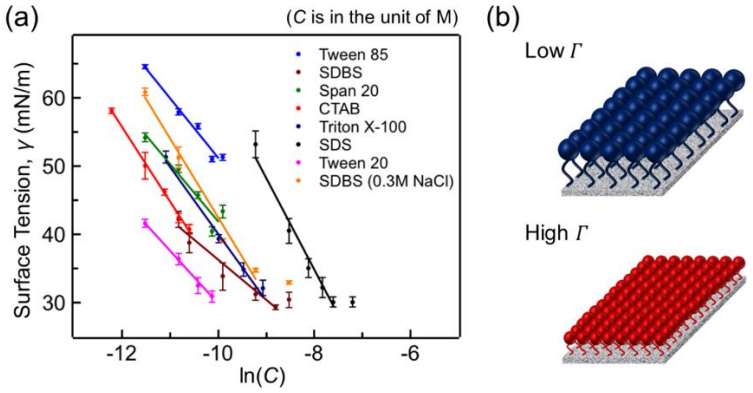


Figure 5.5 (a) surface tension, $\gamma$, as a function of surfactant concentration for different types of surfactants. The solution temperature was 60 ºC and the default NaCl concentration was 0.6 M. For SDBS, an additional NaCl concentration of 0.3 M was also used. We were interested in the slope of the linear portion of "$\gamma$ vs. $\ln(C)$" from which the surface excess concentration, $\Gamma$, can be determined using equation 1. (b) illustration of the concept of surface packing density: compared to "smaller" surfactants (high $\Gamma$, bottom), "larger" surfactants (low $\Gamma$, top) have a lower surface packing density and require less surfactants to saturate a surface of given area.

The breakthrough time, $t_{wetting}$, determined from the data of the wetting experiments (see Fig. D.8 in Appendix D), is linearly correlated with $\Gamma$ in all occasions with the exception of SDS (Fig. 5.6a). Because $\Gamma$ is strongly dependent on ionic strength, solutions dosed with the same concentration of SDBS (0.3 mM) but different concentrations of NaCl (0.3, and 0.6 M) have very different $\Gamma$ which also linearly scales with $t_{wetting}$. In comparison, there is virtually no correlation between $t_{wetting}$ and HLB (Fig. 5.6b), which is consistent with our hypothesis that HLB should

play no role in the kinetics of wetting. Neither is any correlation observed between the breakthrough time and the charge of surfactants (negative for SDS and SDBS, positive for CTAB, neutral for all others).

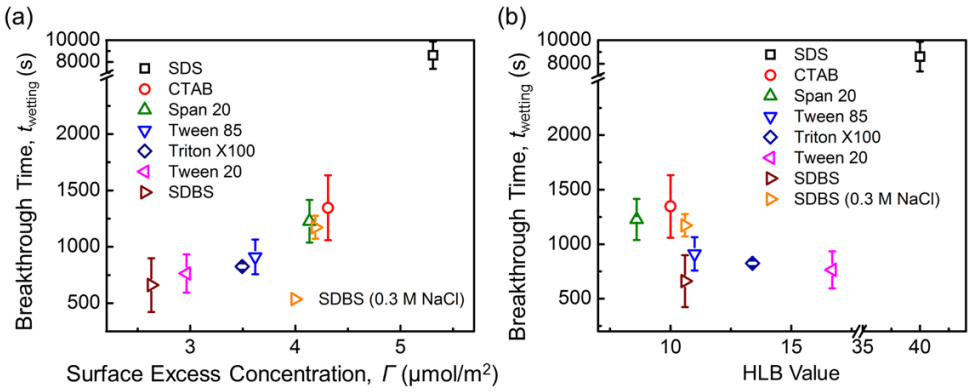


Figure 5.6 (a) Wetting breakthrough time, $t_{wetting}$, as a function of $\Gamma$ estimated from the data in Fig 5.2(a). (b) $t_{wetting}$ as a function of HLB. In each MD experiment, the inlet temperatures of the feed and permeate streams were maintained at 60 and 20 °C, respectively, which resulted in a water vapor flux of 30.5±1.2 L m$^{-2}$ hr$^{-1}$ in our system. In most cases, the feed solutions were 0.6 M NaCl solutions dosed with different surfactants at 0.3 mM. For SDBS, an additional NaCl concentration (0.3 M) was also tested.

The general linear relationship between $t_{wetting}$ and $\Gamma$ can be explained by the kinetic model which suggests that the kinetic rate of pore wetting is essentially determined by how fast the pore surface is saturated by adsorbed surfactants. With this kinetic model, the rate of pore surface saturation is primarily controlled by (1) the rate of surfactant transport from the bulk solution to the wetting frontier, and (2) the surface packing density, which is equivalent to $\Gamma$. Because we controlled the surfactant concentration in the bulk solution and the vapor flux to be same in all experiments, the molar flux of all tested surfactants (except SDS) were similar. Therefore, surfactants with low $\Gamma$, which are "large" surfactants that saturate a unit pores area with less surfactant molecules, promote faster saturation of the pore surface and thus faster wetting. Similarly, "smaller" surfactants with high $\Gamma$ saturate the pore surface more slowly because more surfactant molecules are required to saturate a unit area of surface. Consequently, surfactants with higher $\Gamma$ resulted in slower wetting with longer $t_{wetting}$.

The argument of similar molar flux (for all surfactants except SDS) in the above discussion implicitly assumes that evaporation-induced convection dominates over the concentration gradient-induced diffusion for the axial transport of surfactants from the bulk solution to the

wetting frontier. In fact, the violation of this assumption can be employed to explain the significant deviation of SDS-induced wetting from the linear relationship between $t_{wetting}$ and $\Gamma$ observed in experiments with other surfactants. As shown in Table D2 in Appendix D, the diffusion coefficient of SDS is at least an order of magnitude higher than that of other surfactants. In addition, SDS is also significantly less effective in reducing the surface tension of a solution, which is evidenced by the fact that it has a significantly higher CMC than most other surfactants except for SDBS.

In the context of pore wetting, SDS has a higher critical concentration, $C'$, than most other surfactants (Table D2). This critical concentration is defined as the surfactant concentration that leads to an $LEP'$ (at the wetting frontier) equal to $\Delta P$. The pseudo force equilibrium assumption demands that the actual surfactant concentration at the wetting frontier be maintained as $C'$. With $C'$at the wetting frontier and the diffusion coefficient both being significantly higher than other surfactants, diffusion plays much more important role in the axial transport for SDS than for other surfactants, which explains the significant deviation of SDS-induced wetting from the linear correlation between $t_{wetting}$ and $\Gamma$ for pore wetting induced by other surfactants.

If we employ the full kinetic model that accounts for both the convective and diffusive contributions to surfactant transport, we can simulate $t_{wetting}$ for different types of surfactants considering both the impacts of the surface packing density and diffusion coefficient. The theoretical predictions based on the full kinetic model match reasonably well with the experimental observations (Fig. 5.7), including the data point measured with SDS. The very good agreement between experimental observations and theoretical predictions does not only apply to different surfactants but also to the same surfactant (SDBS in this case) with different background electrolyte concentrations. The ability of the kinetic model to quantitatively predict the experimental results is quite satisfactory especially considering the many simplifying assumptions (e.g. cylindrical pore geometry) made in the model.

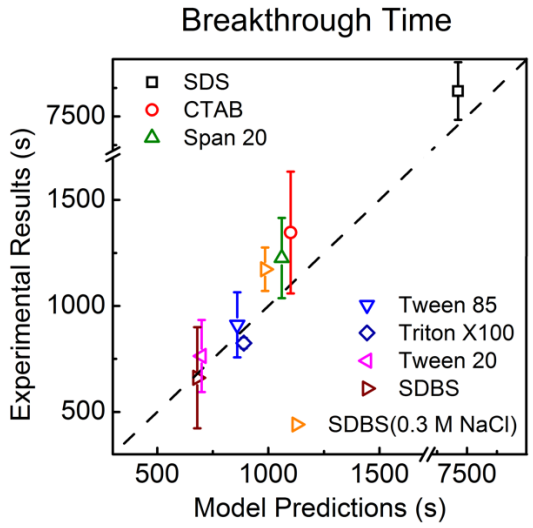


Figure 5.7 Theoretical predictions and experimental observations of the wetting breakthrough time, $t_{wetting}$. The theoretical predictions are simulated using the full kinetic model of surfactant-induced pore wetting as reported in our previous publication [238] and briefly summarized in Appendix D. The dash line represents perfect match between the theoretical predictions and experimental observations.

According to the kinetic model, the critical concentration ($C'$) at the wetting frontier influences the diffusive transport of surfactants because it affects the concentration gradient. While $C'$ is difficult to determine experimentally, simulation results using arbitrary $C'$ from 0.01 mM to the CMC of each surfactant suggest that $t_{wetting}$ is virtually independent of $C'$ except for SDS (Table D2). This further affirms our previous argument that convective contribution dominates the transport of all surfactants but SDS to the wetting frontier. For SDS, simulating $t_{wetting}$ requires more accurate estimation of $C'$ by measuring both the surface tension and contact angle of the solution on a smooth PVDF surface, which has been performed experimentally (Appendix D). Randomly selecting a $C'$ for SDS would lead to a huge range of predicted $t_{wetting}$ from 530s to infinity (i.e. the membrane would never be wetted), which highlights the importance of diffusion in the axial transport of SDS in the pore wetting process.

### 5.5. Conclusion

In this study, we developed and numerically solved a kinetic model for dynamic pore wetting induced by surfactants in MD. This kinetic transport model is developed by solving the coupled convection-diffusion-adsorption mass transport equations using assumptions of pseudo-

equilibrium adsorption and force balance at the wetting frontier, as well as pseudo-steady state for surfactant transport in the boundary layer and within the partially wetted pore. The kinetic model suggests several characteristic dependences of wetting kinetics on bulk surfactant concentration, vapor flux, and transmembrane hydraulic pressure, which have been validated by MD experiments with pore wetting induced by addition of SDS surfactant. We believe the developed model is universally applicable for predicting kinetics of pore wetting induced by other surfactants or any highly surface-active agents that can (1) significantly change the surface tension of an aqueous solution even at low concentration, and (2) strongly adsorb onto the pore surface.

The proposed and validated model reveals several important insights regarding surfactant-induced pore wetting, which are summarized below:

(1) Surfactants promote wetting by reducing the surface tension of the feed solution, not by making the pore surface hydrophilic.

(2) For the above reason, adsorption of surfactants onto the pore surface does not promote wetting. On the contrary, it deters pore wetting by continuously removing the surfactant at the wetting frontier and thereby increasing its LEP.

(3) The kinetics of surfactant-induced pore wetting is determined dominantly by the transport of surfactants to the wetting frontier, which is governed by convection, diffusion, and surface adsorption.

(4) For different surfactant species, surface excess concentration has a strong influence on the kinetics of surfactant-induced pore wetting. For highly effective surfactants that can significantly reduce surface tension with a very low surfactant concentration, surface excess concentration is arguably the single most important property of a surfactant that affects the wetting kinetics. For less effective surfactants, such as SDS, the diffusion coefficient of the surfactants also has a noticeable impact on the wetting kinetics.

These insights will help us better understand pore wetting in MD and develop effective strategies to mitigate pore wetting in MD operations.

**Supporting Information**

See Appendix D.

**Acknowledgement**

This work is supported by National Science Foundation via research grant CBET-1739884. Z. Wang also acknowledge the support from American Chemical Society Petroleum Research Foundation via award ACS-PRF 57353 DNI.

# CHAPTER 6

# STATEGIES FOR FOULING AND WETTING MITIGATION IN MEMBRANE DISTILLATION OPERTATION USING MEMBRANES WITH DIFFERENT WETTIBILITY

This chapter has been published in the journal Water Research as the following peer-reviewed manuscript: Wang Z., and Lin S., Membrane fouling and wetting in membrane distillation and their mitigation by novel membranes with special wettability. Water Research **112** (2017). p. 38-47. doi: 10.1016/j.watres.2017.01.022.

## 6.1. Introduction

Membrane distillation (MD) is a thermal desalination process capable of utilizing low-grade energy to desalinate highly saline water, such as RO brine and shale gas/oil wastewater [16,20,44,87,138]. In a typical MD process, a hydrophobic microporous membrane is used to separate a hot saline water stream (feed) and a cold fresh water stream (distillate). Driven by the trans-membrane temperature difference between the hot feed and cold distillate streams, water evaporates from the feed/membrane interface, transports down the partial vapor pressure gradient, and condenses on the distillate/membrane interface. Although MD has been studied for decades, it has recently gained momentum in academic research and industrial development because it has been proposed as one of the few promising solutions to the desalination of highly saline brine such as shale gas/oil produced water or briny wastewater in zero liquid discharge[1,13,44,93]. Due to the very high salinity, the osmotic pressures of these wastewaters can be significantly higher than the allowable working pressure in reverse osmosis—the state-of-the-art technology for seawater desalination.

The MD membrane is a critical component in an MD system, serving as a barrier for direct liquid water transfer and a medium for water vapor transfer. Conventional MD membranes are hydrophobic and made of common polymeric materials such as polyvinylidene fluoride (PVDF), polypropylene (PP), and polytetrafluoroethylene (PTFE). The hydrophobicity is required to prevent direct liquid permeation through the micropores. However, when hydrophobic membranes are used in MD to treat hypersaline wastewater of a complex composition, two potential problems may lead to MD operation failures [23].

The first potential problem is membrane fouling in which fouling agents (or foulants) attach onto the hydrophobic membrane surface, block the membrane pores, and consequently cause significantly reduced water vapor flux[32,239]. Membrane fouling is a particular concern when hydrophobic membrane is used in MD to treat feed waters with an abundance of hydrophobic contaminants (e.g. oil, hydrophobic organics) due to the strong hydrophobic-hydrophobic interaction[27,29–31]. Recent studies using hydrophobic MD membranes for desalinating brine water rich in oil or organics have shown the rapid and severe flux decline as a result of membrane fouling[33,239,240].

The second major problem that may lead to MD operation failure is membrane wetting. When a hydrophobic membrane is employed in an MD process to desalinate brine water containing amphiphilic molecules, such as surfactants and other amphiphilic organics, the hydrophobic tails of the amphiphilic molecules will attach onto the hydrophobic membrane pore surface, leaving the hydrophilic head exposed and eventually rendering the membrane pores hydrophilic. The consequence of membrane pore wetting is the direct permeation of feed water into the distillate stream and significantly undermined salt rejection rate[44,46–49].

The potential problems of fouling and wetting constraint the applications of conventional hydrophobic MD membrane to treating only relatively "clean" feed water without hydrophobic and amphiphilic contaminants. For desalinating shale/gas wastewater or industrial brines, which are enriched in hydrophobic or/and amphiphilic contaminants, conventional hydrophobic membranes could readily fail due to wetting or/and fouling. In this case, either extensive pretreatments are required to remove the hydrophobic and amphiphilic contaminants before the MD process, which will significantly increase the treatment cost; or advanced membranes that can resist wetting and fouling need to be developed.

Significant advances have been made recently in the materials science community to elucidate the mechanisms of special wettability observed in biological systems and to apply those principles to fabricate artificial interfacial materials with similar special wettability[112]. Two types of special wetting properties have been recently leveraged to enhance MD membrane performance. First, composite membranes with a hydrophobic substrate and a hydrophilic or superhydrophilic surface layer have been developed to impart robust resistance to oil fouling[33,239,240]. Such an approach of integrating a superhydrophilic skin layer has also been employed for fouling control in other membrane processes[105–109,148]. The underlying mechanism for fouling resistance is

the formation of hydration shell on the superhydrophilic coating which renders the membrane surface superoleophobic underwater[82,130,132,146,149,241].

On the other hand, omniphobic membranes have been also developed to mitigate membrane wetting induced by surfactants[44,48,49]. These membranes resist wetting by water and low-surface-tension liquids (e.g. oil) in air, and prevent feed solutions containing surfactants from penetrating into the membrane pores. The key to impart omniphobicity, especially oleophobicity, is to create a rough surface of reentrant structure and very low surface energy[69,242]. Detailed theory regarding the criteria of developing surfaces with robust resistance to wetting by low-surface-tension liquids has been established. Different methods have been also developed to create interfacial materials with omniphobicity using a variety of substrates[204,243–248].

The development of omniphobic membranes and composite membranes with superhydrophilic skin layer has significantly expanded the applications of MD and enabled MD to desalinate more challenging feed water[48,239]. However, a systematic understanding is still lacking regarding how these membranes perform with feed water of different characteristics. For example, while omniphobic membranes robustly resist oil wetting in air, its underwater antifouling performance against oil has not been studied. On the other hand, a previous study has reported that a composite membrane with both hydrophilic and hydrophobic layers was effective in preventing the wetting by feed water containing ethanol, which seems to suggest that a composite membrane may also resist wetting by feed water with surfactants. It is also intriguing to investigate whether each of these two membranes, or both of them, can deliver stable MD performance in complex feed water, such as an oil-in-water emulsion stabilized by surfactants.

In this study, we employ direct contact membrane distillation (DCMD) to systematically investigate the impact of membrane wetting properties on their anti-fouling and anti-wetting performance when used to treat oil-in-water emulsion with and without added synthetic surfactants. Three types of membranes with distinct wetting properties, including a hydrophobic (but oleophilic) membrane, an omniphobic membrane, and a composite membrane with a hydrophobic substrate and a superhydrophilic skin layer, are compared for their wetting properties and MD performance. We also conduct force spectroscopy to assess the underwater interaction between an oil droplet and the three different membranes to elucidate the different observed fouling behaviors.

## 6.2. Materials and Methods

### *6.2.1. Materials and Chemicals*

The hydrophobic PVDF membrane and omniphobic membrane, both with a nominal pore size of 0.45 μm, were purchased from GE Healthcare Life Sciences (Pittsburg, PA), and Pall Corporation (Exton, PA), respectively. This commercial omniphobic membrane belongs to the Versapor® series and is made of acrylic copolymer. Although this Versapore® membrane is developed for venting and moisture control applications and has never been used for MD or any type of water treatment process, we have tested it to be applicable for MD, yielding a flux comparable to the PVDF membrane.

Chitosan (CTS, medium molecular weight, deacetylated chitin), silica nanoparticles, or SiNPs, (LUDOX® HS-40), perfluorooctanoic acid, Triton$^{TM}$ X-100, acetic acid, sodium hydroxide (NaOH) and sodium chloride (NaCl) were all procured from Sigma Aldrich (St. Louis, MO). The crude oil was purchased from Texas Raw Crude Oil (Midland, TX).

### *6.2.2. Fabrication of Composite Membrane with Superhydrophilic Skin Layer*

The composite membrane was fabricated following the procedures reported in literature[120,239]. Briefly, a PFO/CTS nanoparticle-polymer composite was prepared via adding 20 mL of perfluorooctanoate (PFO) aqueous solution (0.1M, acquired from reacting perfluorooctanoic acid with NaOH) to a 100 mL dispersion of CTS and SiNPs (0.2 g CTS dissolved in 1% acetic solution in the presence of 0.3 g SiNPs) dropwise under vigorous stirring. After rinsed with DI water and dried under room temperature, 0.3 g of the PFO/CTS composite was dispersed in 20 mL ethanol and then spray coated onto a PVDF membrane coupon (20 cm × 10 cm) using a spray gun under an air pressure of 0.2 MPa. After heat treatment at 80 °C for 1 h, the resulting composite membrane, namely CTS/PFO-PVDF membrane, was ready to be used in MD experiments. Here, the chitosan was mainly responsible for imparting the hydrophilicity. The SiNPs were added to enhance the surface roughness required to achieve superhydrophilicity. The PFO, a low-surface-energy molecule, was blended to the composite coating to further enhance the anti-fouling performance of the coating. Previous studies have suggested a hydrophilic surface impregnated with low-surface-energy functional groups can outperform a purely hydrophilic

surface in resisting fouling[86,249–251]. It has been suggested that the lower-surface-energy groups serve to promote the release of foulants upon perturbation[252].

### *6.2.3. Membrane Characterization*

The surface morphology of each membrane was characterized using scanning electron microscopy (SEM, Merlin, Zeiss, Thornwood, NY). The wetting properties of the membrane surfaces were quantified by static contact angle (CA) measurements. For each membrane, the in-air CA with water or mineral oil, and the underwater CA with mineral oil were determined by an optical tensiometer (TL100, Attension Finland). The in-air CAs were measured with the sessile drop method, and the underwater CAs were obtained using an approach similar to captive bubble method except that the air phase was replaced by the oil phase. For each membrane, at least five CAs at different locations of the membrane surface were measured.

### *6.2.4. Crude Oil-in-water Emulsions*

Crude oil-in-water emulsions were prepared using two different approaches. In both cases, the resulting emulsions have a salinity of 600 mM (NaCl) and an oil concentration of 500 ppm. With the first approach, the crude oil/water mixture was rigorously stirred at 16,000 rpm for 15 min using a laboratory homogenizer (Fisher Scientific, Pittsburgh, PA) without adding any synthetic surfactant. The second approach differs from the first approach only in that an anionic surfactant (Triton X-100) at a concentration of 100 ppm was added to the emulsion before stirring. We note that 100 ppm is below the critical micelle concentration for Triton-X 100. To compare the two prepared emulsions, microscopic images of the oil droplets in the emulsions were obtained using an optical microscopy (Nikon LV100, Japan) and size distributions of the oil droplets were also determined by dynamic light scattering (DLS) with a Zetasizer (Malvern Nano ZS, UK).

### *6.2.5. Membrane fouling test*

The three different membranes, each of an area of 8 cm × 2.5 cm, were tested in a DCMD system with the two different oil-in-water emulsions as feed solution and deionized water as distillate.

In each test, the influent temperatures of the feed and distillate streams were controlled at 65 and 20 °C, respectively. The flow rates of the feed and the distillate streams were maintained at

500 mL/min (10.7 cm/s in our test cell) and 250 mL/min (5.4 cm/s), respectively. As a result, the hydraulic pressure of the feed stream was slightly higher than that of the distillate stream, which facilitated the detection of membrane wetting. If any pore was wetted, the saline feed water would permeate through the wetted pore to the distillate stream under hydraulic pressure gradient and thereby increase the distillate salinity, providing an unequivocal evidence of pore wetting[44,48,49]. In all MD experiments, the mass and conductivity of the distillate were measured continuously, from which the real time flux and salt rejection rate were calculated.

### *6.2.6. Oil-probe Force Spectroscopy*

Force spectroscopy regarding the underwater oil-membrane interaction was conducted for each membrane using a force tensiometer (Sigma 701, Attension, Finland) to elucidate the different membrane fouling behaviors[104,123,125]. In all measurements, a membrane coupon (2 cm × 2 cm) was first attached onto the bottom of a transparent test cell before the cell was filled with water. A small droplet of mineral oil (~6 μL) was carefully hung onto a ring-shaped force probe underwater in the cell using a syringe. In each measurement, the force probe with the attached oil droplet first approached the membrane surface at a constant speed of 0.3 mm/min, and then retracted from the membrane surface at the same speed immediately after oil-membrane contact. The force applied on the probe at different position was measured by the micro-electro-mechanical senor built in the force tensiometer. For the omniphobic membrane, an additional force spectroscopy was performed in the presence of 100 ppm Triton X-100.

## 6.3. Results and Discussion

### *6.3.1. Membrane Morphology*

The SEM images (Fig. 6.1) show that the pristine PVDF membrane (Fig. 6.1A and 6.1D), the fabricated composite membrane (Fig. 6.1B and 6.1E), and the omniphobic membrane (Fig. 6.1C and 6.1F) have drastically different surface morphology. Compared with the PVDF membrane, the composite membrane has a PFO/CTS composite surface coating with nanoscale roughness imparted by the SiNPs. It can be observed from the cross-section SEM image (Fig. 6.1E) that the PFO/CTS coating was only applied onto the top surface but not the PVDF substrate. On the other hand, the omniphobic membrane has a more stratified morphology that provides the reentrant

structure, which is required for a system to maintain a thermodynamically metastable Cassie-Baxter (C-B) state even with low-surface-tension liquid. In a C-B state, the liquid is supported by a composite surface composed of the porous solid surface and the air trapped within the pores. Because of the non-wetting requirement in MD application, the feed solution-membrane contact in MD should always be in a C-B state. The reentrant structure is critical for maintaining a C-B with low-surface-tension liquid because only with such a structure the entrance of low-surface-tension liquid into the pores can possibly be energetically unfavorable. For more details regarding reentrant structure and the mechanism via which it imparts oleophobicity, interested readers are referred to the abundant literature in materials science on omniphobic surface development.[44,69,112,204,205,242,253,254]. The presence of nanoparticle clusters within the porous structure also create additional multiscale reentrant structure to impart more robust resistance against pore wicking by oil[255].

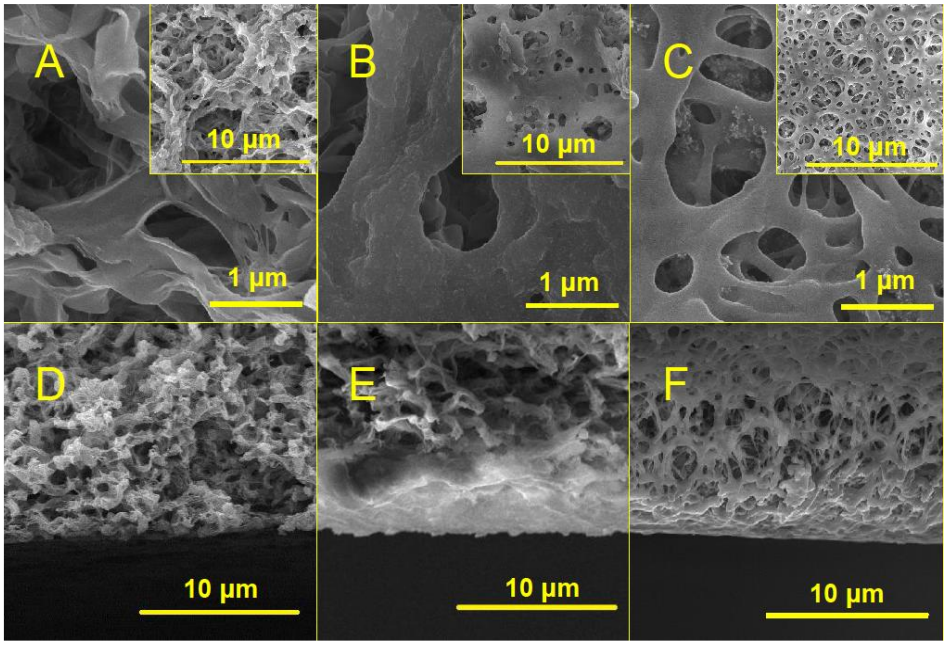


Figure 0.1 Top-view SEM images of the local surface morphology for (A) PVDF membrane, (B) PFO-PVDF composite membrane, and (C) omniphobic membrane. The insets in (A), (B) and (C) show the membrane surface morphology at a larger scale. Cross-section SEM images of (D) PVDF membrane, (E) PFO/CTS-composite membrane, and (F) commercial omniphobic membrane.

*6.3.2. Membrane wetting properties*

The CAs that quantify the membrane wetting properties are shown in Fig. 6.2. Both the PVDF membrane and the omniphobic membrane were in-air hydrophobic with in-air water CAs of

105.3±2.1° (Fig. 6.2A) and 132.5±0.9° (Fig. 6.2C), respectively. The coated surface of the composite membrane was in-air hydrophilic with an in-air water CA of 15±1.3° (Fig. 6.2B) due to the presence of the hydrophilic coating. The PVDF membrane was in-air superoleophilic, with no observable in-air oil CA (Fig. 6.2D). Interestingly, the composite membrane underwent an oleophilic-to-superoleophilic transition, with the in-air oil CA changing from its initial value of 55.4±0.9° to 0° in 10 minutes (Fig. 6.2E). The dynamic wetting of a surface with heterogeneous surface energy has been reported[256], but its detailed mechanism remains unclear. The reconfiguration of surface functional groups has been suggested to be a possible mechanism. For dynamic wetting of the composite surface by an oil droplet, it was possible that the system was originally in a Cassie-Baxter state as the oil was in contact with the low-surface-energy perfluoroalkyl chains in the PFO. The prolonged contact between the oil droplet and the PFO/CTS surface coating eventually became dominated by the interaction between oil and the underlying CTS which promoted membrane wetting. However, this cannot explain why similar dynamic wetting behavior was not observed with a water droplet on the composite membrane surface. It is worth noting that a previous study has reported a superhydrophilic-superoleophobic surface on which the dynamic wetting of water was observed yet the oil CA was ultra-high and stable. Moreover, dynamic wetting of membrane has also been observed with commercial PTFE membranes contacting different low-surface-tension liquids[44], in which the time scale of transitioning to a fully wetted surface varied significantly depending on the contacting liquids. In general, membrane dynamic wetting is a widely observed yet relatively poorly understood phenomenon that warrants further investigation. The hydrophobic PVDF membrane and the composite membrane were both wicked by mineral oil in air, as suggested by non-observable in-air CAs (Figure 6.2D and 6.2E). In comparison, the omniphobic membrane was not subject to oil wicking (Figure 6.2F) due to its oleophobicity made possible by the combination of reentrant morphology and the low-surface-energy of the materials.

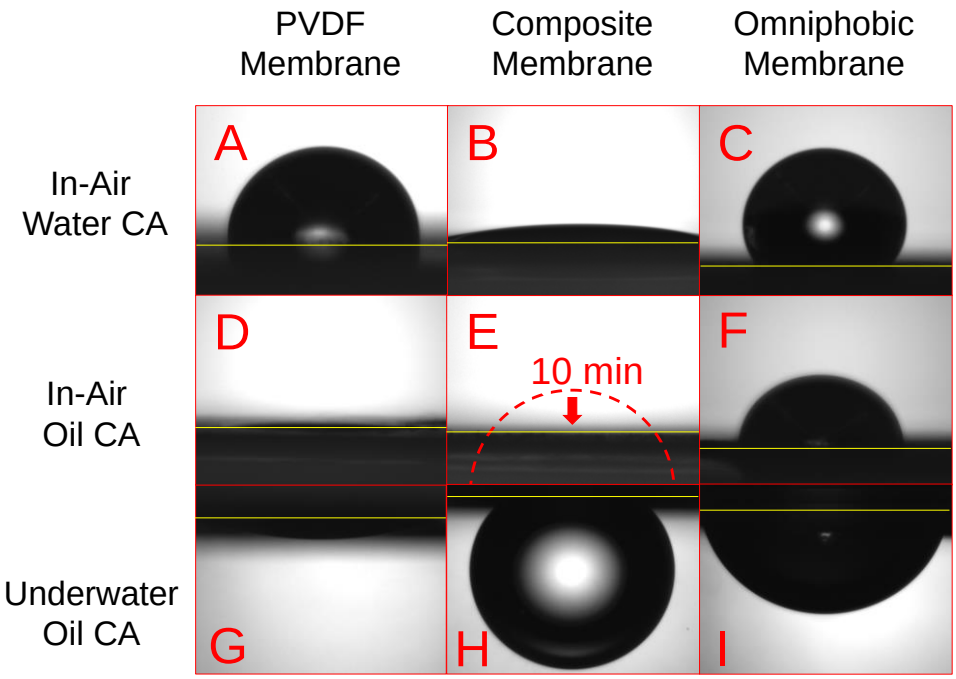


Figure 0.2 In-air water CA of (A) the PVDF membrane, (B) the composite membrane, and (C) the ominphobic membrane; in-air oil CA of (D) the PVDF membrane, (E) the composite membrane, and (F) the omniphobic membrane; underwater oil CA of the (G) the PVDF membrane, (H) the composite membrane, and (I) the omniphobic membrane.

We also measured the underwater oil CA due to its strong relevance in membrane oil fouling. The PVDF membrane was underwater oleophilic with an underwater oil CA of 23.8±1.8° (Fig. 6.2G), which can be attributed to the strong attractive hydrophobic-hydrophobic interaction between the membrane and the oil droplet. In comparison, the composite membrane was underwater highly oleophobic with an underwater oil CA of 139.3±1.6°. This underwater oleophobicity can be explained by the strong repulsive hydration force experienced by the oil droplet when it attempted to wet the superhydrophilic CTS/PFO coated surface[239]. The adhesion between the mineral oil and the CTS/PFO underwater, which is required for the mineral oil to wick into the porous CTS/PFO layer, necessitates the dehydration of the CTS/PFO which is energetically highly unfavorable[128,130–132].

The wetting properties of the omniphobic membrane were significantly different from those of the PVDF and the CTS/PFO membrane. Non-zero CAs were observed for both water and oil in air as well as for oil underwater. Another key requirement to achieve omniphobicity, in addition to the reentrant structure, is that the solid materials of the porous structure is of low surface energy.

Therefore, it should be expected that an omniphobic membrane is underwater oleophilic due to the hydrophobic-hydrophobic interaction between oil and the low-surface-energy membrane materials. However, the underwater oil CA of the omniphobic membrane (73.8±0.7°), though lower than 90º, was significantly higher than that of the PVDF membrane. This is because the complete wetting of a membrane requires the transition from a C-B state to a Wenzel state via pore wicking, which did not occur to the omniphobic membrane due to the reentrant structure. Nonetheless, the underwater oil CA of the omniphobic membrane was appreciably lower than that of the CTS/PFO membrane, which suggests possibly favorable attachment of oil droplets onto the omniphobic membrane and consequently the blocking of membrane pores by the attached oil droplets in MD operations.

*6.3.3. Characterizations of crude oil-in-water emulsions*

The prepared emulsions were highly turbid (Fig. 6.3A and 6.3B insets) and stable with no observed phase separation for at least 24 h. The stability of the emulsion with Triton X-100 was attributed to the presence of the synthetic surfactant, Triton X-100. On the other hand, the stability of the emulsion without synthetic surfactant can be ascribed to the natural amphiphilic molecules existing in the crude oil that acted as surfactants. These naturally occurring surfactants include, but are not limited to, asphaltenes, naphthenic acid, carboxylic acid and other oil-soluble acids and bases[134,135].

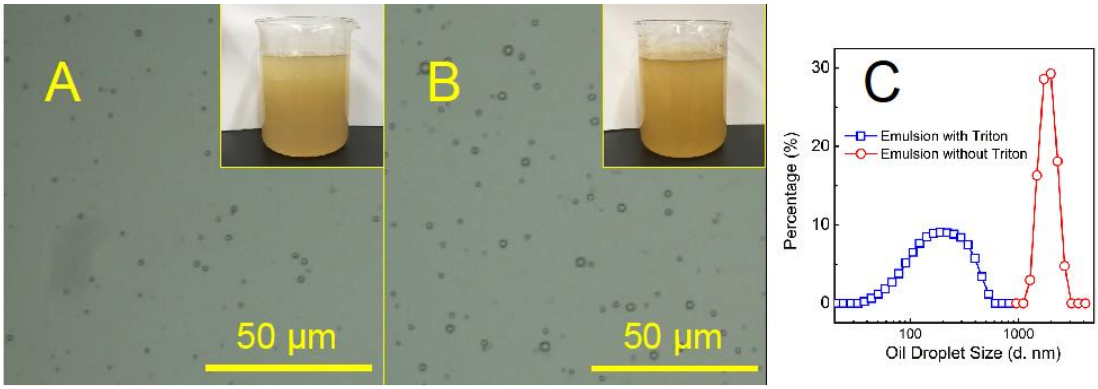


Figure 0.3 Microscopic images of (A) emulsion with Triton X-100, and (B) emulsion without any synthetic surfactant. The insets show the photographic images of the emulsions. (C) The distributions of hydrodynamic diameters of crude oil droplets in the emulsions measured by dynamic light scattering. The emulsions were kinetically stable for at least 24 h with no phase separation observed.

Comparing the microscopic images of the two emulsions, the crude oil droplets in the emulsion with surfactants (Fig. 6.3A) were smaller than that in the emulsion without surfactant (Fig. 6.3B). From the DLS measurements, the oil droplets in the emulsion with and without Triton X-100 showed distributions of hydrodynamic diameter of 209±110, 897±330 nm respectively, which is in accordance with the microscopic images. Triton X-100 decreased the oil droplet size as it reduced the oil droplet surface tension[257,258].

### *6.3.4. Membrane performance with oil-in-water emulsion without synthetic surfactants*

With the crude oil-in-water emulsion without synthetic surfactant, the PVDF was fouled rapidly, which resulted in significant flux decline within two hours of operation (Fig. 6.4a). This is consistent with experimental observations in previous studies and the ultralow underwater oil CA shown in Fig. 6.2. The strong hydrophobic-hydrophobic interaction between the crude oil and the PVDF membrane promoted the attachment of oil to the membrane surface and the subsequent wicking of the membrane pores, thereby eliminating available pores for vapor permeation.

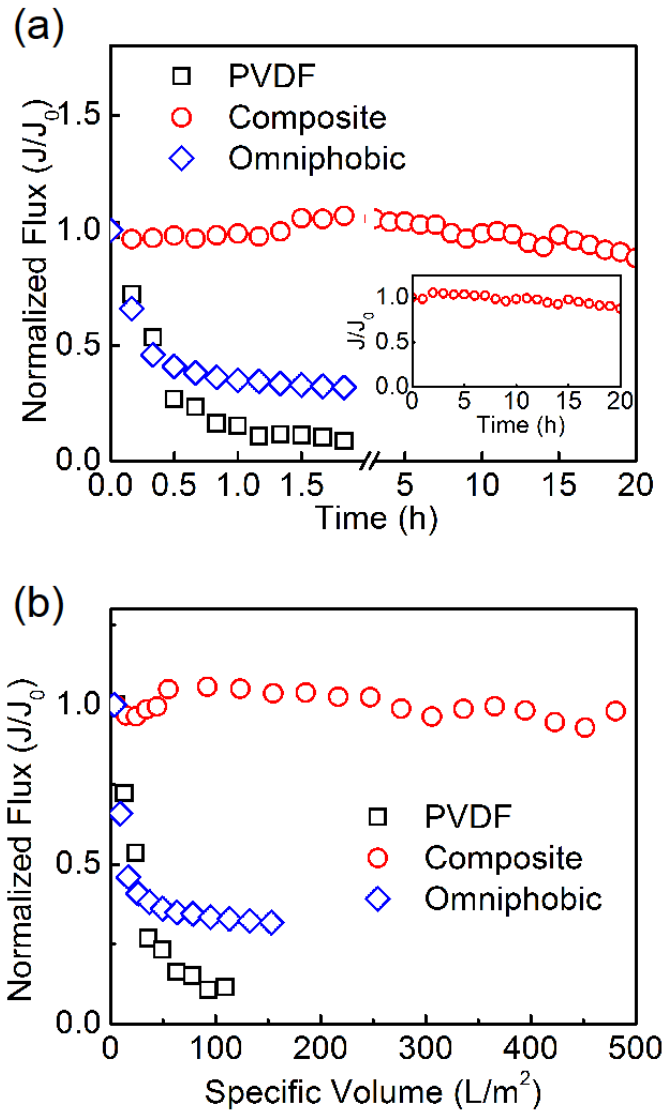


Figure 0.4 Normalized water fluxes of the PVDF membrane (black squares), the composite membrane (red circles), and the omniphobic membrane (blue diamonds) over (a) time, and (b) specific volume of permeate water normalized by the membrane area in DCMD experiments using prepared crude oil-in-water emulsion without synthetic surfactant as the feed solution. The normalized fluxes were the measured absolute fluxes normalized by the initial fluxes. The influent temperatures of the feed and distillate streams were 65 and 20 ºC, respectively. The cross-flow velocities on the membrane for the feed and distillate streams were 10.7 and 5.4 cm/s, respectively. The initial fluxes for the PVDF membrane, the composite membrane and the omniphobic membrane were 35.67, 30.15 and 25.19 LMH, respectively. The salt rejection rates for all membranes are over 99.9% in all experiments. The inset in (a) is the DCMD result for composite membrane operating with the same feed water over 20 hours.

Similar fouling behavior was also observed for the omniphobic membrane (blue diamonds on Fig. 6.4). As discussed in section 6.3.2, although the underwater CAs with oil were drastically different between the omniphobic membrane and the hydrophobic PVDF membrane due to the presence of reentrant structure in the omniphobic membrane, the low-surface-energy material comprising the omniphobic membrane was still attractive to oil via the hydrophobic-hydrophobic interaction underwater. Such an attraction led to the spreading of the oil droplets on the membrane surface, which eliminated the available pores of the omniphobic membrane for vapor transfer and thereby led to significant flux decline. The major difference in fouling between the PVDF and the omniphobic membranes, however, was the permeation of oil into the pores of the PVDF membrane but not the omniphobic membrane. Evidences in support of such difference include the underwater oil CA for both membranes reported in section 6.3.2, as well as the force curves measured for the interaction between an oil droplet and both membranes, which will be discussed in detail in section 6.3.6.

In a stark contrast, the composite membrane was able to deliver a highly stable performance with negligible flux decline in 20 h (red circles on Fig. 6.4a). The excellent fouling resistance of the composite membrane was attributable to the presence of the superhydrophilic PFO/CTS coating which created a hydration layer on the membrane surface. The strong and repulsive hydration force prevented the oil from attaching onto the surface, thereby keeping the pores open and available for vapor transfer. On the other hand, the low-surface-energy perfluoro functional groups in the PFO/CTS coating served to promote the release of any attached oil foulant upon local hydrodynamic perturbation[252]. Our recent study has shown that the PFO/CTS coating was more effective in mitigating oil fouling in MD than a pure crosslinked CTS coating which was superhydrophilic but without low-surface-energy functional groups[249]. Similar improvements on anti-fouling performance by the integration of low-surface-energy functional groups into superhydrophilic matrixes have also been observed in other pressurized membrane processes[86,252,259–261].

For all three membranes, the calculated salt rejection rates were all over 99.9%. We therefore conclude no membrane wetting occurred with this feed solution containing no synthetic surfactant. The natural surfactants that stabilized the oil-in-water emulsions did not induce membrane pore wetting even for PVDF membrane which has been demonstrated to be very susceptible to wetting by surfactants[44]. It was likely that the naturally occurring surfactants were mostly bound to the

oil-water interface and did not exist substantially as unassociated surfactants in the feed water due to their relatively low concentrations.

*6.3.5. Membrane performance with oil-in-water emulsion stabilized by synthetic surfactants*

When the crude oil-in-water emulsion stabilized by synthetic surfactants (Triton X-100) was used as the feed solution in MD, it completely changed the membrane performance. For the PVDF membrane, very rapid fouling was observed, leading to drastic flux decline within 10 min (Fig. 6.5a). The fouling of the PVDF membrane by feed solution stabilized by Triton X-100 seemed to be faster than that with feed solution without synthetic surfactants (Fig.6.4). During this fouling stage, the salt rejection remained near perfect (Fig. 6.5b), implying that the membrane pores were not yet wicked through by the feed solution. Most interestingly, the fouling stage only lasted for about 10 min before pore wetting became dominant. Both the increase of permeate flux, which eventually surpassed the initial flux, as well as the dramatically reduced salt rejection, which eventually became zero, suggest rapid and severe pore wetting. Previous studies have shown failure of MD due to membrane pore wetting by unbound anionic surfactants[44,48,49]. Here, the wetting could be caused by either the surfactants that bound directly to the membrane pores or by surfactants that bound to the absorbed oil on the surface of the membrane pores, although the exact contributions are difficult to determine.

The composite membrane, which robustly resisted fouling against crude oil-in-water emulsion without synthetic surfactant, was highly susceptible to pore wetting when the feed solution contained Triton X-100 (Fig. 6.5). The absence of flux decline suggests that no fouling occurred. Therefore, the wetting was attributable to the free surfactants (i.e. unbound to oil droplets) but not oil-bound surfactants. The unbound surfactants were able to transport across the superhydrophilic skin layer and absorb onto the underlying hydrophobic PVDF substrates, which rendered the membrane pores hydrophilic, appreciably reduced the liquid entry pressure, and allowed direct permeation of the saline feed water through the pores. The failure of the composite membrane in MD performance was similar to that of the PVDF membrane in both the degree and the kinetics of wetting: the salt rejection rate decreased to almost zero in just about half an hour (Fig. 6.5b). The major difference was the absence of the fouling stage for the composite membrane with a superhydrophilic surface.

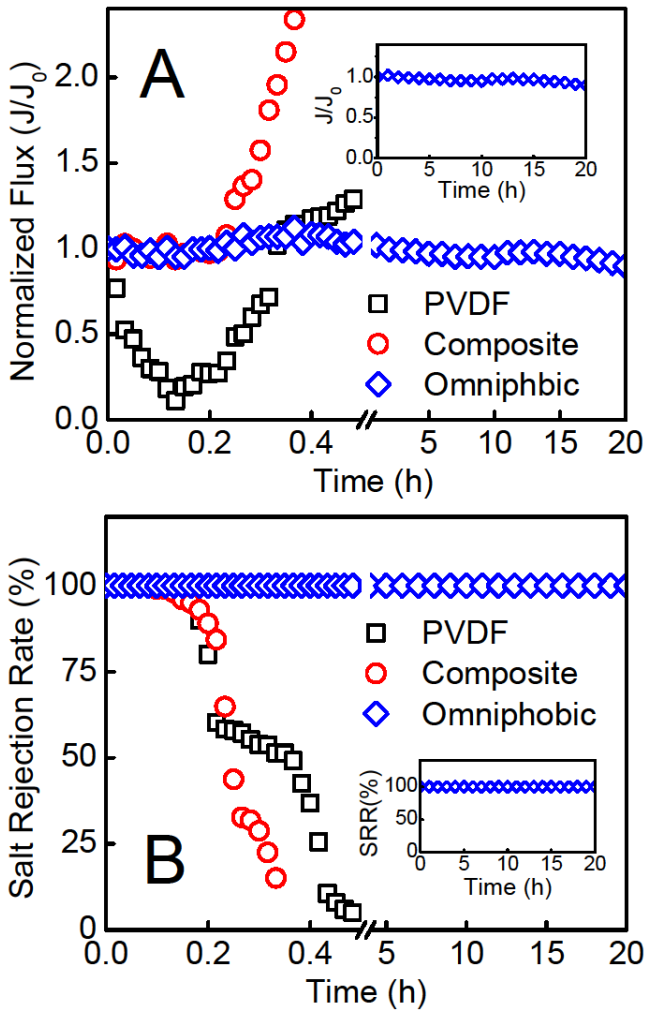


Figure 0.5 (a) Normalized water fluxes for the PVDF membrane (black squares), the composite membrane (blue diamonds), and the omniphobic membrane (red circles) over time in DCMD experiments using high-surfactant-content crude oil-in-water emulsion as feed. The experimental conditions were the same as those described in Fig. 6.4. The initial fluxes for the PVDF membrane, composite membrane and omniphobic membrane were 36.15, 30.76 and 24.46 L/($m^2hr^1$), respectively. (b) Corresponding salt rejection rates for the PVDF membrane (black squares), the composite membrane (blue diamonds), and the omniphobic membrane (red circles) over time in the DCMD experiments. The insets in both (a) and (b) show the DCMD results for the omniphobic membrane operating with the same feed water over a long time period.

In comparison, the omniphobic membrane exhibited excellent anti-fouling and anti-wetting performance in DCMD experiments using crude oil-in-water emulsion stabilized by synthetic surfactants as the feed solution: no flux decline or decrease in salt rejection rate was observed over 20 h of operation (Fig. 6.5), which suggested the absence of fouling or wetting. Previous studies

have shown outstanding anti-wetting performance of omniphobic membranes when feed solution was dosed with free surfactants[44,48,49]. It has been suggested that the combination of re-entrant structure and low surface energy sustains a metastable Cassie-Baxter state for the contact between an omniphobic membrane with low surface tension liquids. With the exact same mechanism, the unbound surfactants in the feed solution did not induce pore wetting of the omniphobic membrane in our experiments. A recent study also showed that an omniphobic membrane delivered significantly more stable performance than a PVDF membrane when being used to desalinate real shale gas wastewater[50].

The omniphobic membrane performed very differently with different feed solutions: we have already shown, in section 6.3.4, that crude oil-in-water emulsion without synthetic surfactants readily fouled the omniphobic membrane; however, when the emulsion was stabilized by synthetic surfactants, Triton X-100, no fouling was observed over 20 h of MD operation (Fig. 6.5). In an abundance of surfactants in the emulsion, the crude oil droplets were "wrapped" by the surface-adsorbed surfactants and thereby became 'hydrophilic'. The hydrophilic oil droplets were not able to attach onto the membrane surface and block the membrane pores, because not only the hydrophobic-hydrophobic attraction was eliminated but the oil droplets were also stabilized by a hydration shell due to the strong affinity between the hydrophilic heads of the surfactants and the surrounding water.

### *6.3.6. Force spectroscopy to elucidate oil-membrane interaction*

To acquire fundamental understandings of the interaction between oil and membranes with different special wetting properties, underwater force spectroscopy was conducted for each membrane using an oil droplet as the force probe. The force curves from the force spectroscopy are shown in Fig. 6.6, showing a unique behavior for the interaction between each membrane with the oil droplet probe. In each measurement, the oil droplet probe first approached the membrane and retracted immediately after contacting the membrane, both at the same speed. Due to oil-membrane adhesion, the retraction stretched the oil droplet and eventually split the droplet into two portions with one remaining on the probe and the other retained by the membrane surface. Physically, there should be no baseline adhesion force before the oil droplet contacted the membrane and after the split of the oil droplet, as there was no oil-membrane interaction in both cases. However, the measured "pseudo-adhesion-forces", which were essentially the force exerted

on the force sensor of the tensiometer, could be different for the two baselines in the receding stage due to the reduction of the oil droplet volume as a result of the split. The decrease of the oil droplet volume caused the simultaneous decrease of the flotation force, gravitational force, and viscous force (for constant-speed movement), which collectively led to a net positive pseudo-adhesion-force compared to the baseline before splitting. Such a baseline difference represents the amount of oil droplet retained by the membrane and thus complements the actual adhesion force in assessing the oil-membrane interaction.

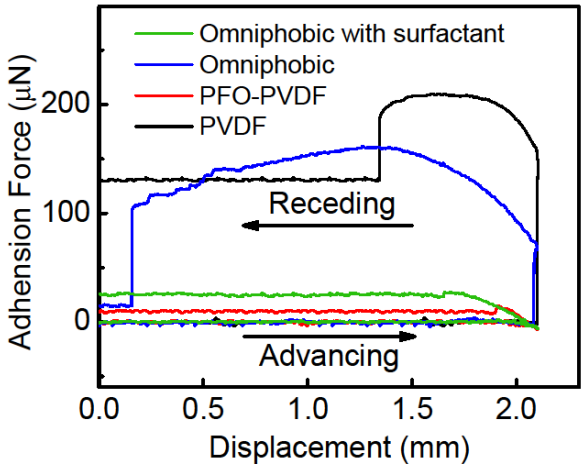


Figure 0.6 Force curves for the interactions between the PVDF membrane (black curve), the composite membrane (red curve), and the omniphobic membrane (blue and green curves) and a mineral oil droplet. The force curves display the forces measured by the tensiometer sensor as a function of probe displacement. All force curves were collected for the oil-membrane interaction under DI water, with the exception for the one that was collected in a Triton-X solution (the green curve). The initial position of the oil droplet and the initial force applied on the oil droplet were both set as zero.

For the PVDF membrane, upon the physical contact between the oil droplet and the membrane surface, there was a drastic increase in the adhesion force. This strong attraction between the PVDF membrane surface and the approaching oil droplet is attributable to the strong and attractive hydrophobic-hydrophobic interaction[241]. The underwater adhesion force between the oil droplet and the PVDF membranes (~200 μN) was significantly stronger than that of the composite membrane and the omniphobic membrane. In addition, a large fraction of oil was retained by the PVDF membrane, which reduced the volume of the oil droplet probe that translated to a net force of ~130 μN for the new baseline in the receding stage.

The oil droplet interacted with the composite membrane in a drastically different manner compared to that with the PVDF membrane. First of all, no strong adhesion force was detected upon the contact between the oil droplet and the superhydrophilic surface of the composite membrane. On the contrary, a small repulsion (reflected as negative adhesion force) was observed, most likely due to the repulsive hydration force. Stronger repulsion was likely to be observed if we further pressed the oil droplet probe against the membrane surface. However, we intentionally chose to retract immediately right after the oil-membrane contact because the ring-shaped tensiometer probe (to which the oil droplet was hung) could be forced into oil droplet and generate information irrelevant to the actual oil-membrane interaction. Furthermore, the pseudo-adhesion force for the baseline in the receding stage was very low compared to that with the PVDF membrane, suggesting little retention of oil on the membrane surface due to the very weak adhesion between the oil and the superhydrophilic surface of membrane.

The interactions between the oil droplet and the omniphobic membrane were the most interesting. For the interaction in DI water, similar to the interaction with PVDF membrane, a sudden increase in adhesion force was observed at the end of the advancing stage due to the hydrophobic-hydrophobic interaction. This is consistent with the results of our fouling experiments which showed similar fouling behaviors for both the hydrophobic PVDF membrane and the omniphobic membrane. However, the fraction of oil retained by the omniphobic membrane was significantly lower than that by the PVDF membrane, as indicated by the very low pseudo-adhesion force measured in the baseline of the receding stage. In fact, the fraction of oil droplet retained by omniphobic membrane was even similar to that retained by the composite membrane with a superhydrophilic surface, even though the two surfaces have drastically different upon-contact interactions with the oil droplet. In this regard, the omniphobic membrane can be considered “attractive but not adhesive” to oil, which is consistent with the observation in the CA measurements that the oil droplet spread reasonably well on the omniphobic membrane surface but did not penetrate into the membrane pores because of the reentrant structure.

The presence of the excess synthetic surfactants, Triton X-100, in the solution where the force curve was measured, drastically changed the oil-membrane interaction. The force curve for the interaction of the oil droplet with the omniphobic membrane in the presence of the surfactants was similar to that with the composite membrane in DI water. The observation of the oil-membrane interaction in the presence of surfactants was very interesting but not particularly surprising. As

discussed in section 6.3.5, the surfactants 'wrapped' the oil droplets adsorbing onto the oil-water interface and rendered the oil droplets hydrophilic. Consequently, the attractive oil-membrane interaction was significantly reduced due to hydration force resulting from strong hydration of the hydrophilic heads of the adsorbed surfactants. Similar behavior of fouling mitigation has also been observed in a previous study in which Pickering emulsion stabilized by nanoparticles showed appreciably lower membrane fouling propensity in ultrafiltration compared to an emulsion stabilized simply by naturally occurring surfactants[148].

## 6.4. Conclusion

To successfully utilize MD to desalinate challenging saline wastewater with a complex composition, such as shale oil/gas produced wastewater or industrial brine, the selection of proper MD membrane is of vital importance. With the recent innovations in membrane materials, three types of membranes are currently available for MD operations, including conventional hydrophobic membranes, composite membranes with a superhydrophilic surface and a hydrophobic substrate, and omniphobic membranes. This study employs CA measurements, DCMD fouling and wetting experiments, as well as oil-probe force spectroscopy to systematically investigate the performance of different MD membranes for desalinating saline oil-water emulsions.

When the oil emulsion was stabilized only by a limited amount of naturally occurring surfactants, severe fouling was observed for both the hydrophobic and the omniphobic membranes due to the very low surface energy of these membranes that resulted in the attractive hydrophobic-hydrophobic interaction. However, the omniphobic membrane differed from the hydrophobic membrane in that the oil droplets could not penetrate into the pores of the omniphobic membrane due to the reentrant structure. The appropriate membrane to be employed for such a feed solution is the composite membrane with a superhydrophilic surface that has been shown to be capable of mitigating oil fouling and sustaining robust MD operation.

For feed solution containing crude oil droplets stabilized by excess synthetic surfactants, the membrane performance became dramatically different. Both the composite membrane and the hydrophobic PVDF membrane were eventually completely wetted by the excess surfactants, leading to near-zero salt rejection. While no fouling of the composite membrane was observed, the PVDF membrane was rapidly fouled first before wetting occurred. The omniphobic membrane,

on the other hand, was able to resist both fouling and wetting with this feed solution because the omniphobic membrane was intrinsically anti-wetting (as shown in previous studies) and the emulsified oil droplets became hydrophilic due to adsorbed surfactants on the oil-water interface.

**Acknowledgement**

The authors acknowledge the financial support from Bureau of Reclamation, Department of Interior, via DWPR Agreement R15AC00088.

# CHAPTER 7

# CONCLUSIONS AND FUTURE WORK

Membrane fouling and wetting are two prominent challenges limiting the wide application of membrane distillation (MD) in industry. In this dissertation, the mechanisms and mitigation strategies of membrane fouling and wetting in MD have been investigated. For the membrane fouling problem, it has been long known that the conventional hydrophobic membrane is prone to fouling by hydrophobic contaminants (e.g. oils) due to the strong hydrophobic-hydrophobic interaction underwater. In this dissertation, we utilized a composite membrane with an in-air superhydrophilic/underwater oleophobic surface layer and a hydrophobic substrate in MD operation with oily feed and found that the composite membrane can largely mitigate oil fouling problem because of the elimination of hydrophobic-hydrophobic interaction. In addition, we revealed that besides surface wetting property, the surface charge is also able to influence the fouling resistance of the MD membrane. For membrane wetting problem, despite of the efforts spent on mitigation strategy, the fundamental mechanism still remains unclear. To unveil the mechanism of membrane pore wetting, we firstly developed a novel impedance-based technique that is able to monitor the membrane wetting pore process in MD operations and then exploited this technique to study the membrane pore wettings induced by two different wetting agents, ethanol (a water-miscible and low-surface-tension liquid) and Triton X-100 (amphiphilic molecules). The results indicate that membrane pore wettings resulted from these two different wetting agents share the same wetting criterion but exhibit distinctive kinetics, and the difference in wetting dynamics stems from the adsorption of Triton X-100 onto the membrane pore surface. Furthermore, we developed a mathematical model for surfactant-induced membrane pore wetting process that can quantitatively predict the pore wetting breakthrough time regarding the MD operation conditions and surfactant properties. After all the studies on the mechanisms of membrane failures and mitigation strategies, we compared the performances of MD membranes with different wettability in MD operations with different types of feed, and developed a general membrane selection strategy for sustaining robust MD operations depending on feed type. A detailed summary of the conclusions from the main chapters of this dissertation is provided in the following:

*Chapter 2.* Inspired by the development of surface materials with special wettability in material science community, a composite membrane with an in-air superhydrophilic/underwater oleophobic surface layer and a hydrophobic substrate has been fabricated, characterized, and employed in direct contact membrane distillation (DCMD) operation with crude oil-in-water emulsion as feed. Compared with the conventional hydrophobic MD membrane, the composite MD membrane exhibited excellent fouling resistance in the DCMD operation. The oil probe force spectroscopy acquired with a force tensiometer indicates that the excellent fouling resistance of the composite membrane can be attributed to the elimination of the strong hydrophobic-hydrophobic interaction between the hydrophobic membrane surface and the oil droplet underwater. The results from this chapter suggest that composite membranes with asymmetric wettability can enable MD to desalinate hypersaline wastewater with high concentrations of hydrophobic contaminants.

*Chapters 3.* The efforts of developing anti-fouling membranes have so far been focusing on tailoring membrane surface wetting properties, whereas the impacts of surface charge are often eclipsed. In this chapter, we investigated the synergistic impact of surface wetting property and surface charge on anti-fouling property of the MD membrane. Two composite membranes with different surface charges were fabricated. The fabricated composite membranes and the pristine hydrophobic membrane were firstly characterized using contact angle measurements, and then tested in DCMD operations with crude oil-in-water emulsion as feed, respectively. It was found that the negatively charged composite membrane performed the best in mitigating membrane fouling by the negatively charged oil emulsion, followed by the positively charged composite membrane, with the pristine hydrophobic membrane being the most susceptible to oil fouling in MD operations. Oil probe force spectroscopy has been conducted for each membrane, and the results corroborated with the contact angle measurement results to unveil the anti-fouling mechanism associated with surface charge.

*Chapter 4.* Pore wetting is an important failure mechanism unique to MD. While it is well known that both low-surface-tension and water miscible liquids, such as alcohols, and amphiphilic molecules, such as surfactants, are effective wetting agents, the detailed mechanisms for these agents to induce pore wetting remain unclear. In particular, the role of surface adsorption in surfactant-induced wetting remains to be elucidated. To obtain the fundamental insights to

understanding the mechanism of pore wetting, we developed a novel and simple method, based on measurement of cross-membrane impedance, for monitoring the dynamics of membrane pore wetting and enabling early detection of imminent wetting-based membrane failure. Using this wetting monitoring method, we experimentally probed the kinetics of wetting frontier propagation induced by different wetting agents including ethanol and Triton X-100 surfactant. We demonstrated that ethanol-induced wetting is instantaneous whereas surfactant-induced wetting is dynamic with its kinetic rate dependent on several critical factors. We also developed a theoretical model to qualitatively explain the important features experimentally observed in surfactant-induced membrane pore wetting. Specifically, it was found that the kinetics of surfactant-induced wetting strongly depends on the vapor flux and the bulk concentration of surfactants in the feed solution, but surprisingly not on the transmembrane hydraulic pressure difference. The results from this chapter also suggest that while the presence of surfactants promotes wetting, adsorption of surfactants onto pore surface actually deters pore wetting instead of promoting it by rendering the surface hydrophilic.

*Chapter 5.* To enrich the understanding of the mechanism of surfactant-induced pore wetting in MD, in this chapter, we developed a mathematical model, based on surfactant transport in a partially wetted membrane pore under the pseudo-steady state assumption, to quantify the kinetics of pore wetting. The developed model predicted several key dependences of wetting kinetics on operating parameters and solution properties, which were highly consistent with results from MD experiments using feed solution containing sodium dodecyl sulfate. It was found that kinetics of pore wetting is strongly dependent on vapor flux, surfactant concentration, but relatively independent of the transmembrane hydraulic pressure. The critical surfactant concentration below which pore wetting does not occur was also predicted by the wetting model. In addition, the wetting propensity of different surfactant species was investigated, and the membrane pore wetting predictions from the developed model matched the experimental results very well, which further validated the developed model. The results indicate that for membrane wettings induced by different surfactants, the surface excess concentration is the most important surfactant property in affecting the pore wetting kinetics. Other parameters of a surfactant, such as molecular charge and hydrophilic-lipophilic balance, have no observable direct impact on the wetting kinetics.

*Chapter 6.* In this chapter, we systematically investigated the impact of the surface wetting properties on the membrane wetting and/or fouling behaviors in MD. Specifically, we compared the wetting and fouling resistance of three types of membranes of different wetting properties, including hydrophobic and omniphobic membranes as well as composite membranes with a hydrophobic substrate and a superhydrophilic top surface. We challenged the MD membranes with hypersaline feed that contained a relatively high concentration of crude oil with and without added synthetic surfactant, Triton X-100. We found that the composite membranes with superhydrophilic top surface were robustly resistant to oil fouling in the absence of Triton X-100, but were subject to pore wetting in the presence of Triton X-100. On the other hand, the omniphobic membranes were easily fouled by oil-in-water emulsion without Triton X-100, but successfully sustained stable MD performance with Triton X-100 stabilized oil-in-water emulsion as the feed solution. In contrast, the conventional hydrophobic membranes failed readily regardless whether Triton X-100 was present, although via different mechanisms. These findings are corroborated by contact angle measures as well as oil-probe force spectroscopy. This chapter provides a holistic picture regarding how a hydrophobic membrane fails in MD and how we can leverage membranes with special wettability to prevent membrane failure in MD operations.

*Future Work.* This dissertation can be further extended from the following perspectives:

- The composite MD membrane should be further tested with real hypersaline wastewater rich of hydrophobic contaminants (e.g. shale oil/gas produced water) as feed to confirm its practical viability in field work.
- Besides surface wettability and surface charge, other surface properties of MD membrane can be further investigated to construct MD membranes with more robust fouling resistance.
- The mechanism of membrane pore wetting induced by inorganic fouling (e.g. salt scaling) still remains unknown and needs to be explored.
- A novel MD membrane that has simultaneous fouling and wetting resistances is needed.

APPENDIX A

SUPPLEMENTARY MATERIALS FOR CHAPTER 2

## Membrane Porosity Quantification

The porosity of the membrane was defined as the volume of the pores divided by the total volume of the membrane. The flat-sheet membrane porosity $\varepsilon$ was determined by gravimetric method and calculated by the following equation[262]:

$$\varepsilon = \frac{m_1 - m_2}{\rho_L \cdot A \cdot l} \quad (A\,1)$$

where $m_1$ is the weight of the wet membrane, $m_2$ is the weight of the dry membrane, $\rho_L$ is the liquid density, $A$ is the effective area of the membrane and $l$ is the membrane thickness. The liquid used for porosity measurement named Porefil was supported by IB-FT GmbH (Germany) and its surface tension and density were 16 dyn/cm and 1.87 g/ml, respectively.

## Pore Size Distribution

The pore size distribution of the membrane was investigated by using a Capillary Flow Porometer, CFP (Porolux 1000, IB-FT GmbH, Germany). The membrane sample was fully wetted with the Porefil, and then the measurement was carried out following the procedure described in literature[121]. The CFP was fully automated to generate the pore size distribution following the cited method.

## Liquid Entry Pressure

The liquid entry pressure (LEP) of water was obtained using the method described by Smolders and Franken[122]. The membrane sample with effective area of 2.69 $cm^2$ was assembled into a test membrane cell filled with distilled water. Hydraulic pressure was gradually increased by regulating the outlet pressure of the nitrogen cylinder. The minimum applied pressure at which a continuous liquid flow was observed was recorded as the LEP.

## Chemical Evidence for Surface Modification

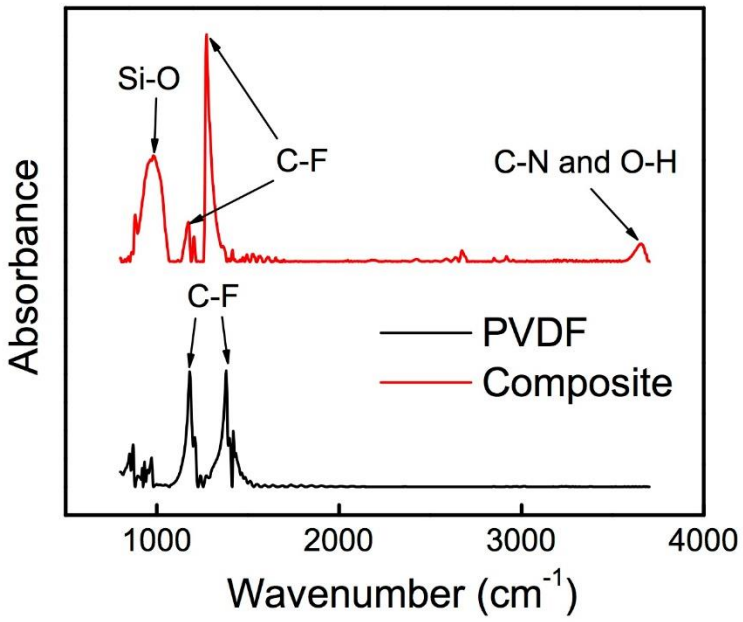


Figure A.1 Polarization Modulation-Infrared Reflection-Adsorption Spectroscopy (PM-IRRAS) for the PVDF and the modified surface of the composite membrane. The major difference between the two spectra is the presence of additional bonds such as Si-O, C-N, and O-H that are characteristic of the nanocomposite (silica nanoparticles/chitosan/PFO) employed for surface modification.[263–266]

APPENDIX B

SUPPLEMENTARY MATERIAL FOR CHAPTER 3

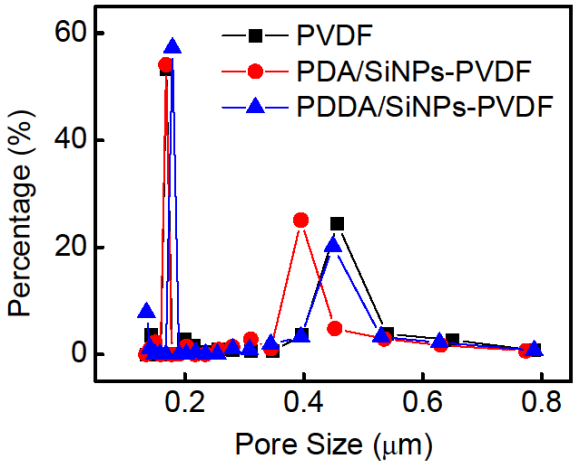


Figure B.1 Pore size distributions of PVDF membrane (black squares), PDA/SiNPs-PVDF composite membrane (red circles) and PDDA/SiNPs-PVDF composite membrane (blue triangles). The distributions are bimodal in all cases.

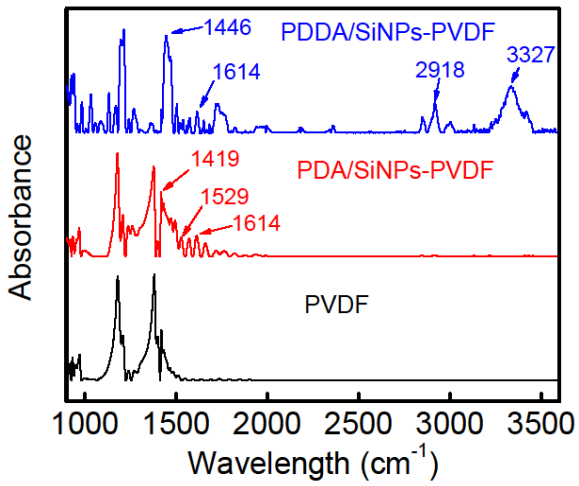


Figure B.0.2 Infrared absorbance spectra obtained from PMIRRAS for the PVDF membrane (black curve), PDA/SiNPs-PVDF composite membrane (red curve) and PDDA/SiNPs-PVDF composite membrane (blue curve). In the spectrum of PDA/SiNPs-PVDF composite membrane, the peak at 1617 $cm^{-1}$ resulted from C=C resonance vibration in the aromatic ring and N-H bending; the peak at 1529 $cm^{-1}$ was attributed to the N-H shearing vibration and N-O stretching; the peak at 1419 $cm^{-1}$ was attributable to phenolic O-H deformation and phenolic C-O stretching

[267,268]. In the spectrum of PDDA/SiNPs-PVDF composite membrane, the peaks at 1614 $cm^{-1}$ was owing to the deformation vibration of N-H; the peaks at 1446 $cm^{-1}$ and 2918 $cm^{-1}$ were resulted from C-H bending; the peak at 3327 $cm^{-1}$ was attributed to a deformation vibration of N-H and a stretching vibration of $–NR_3^+$

APPENDIX C

SUPPLEMENTARY MATERIAL FOR CHAPTER 4

**Selection of Frequency for Impedance Measurement**

The selection of a specific frequency for measuring the time-resolved impedance across the MD membrane follows two basic principles. First, the phase should not be close to zero so that capacitive contribution becomes insignificant. Second, the initial overall impedance should be reasonably high before any wetting occurs so that the measurement of the impedance change can be more accurate. Following these rules, we conducted an EIS measurement in the frequency range of $10^3$ to $10^6$ Hz and summarized the dependence impedance and phase on frequency in a Bode plot (Figure C.1). The measurement was conducted in an operating DCMD system with surfactant-free saline feed solution. Based on these spectra, we chose a working frequency of $10^5$ Hz. Other medium frequencies should also work, as long as they are not too high in which case the impedance is too low, or not low in which case the phase is too high (close to 0).

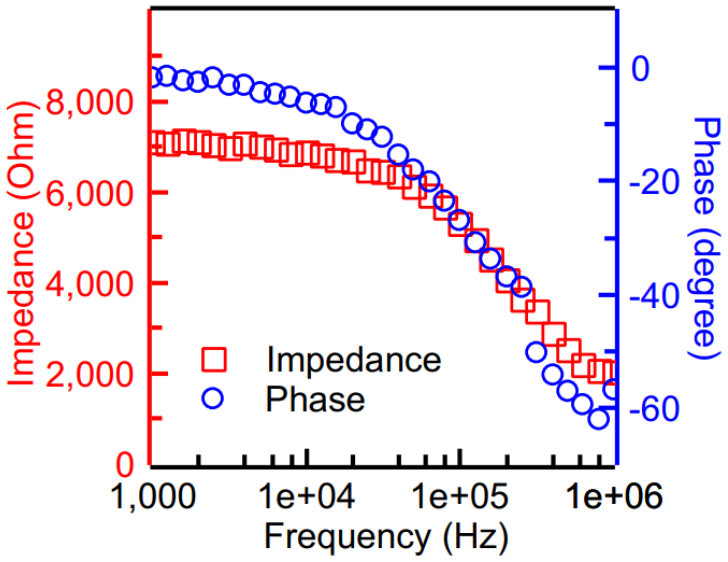


Figure C.1 Impedance (red squares, left Y-axis) and phase angle (blue circles, right Y-axis) spectra of a PVDF membrane in DCMD operation with 0.6 M NaCl solution on feed side and DI water on permeate side.

**Justification of using transmembrane hydraulic pressure instead of feed hydraulic pressure for wetting analysis**

In this analysis, we present the proof that the transmembrane hydraulic pressure, $\Delta P$, instead of the hydraulic pressure of the feed stream, should be used to compared LEP as a criterion for pore wetting. Such a proof was first given by Zmievskii[207] and is simply summarized here. We start with conducting a force balance analysis on the water and air trapped in an ideal cylindrical pore between the feed solution and the distillate (Figure C.2).

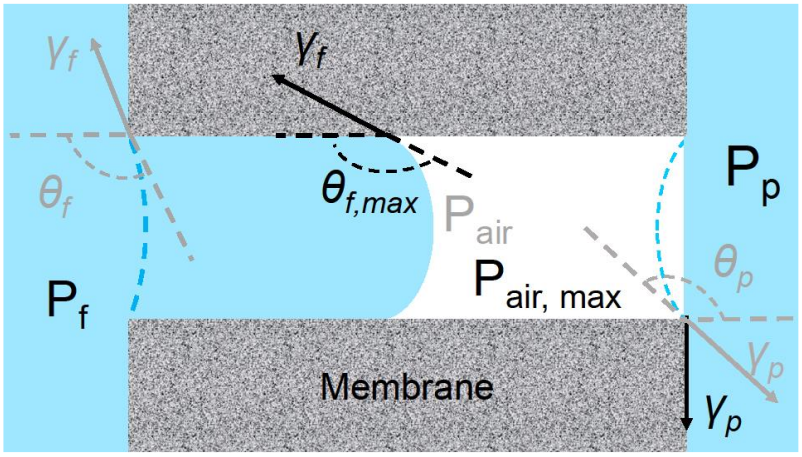


Figure C.2 Schematic of membrane pore wetting in DCMD. $P_f$ and $P_p$ are the applied hydraulic pressures on the feed and permeate sides, respectively. $P_{air}$ is the pressure of the trapped air in the membrane pore. $\gamma_f$ and $\gamma_p$ are the surface tensions of the feed and permeate solutions, respectively. $\theta_f$ and $\theta_p$ are the contact angles of the feed and permeate solutions on the PVDF membrane surface, respectively.

Let us assume that the hydraulic pressure on the feed side, $P_f$, is higher than that on the distillate side, $P_p$, so that $\Delta P$ is always positive. The force balance for the feed solution and distillate within the pore can be described by the two following equations:

$$P_f \pi R^2 = P_{air} \pi R^2 + (-\cos\theta_f)\gamma_f 2\pi R \quad \text{(C1)}$$

$$P_p \pi R^2 = P_{air} \pi R^2 + (-cos\,\theta_p)\gamma_p 2\pi R \quad \text{(C2)}$$

where $R$ is the radius of the membrane pore; $P_{air}$ is the pressure of air trapped in the membrane pore; $\theta_f$ and $\theta_p$ are the intrinsic contact angles of the feed solution and the distillate on the membrane material, respectively; $\gamma_f$ and $\gamma_p$ are the surface tensions of the feed solution and distillate, respectively.

When feed solution has not yet intruded into the membrane pore, increasing $P_f$ first increases $\theta_f$. But $P_{air}$ remains constant because the increasing curvature of feed/air interface barely changes the volume of the air trapped in the pore. Based on equation C1, the increased hydraulic pressure on the feed solution is balanced by the increased interfacial force caused by an increased $\theta_f$. As $P_f$ further increases, $\theta_f$ will reach a maximum, $\theta_{f,max}$, that is determined by the surface tensions of the feed solution and membrane material. Further increasing $P_f$ will lead to intrusion of the feed solution into the pore, which will in turn compress the air trapped in the pore and increase its pressure.

Once the air pressure starts to increases, force balance on the distillate (equation C2) dictates that $\theta_p$ decreases because $P_{air}$ increases yet $P_p$ remains constant. As $P_{air}$ continues to increase, $\theta_p$ will become less than zero and an air bubble will emerge in the distillate until $\theta_p$ reaches $-90°$. Further increase of $P_{air}$ will cause detachment of air bubble, which will result in destabilization of the system and complete pore wetting. At this critical point of pore wetting, equations C1 and C2 can be combined to obtain equation C3, with $\theta_f = \theta_{f,max}$ and $\theta_p = -90°$:

$$\left(P_f - P_p\right)\pi R^2 = \left(-\cos\theta_{f,max}\right)\gamma_f \cdot 2\pi R \tag{C3}$$

Rearranging equation C3 yields equation C4:

$$\Delta P = P_f - P_p = \frac{-2\gamma_f}{R}\cos\theta_{f,max} = LEP \tag{C4}$$

Equation C4 suggests that at the critical point of pore wetting, LEP should be equal to the transmembrane hydraulic pressure difference, $\Delta P$, not the feed hydraulic pressure, $P_f$. Therefore, the criterion for pore wetting is that $\Delta P > LEP$.

**Derivation of Equation 4.3**

According to Poiseuille equation[269,270],

$$\Delta P - LEP = \frac{8\mu l Q}{\pi r^4} \tag{C5}$$

where $\Delta P$ is the applied transmembrane pressure, $LEP$ is the liquid entry pressure of the membrane pore, $l$ is the distance between the wetting frontier and the pore entrance, $\mu$ is the dynamic viscosity, $Q$ is the volumetric flow rate (i.e. $Q = \pi r^2 \frac{dl}{dt}$), $r$ is the pore radius. Rearranging equation C5 gives

$$ldl = \frac{8(\Delta P - LEP)\mu}{r^2}dt \tag{C6}$$

Integrating equation C6 from $l = 0$ to $l$, and $t = 0$ to $t$, we can obtain,

$$\frac{l^2}{2} = \frac{(\Delta P - LEP)r^2}{8\mu}t \tag{C7}$$

We can get equation C8, which is equation 4.3 in the main text, from rearranging equation C7

$$l(t) = \sqrt{\frac{R^2}{4\mu}(\Delta P - LEP)t} \tag{C8}$$

In our experiments, $r = 0.225\ \mu m$, $\mu = 0.47\ mPa \cdot s$, for $\Delta P - LEP = 0.25\ kPa$, which is a very small pressure, the time $t$ it takes for the liquid to penetrate through the entire membrane ($l(t) = d_0$, where the membrane thickness $d_0 = 180\ \mu m$) is calculated to be $1.22\ s$.

**Partial Differential Equation for Surfactant Transport**

The partial differential equation regarding the diffusion-convection-adsorption of surfactant within a partially wetted pore[209],

$$\frac{\partial c}{\partial t} + \frac{2}{r}\frac{\partial \tau}{\partial t} = D\frac{\partial^2 c}{\partial x^2} + D_{sl}\frac{2}{r}\frac{\partial^2 c}{\partial x^2} - (\frac{J}{\varepsilon} + v_s)\frac{\partial c}{\partial x} \tag{C9}$$

Where $c$ (abbreviation for $c(x,t)$) is the concentration of surfactants at position $x$, and time $t$, $\tau$ is the surface concentration of the surfactant on the pore surface, $R$ is the pore radius, $D$ is the diffusion coefficient of surfactants in the solution, $D_{sl}$ is the surface diffusion coefficient over the filled portion of the pore, $J$ is the vapor flux, $\varepsilon$ is the porosity of the membrane, $v_s$ is the moving speed of the solution in the pore ($v_s \ll \frac{J}{\varepsilon}$ in our experiments). The initial conditions for the equation is $c = 0$ except for $c(0,0) = c_0$, where $c_0$ is the surfactant concentration in the bulk solution. The left-hand-side boundary condition is $c(0,t) = c_0$, and the right-hand-side boundary condition is $c(l,t) = c'$, where $c'$ is the critical concentration of surfactant that satisfies $LEP = \Delta P$.

**Relative Insignificance of Axial Diffusion**

According to literatures[212,271,272], $D = 4 \times 10^{-7} cm^2 s^{-1}$, and the adsorption occurs so fast that the pore surface would be saturated immediately as the solution is in contact with the pore

surface ($\frac{\partial \tau}{\partial t} = 0$ for $c \neq 0$). We can solve a specific case of the PDE at steady state with $J = 14$ L m$^{-2}$ h$^{-1}$ (relatively low), $c_0 = 0.08\, mM$, $c^* = 0$ (the extreme case), and $l = 30\ \mu m$ (less than 20% of the membrane thickness). The result is plotted in Figure C.3. In this specific case, the diffusion term at the pore entrance, $D \frac{dc}{dx}\Big|_{x=0}$, is only 3.22% of the convection term, $Jc_0$. This suggests that except for the beginning of the wetting when $l$ is very short, axial diffusion is relatively insignificant compared to convection for surfactant transport, and can thus be numerically ignored. When a higher $J$ or/and $c^*$, the axial diffusion at the pore entrance will become even more negligible compared to convection.

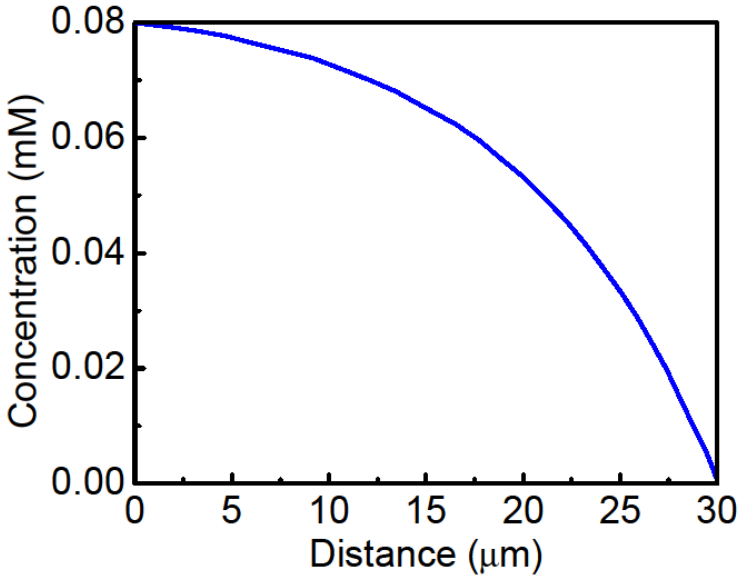


Figure C.3 The concentration profile of Triton X-100 in the solution for $l = 30\ \mu m$. In this specific case, the bulk concentration $c_0 = 0.08\, mM$, the critical concentration $c^* = 0$, the diffusion coefficient $D = 4 \times 10^{-7} cm^2 s^{-1}$, and the vapor flux with $J = 14$ L m$^{-2}$ h$^{-1}$.

**Derivation of Equation 4.8**

As the membrane is equivalent to a parallel circuit of a resistor and a capacitor and at a high frequency (100 kHz), the transmembrane impedance is approximately equal to the impedance of the capacitor. The capacitance of the capacitor $C$ can be calculated as

$$C = \frac{\varepsilon_p A}{d} \tag{C10}$$

Where, $\varepsilon_p$ is the permittivity of the air, $A$ is the area of the air, $d$ is the distance between the two air-liquid interfaces across the membrane. Following the equation of capacitor impedance calculation, the transmembrane impedance $Z$ can be obtained with the frequency $\omega$ and imaginary unit $i$

$$Z = \frac{1}{i\omega C} \tag{C11}$$

The distance $d$ can be expressed using the membrane thickness $d_0$, and the position of the wetting frontier at time $t$, $l(t)$:

$$d = d_0 - l(t) \tag{C12}$$

Combining equations C10 to C12 yields

$$Z = \frac{d_0 - l(t)}{i\omega\varepsilon_p A} \tag{C13}$$

Normalizing $Z$ with $Z_0$ yields

$$\frac{Z}{Z_0} = \frac{d_0 - l(t)}{d_0} \tag{C14}$$

which is equation 4.8 in the main text.

**Surface Tension Measurements**

The results of surface tension measurement using pedant drop method are shown in Figure C.4. Figure C.4 suggests that both the 20 wt% ethanol salty solution (red circles) and 50 ppm Triton X-100 salty solution have a surface tension of ~35 mN/m. Therefore, in our wetting experiments to compare the wetting behaviors of ethanol and Triton X-100, 20 wt% ethanol salty solution and 50 ppm Triton X-100 salty solution were chosen as the feed solutions, respectively.

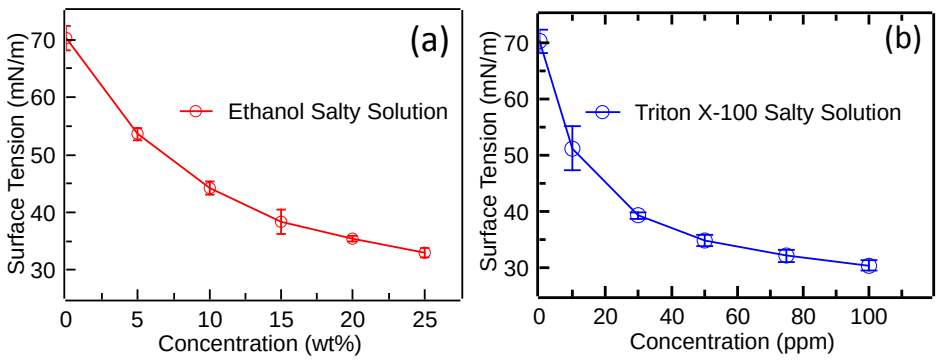


Figure C.4 The surface tensions of 0.6 M NaCl aqueous solutions with different concentrations of (a) ethanol (red circles), and (b) Triton X-100 (blue squares) at 60 °C.

**Water Flux and Salt Rejection Rate**

The normalized water fluxes and salt rejection rate as functions of time in DCMD experiments are shown in Figure C.5, C.6, C.7, C.8, and C.9. In all DCMD experiments, the baseline normalized water flux was 1, and the initial salt rejection rate was near 100%. As the membrane became wetted, some membrane pores were fully wicked through by the feed solution, resulting in a drastically reduced salt rejection rate and significantly increased normalized water flux. The increase of normalized water flux could be attributed to the fact that the fully wicked-through membrane pores became available for convective liquid water flow. As the hydarulic pressure on the feed side was controlled to be higher than that on the distillate side, the convective water flow through the wicked-through pores was always from the feed stream to the distillate stream. Because such a hydraulic pressure driven convective water flux was significantly faster than the vapor flux driven by partial vapor pressure difference, the total water flux, as a sum of the liquid flux and vapor flux, increased as more pores became fully wicked through.

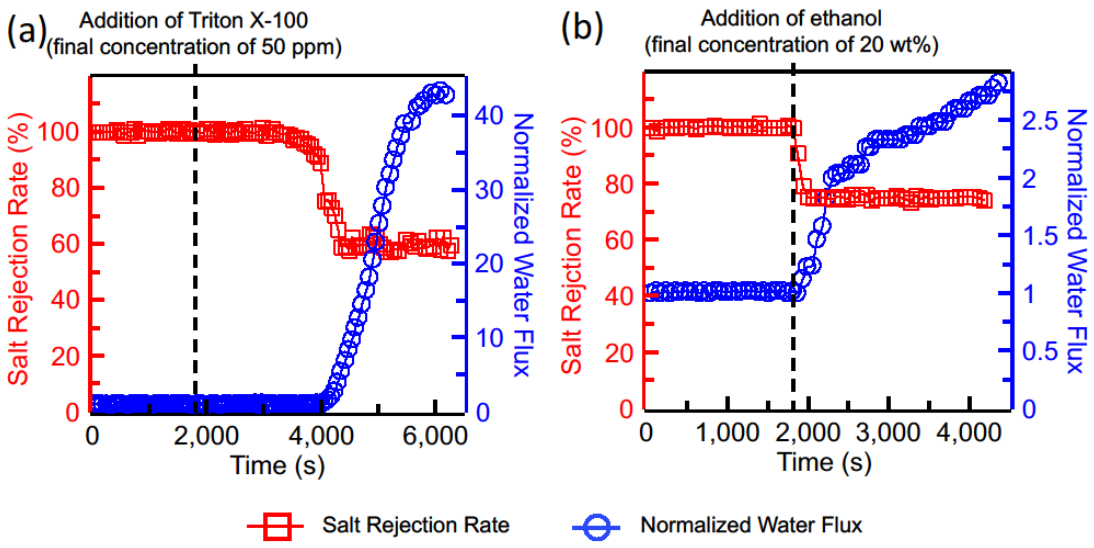


Figure C.5 Salt rejection rate (red rectangle, left Y-axis) and normalized water (liquid and vapor) flux (blue circle, right Y-axis) in DCMD experiments the impedance and salt rejection rate of which are reported in Figure 4.3 of the main text. The water fluxes are normalized by the initial water fluxes of the respective measurements. The initial water (only vapor, no liquid) fluxes in (a) and (b) were 29.48 and 29.95 LMH, respectively.

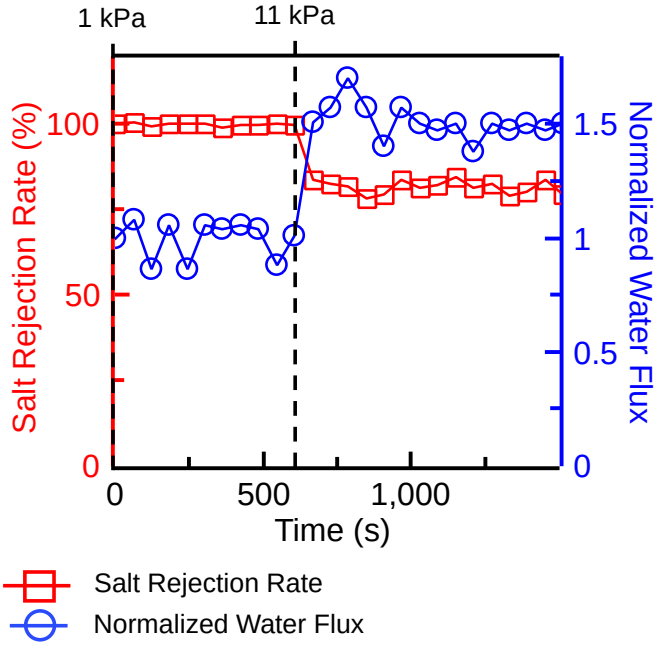


Figure C.6 Salt rejection rate (red rectangle, left Y-axis) and normalized water (liquid and vapor) flux (blue circle, right Y-axis) in DCMD experiments the impedance and salt rejection rate of which are reported in Figure 4.4 of the main text. The water flux is normalized by the initial water flux. The initial water (only vapor, no liquid) flux was 29 LMH.

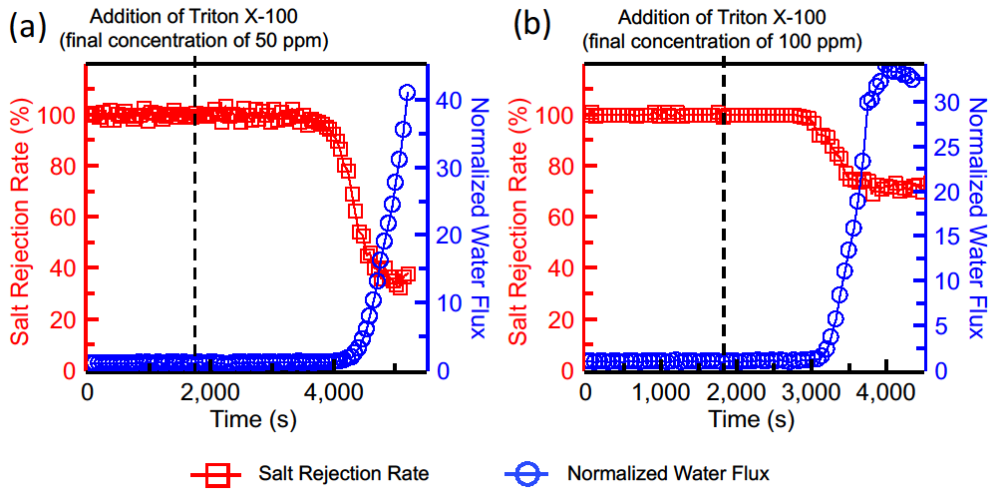


Figure C.7 Salt rejection rate (red rectangle, left Y-axis) and normalized water (liquid and vapor) flux (blue circle, right Y-axis) in DCMD experiments the impedance and salt rejection rate of which are reported in Figure 4.5a of the main text. The water fluxes are normalized by the initial water fluxes of the respective measurements. The initial water (only vapor, no liquid) fluxes in (a) and (b) were 29.48 and 29 LMH, respectively.

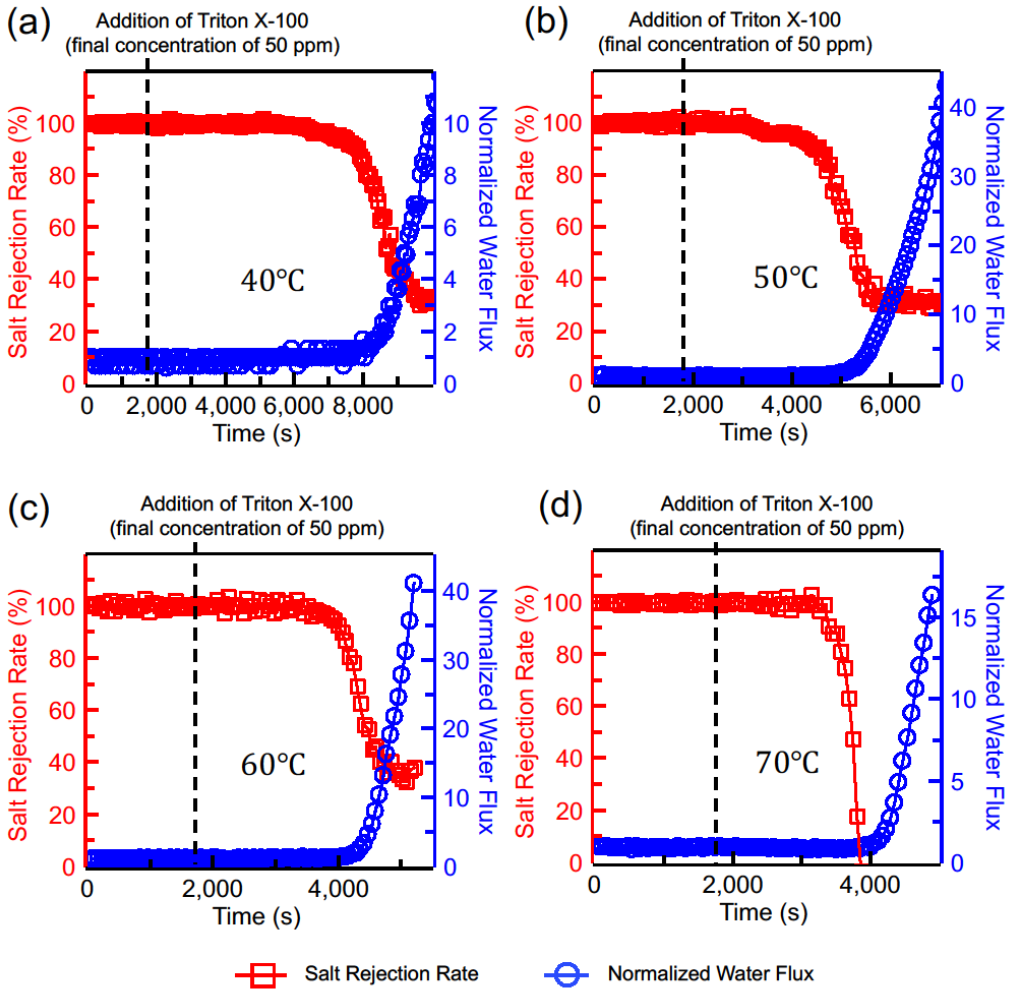


Figure C.8 Salt rejection rate (red rectangle, left Y-axis) and normalized water (liquid and vapor) flux (blue circle, right Y-axis) in DCMD experiments the impedance and salt rejection rate of which are reported in Figure 4.5b of the main text. The water fluxes are normalized by the initial water fluxes of the respective measurements. The initial water (only vapor, no liquid) fluxes in (a) (b), (c), and (d) were 8.60, 14.97, 29.95, and 47.13 LMH, respectively.

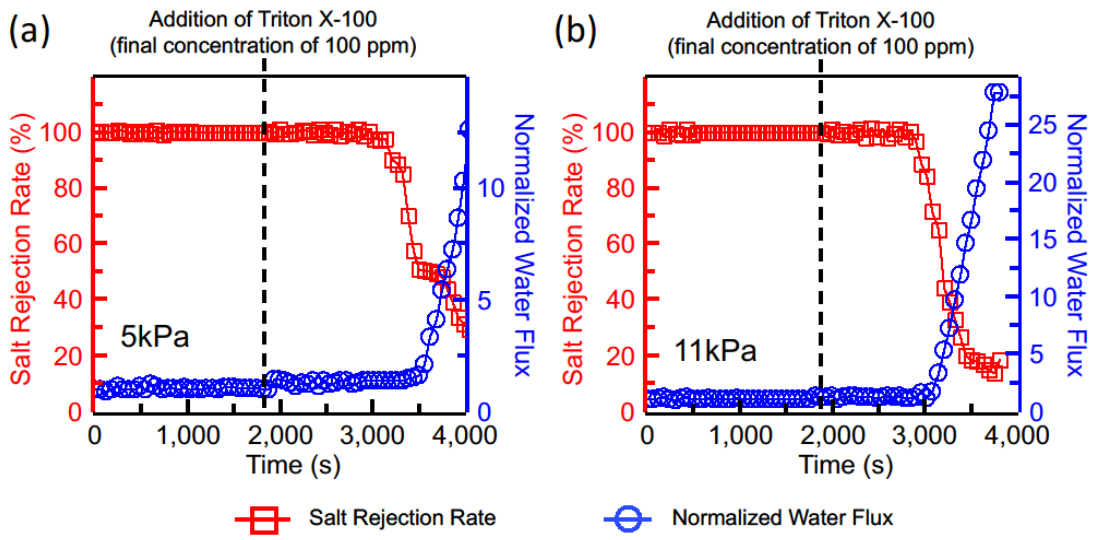


Figure C.9 Salt rejection rate (red rectangle, left Y-axis) and normalized water (liquid and vapor) flux (blue circle, right Y-axis) in DCMD experiments the impedance and salt rejection rate of which are reported in Figure 4.6 of the main text. The water fluxes are normalized by the initial water fluxes of the respective measurements. The initial water (only vapor, no liquid) fluxes in (a) and (b) were 28.85, and 29.48 LMH, respectively.

APPENDIX D

SUPPLEMENTARY MATERIAL FOR CHAPTERS 5

**Derivation of mass balance equation for surfactants (Eq. 5.3).**

Eq. 5.3 with a slight modification is shown below and denoted as Eq. 5.3'. Eq. 5.3 in the main text can be obtained by dividing both sides of Eq. 5.3' by $\pi R^2$. Eq. 5.3 or Eq. 5.3' describes the mass balance of surfactants in the control volume (CV, including boundary layer and pores). The definition of each term can be found in the main text and the nomenclature. Here, we provide a more detailed description of the meaning of each term.

$$\begin{aligned}\frac{\pi R^2}{\varepsilon}\left(J_w c_0 - D\frac{\partial c(x,t)}{\partial x}_{x=0}\right)dt \\ = \frac{\pi R^2}{\varepsilon}\int_0^{\delta_b}[c(x,t+dt)-c(x,t)]dx \\ + \left\{\int_{\delta_b}^{\delta_b+l(t+dt)}[\tau(x,t+dt)2\pi R(1-\varepsilon)+c(x,t+dt)\pi R^2]dx\right. \\ \left. - \int_{\delta_b}^{\delta_b+l(t)}[\tau(x,t)2\pi R(1-\varepsilon)+c(x,t)\pi R^2]dx\right\}\end{aligned} \tag{5.3'}$$

Here we consider a cylindrical pore of radius R and its corresponding portion in the boundary layer. Because the boundary layer has no solid material and is 100% porous, the area of the boundary layer corresponding to a pore of an area $\pi R^2$ is $\pi R^2/\varepsilon$. The first term on the left-hand-side (LHS), $J_w c_0 \pi R^2/\varepsilon$, is the convective flux of the surfactants into the CV corresponding to a pore (including the boundary layer outside the pore). The second term on the LHS is the diffusive flux of surfactants into the same CV. The first integral on the right-hand-side (RHS) represents the accumulation of surfactants in the boundary layer from $t$ to $t + dt$.

The first part of the second integral on the RHS, $\int_{\delta_b}^{\delta_b+l(t+dt)}\tau(x,t+dt)2\pi R(1-\varepsilon)dx$, quantifies the amount of surfactant on the pore surface at time $t + dt$. The term $(1-\varepsilon)$ accounts for the fact that a pore does not have continuous, non-porous wall across the thickness of the membrane. Rather, we assume the isotropy for the membrane porosity so that the available area of solid surface in the pore is $(1-\varepsilon)$ of the area calculated using a cylindrical tube (i.e.

$\pi R^2 l(t + dt)$). The second part of the second integral on the RHS is the amount of surfactant in the solution within the pore. The third integral on the RHS is almost exactly the same as the second integral on the RHS except for a different time point, $t + dt$ (instead of t). Together, the difference between the second and the third integrals on the RHS represents the accumulation of surfactants within a pore (not including the boundary layer). The RHS quantifies the accumulation of surfactants within a CV including both the pore and the boundary layer.

**Surfactant adsorption isotherm.**

Assuming Langmuir adsorption isotherm for SDS adsorption onto PVDF surface[227,273], the area density of the adsorbed SDS on PVDF surface, $\tau$, can be expressed as

$$\tau = \tau_{max} \frac{Kc}{1 + Kc} \quad \text{(D1)}$$

where $\tau_{max}$ is the maximum area density of SDS on PVDF surface and K is an equilibrium constant that governs the partition of SDS between the pore surface and the solution phase. According to literature[227], K can be approximated as 180 $mM^{-1}$. In our study, the minimum $c_0$ we utilized was over 0.1 mM. According Eq. D1, with $K = 180\ mM^{-1}$ and $c = 0.1\ mM$, $\tau = 0.95\tau_{max}$. With all other concentrations tested, the pore surface can be considered to be practically saturated with SDS as long as it is in contact with the solution, in which case we can simplify the Langmuir adsorption isotherm to a stepwise adsorption isotherm:

$$\tau = \begin{cases} \tau_{max}, c > 0 \\ 0, c = 0 \end{cases} \quad \text{(D2)}$$

**Summary of experimental conditions of DCMD wetting experiments**

Table D1. . Summary of experimental conditions of DCMD wetting experiments

| Experiment No. | SDS concentration (mM) | Feed temperature (°C) | Permeate temperature (°C) | Feed velocity (m/s) | Permeate velocity (m/s) |
|---|---|---|---|---|---|
| (1) | 0.85 | 60 | 20 | 0.29 | 0.18 |
| (2) | 0.77 | 60 | 20 | 0.29 | 0.18 |
| (3) | 0.68 | 60 | 20 | 0.29 | 0.18 |
| (4) | 0.60 | 60 | 20 | 0.29 | 0.18 |
| (5) | 0.51 | 60 | 20 | 0.29 | 0.18 |
| (6) | 0.43 | 60 | 20 | 0.29 | 0.18 |
| (7) | 0.34 | 60 | 20 | 0.29 | 0.18 |
| (8) | 0.17 | 60 | 20 | 0.29 | 0.18 |

| | | | | | |
|---|---|---|---|---|---|
| (9) | 0.43 | 70 | 20 | 0.29 | 0.18 |
| (10) | 0.43 | 65 | 20 | 0.29 | 0.18 |
| (11) | 0.43 | 55 | 20 | 0.29 | 0.18 |
| (12) | 0.43 | 50 | 20 | 0.29 | 0.18 |
| (13) | 0.43 | 40 | 20 | 0.29 | 0.18 |
| (14) | 0.43 | 35 | 20 | 0.29 | 0.18 |
| (15) | 0.43 | 62 | 20 | 0.18 | 0.18 |
| (16) | 0.43 | 62 | 20 | 0.29 | 0.02 |

**Water fluxes and salt rejection rates data for Fig. 5.2.**

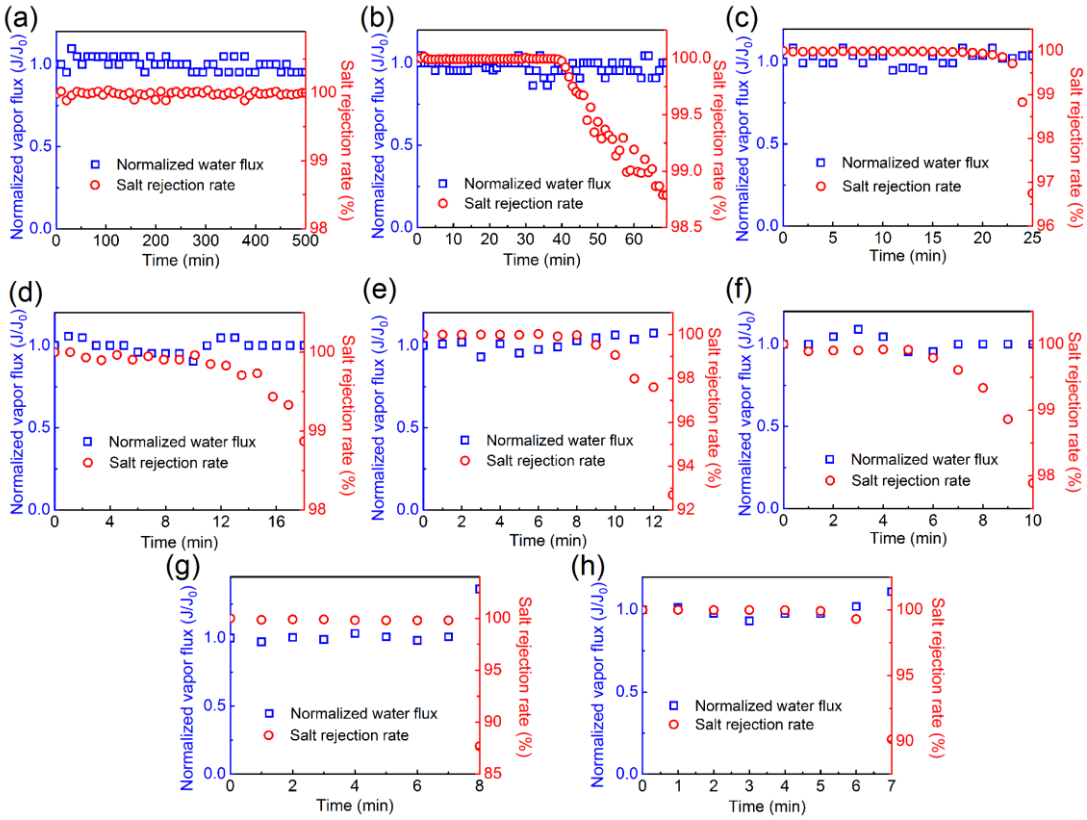


Figure D.1 Normalized water fluxes and salt rejection data for DCMD membrane wetting experiments (experiments 1-9 in Table D1). In each panel, the water vapor fluxes were normalized by the initial vapor flux. The initial water vapor fluxes were (a) 31.2, (b) 32.7, (c) 32.2, (d) 31.2, (e) 31.4, (f) 32.7, (g) 31.8, and (h) 33.5 L $m^{-2}$ $h^{-1}$, respectively. The transmembrane hydraulic pressure in all the experiments was 6 kPa. We note that after the membrane was wetted, the normalized water flux increased over unity. This is because the higher hydraulic pressure of the feed stream (than that of the distillate stream) drives convective flow of feed solution through the wetted pores, thereby increasing the total flux.

**Water fluxes and salt rejection rates data for Fig. 5.3.**

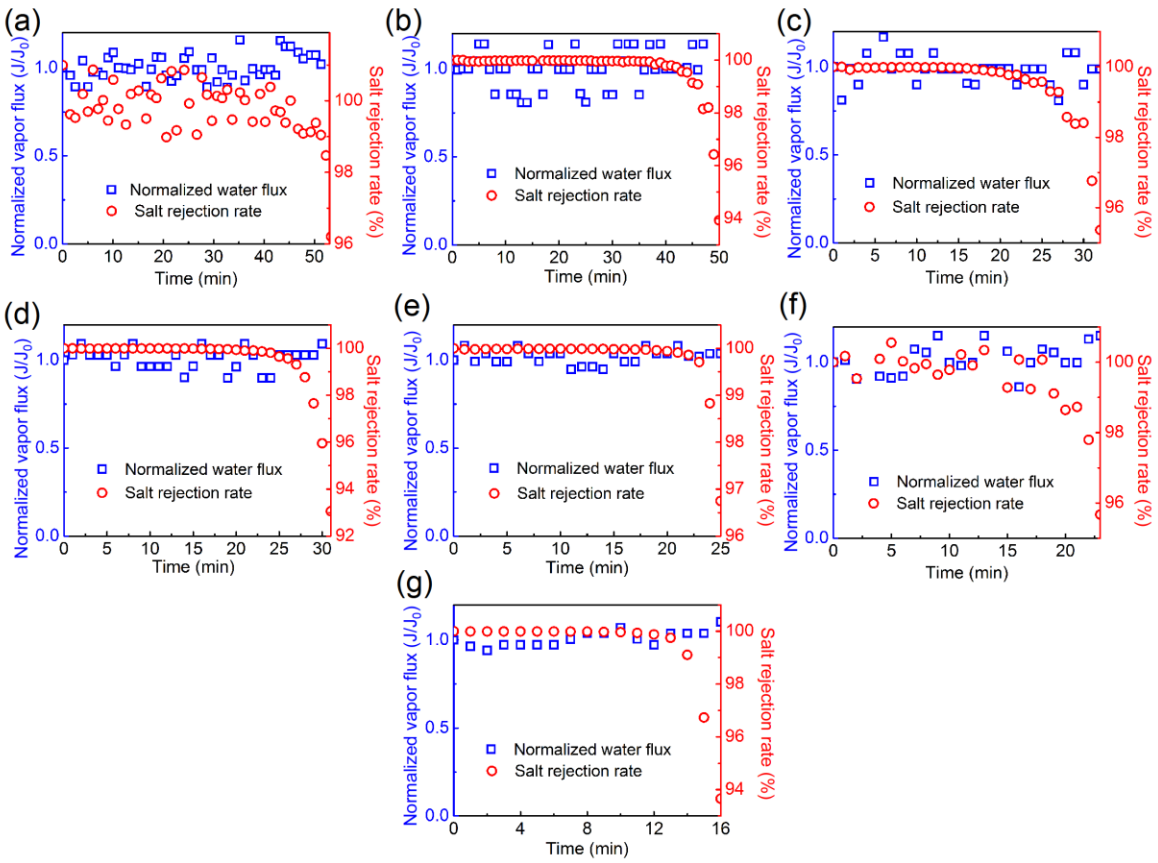


Figure D.2 Normalized water fluxes and salt rejection rates data for DCMD membrane wetting experiments (experiments 6 and 10-14 in Table D1) with initial vapor fluxes of (a) 6.0, (b) 10.3, (c) 16.5, (d) 23.1, (e) 32.2, (f) 39.2, and (g) 45.8 L $m^{-2}$ $h^{-1}$, respectively. In each panel, the water fluxes were normalized by the initial vapor flux. The SDS concentration of 0.43 mM and the transmembrane hydraulic pressure of 6 kPa were used in all the experiments. The normalized water flux increased over unity after wetting occurred, as explained in the caption Fig. D1.

**Water fluxes and salt rejection rates data for Fig. 5.4.**

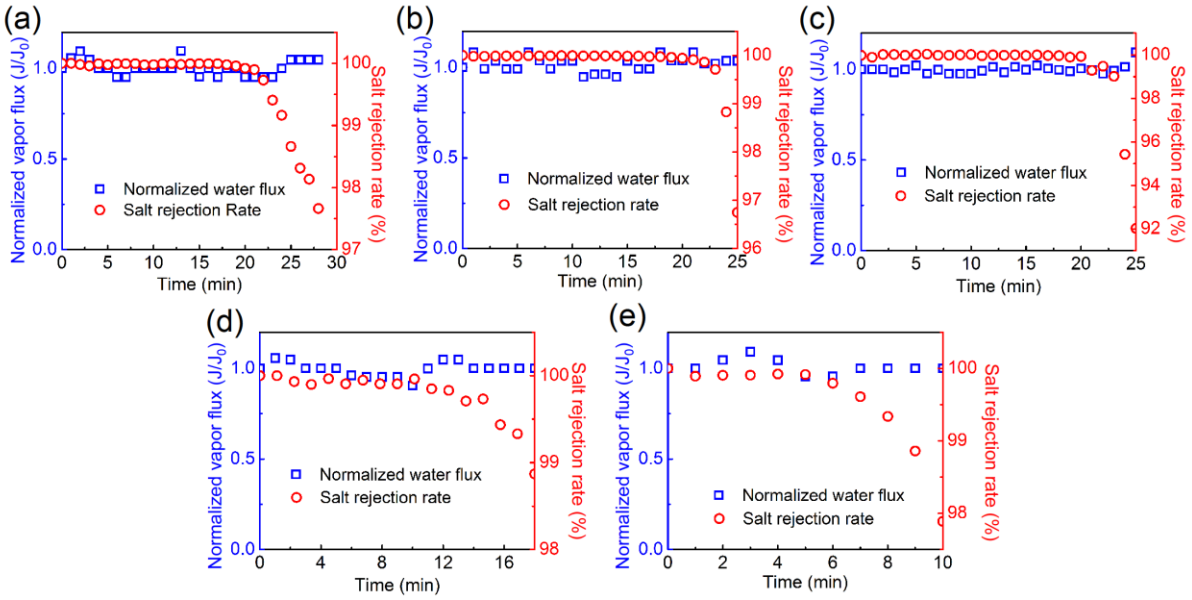


Figure D.3 Normalized water fluxes and salt rejection rates data for DCMD membrane wetting experiments (experiments 6, 15 and 16 in Table D1) with SDS concentration of 0.43 mM and transmembrane hydraulic pressure of (a) 0 kPa, (b) 6 kPa, and (c) 13 kPa, respectively. Normalized water fluxes and salt rejection rates data for DCMD membrane wetting experiments (experiments 5 and 3 in Appendix C) with transmembrane hydraulic pressure of 6 kPa and SDS concentration of (d) 0.51 mM and (e) 0.68 mM, respectively. In each panel, the water fluxes were normalized by the initial vapor flux. The initial vapor fluxes were (a) 31.2, (b) 32.2, (c) 33.5, (d) 31.2 and (e) 32.7 L $m^{-2}$ $h^{-1}$, respectively. The normalized water flux increased over unity after wetting occurred, as explained in the caption Fig. D1.

**Surface roughness of the reconstructed PVDF film**

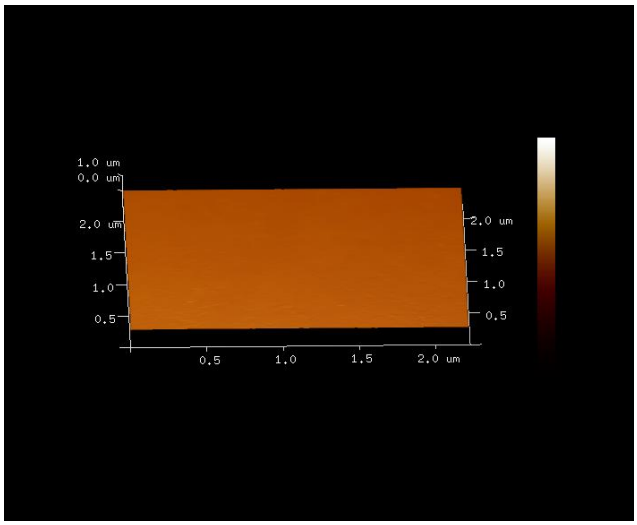

Figure D.4 AFM images of the PVDF film reconstructed from porous PVDF membrane. The measured Ra and Rq were 2.5 and 3.12 nm, respectively. No pore was observed and the roughness

is negligibly small. Therefore, CA measured using this film can be considered as an approximation of the intrinsic CA.

**Surface tensions of SDS solutions with different concentrations**

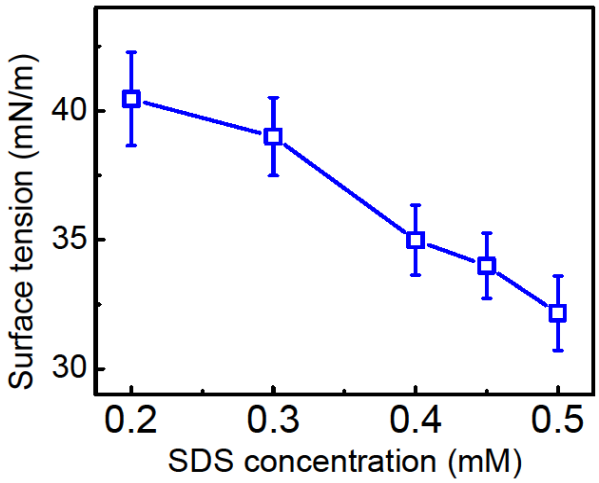


Figure D.5 Surface tensions of NaCl solutions (0.6 M) with different concentrations of SDS.

**Intrinsic contact angles of NaCl solutions with different concentrations of SDS on a PVDF surface;**

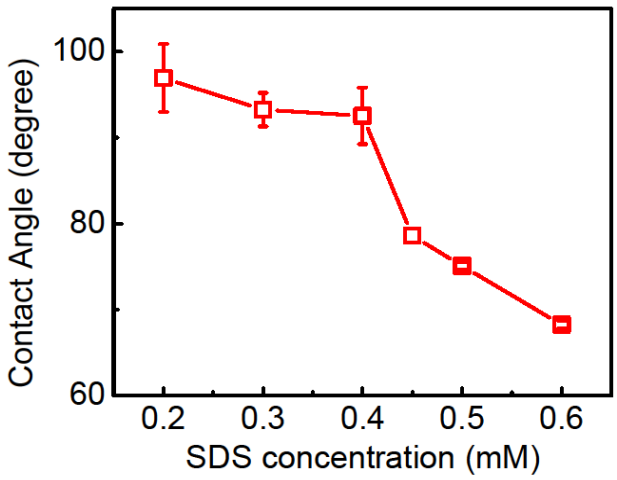


Figure D.6 Intrinsic contact angles of NaCl solutions (0.6 M) with different concentrations of SDS on PVDF surface.

**Estimated LEP for NaCl solutions with different SDS concentrations**

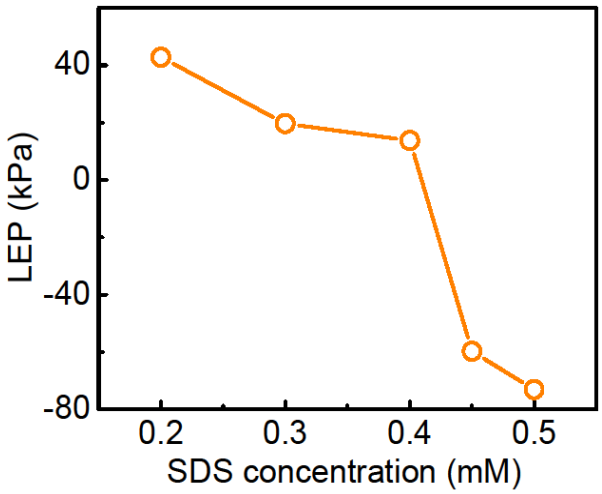


Figure D.7 Estimated LEP of the PVDF membrane for NaCl solutions with different SDS concentrations. These values were calculated using Eq. 5.2 based on the surface tensions (Fig. D5) and intrinsic contact angles (Fig. D6) of NaCl solutions with different SDS concentrations.

## Results of Membrane Wetting Experiments

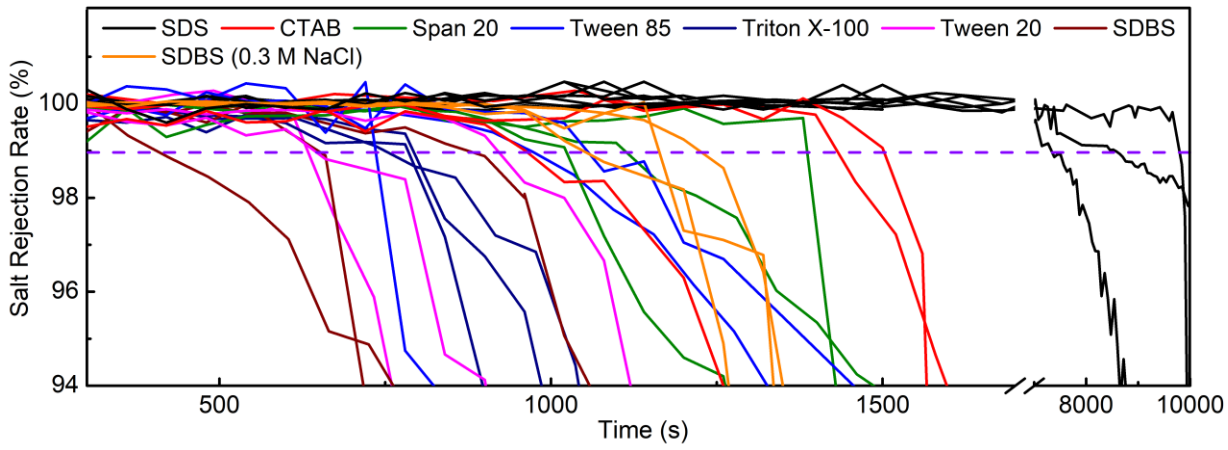


Figure D.8 Salt rejection rate as a function of time in DCMD wetting experiments. Each curve represents the change of salt rejection rate in a wetting experiment, and the color of the curve specifies the surfactant species utilized in the experiment. The purple dash line denotes to a salt rejection rate of 99%, which is defined as the criterion for the breakthrough of the membrane pore

by salty feed solution. The breakthrough time is attained as the time at which a curve drops below the purple dash line.

## Model Parameters for Different Surfactant Species

In each model simulation, the water flux $J_w$ was 30.5 L $m^{-2}$ $hr^{-1}$, and the bulk concentration for surfactants was 0.3 mM. The maximum packing density of surfactant on the pore surface $\tau_{max}$ was approximated using the measured surface excess concentration and the coefficients of determination for surface excess concentrations $R^2$ were also provided. The diffusion coefficient $D$ of each surfactant was acquired from literatures[225,272,274–278].The critical concentrations $C'$ for SDS was estimated using the following equation with an LEP of 6 kPa (i.e. the transmembrane pressure in the experiments)

$$\text{LEP} = -\frac{2\gamma(C')\cos(\theta(C'))}{R}$$

where $\gamma(C')$ and $\theta(C')$ are the surface tension of the solution and its contact angle on a PVDF surface, respectively, both being a function of $C'$ (ref [25] in the main text for more details). For other surfactants, we performed the simulations using $C'$ from 0.01 mM (extremely low) to the CMC of the surfactants from the surface tension measurements. We note that LEP does not change when $C'$ is beyond CMC because $\gamma(C')$ and $\cos(\theta(C'))$ becomes constant when $C'$ is beyond CMC. We find that for all other surfactants except SDS, the choice of $C'$ within this range does not have any appreciable impact on the simulated $t_{\text{wetting}}$ because diffusion is unimportant compared to convection in the axial transport of these surfactants. A summary of surface excess concentration, $\Gamma$, coefficient of determination $R^2$ (for $\Gamma$), critical concentration, $C'$, diffusion coefficient, $D$, and the simulated $t_{\text{wetting}}$ for different surfactant species are shown in Table D2.

Table D2. The parameters for model prediction of pore wetting by different surfactant species (corresponding to Fig. 5.7 in the main text)

| **Surfactant Species** | $\Gamma$ ($\times 10^{-6}\ mole\ m^{-2}$) | $R^2$ (for $\Gamma$) | C' (mM) | $D$ ($\times 10^{-10}\ m^2\ s^{-1}$) | $t_{\text{wetting}}$ (C'=0.01 mM) | $t_{\text{wetting}}$ (C'=CMC) |
|---|---|---|---|---|---|---|
| SDS | 5.31 | 0.977 | 0.36 | 7.3 | 7130 (C'=0.36 mM) | |
| Triton X100 | 3.50 | 0.990 | 0.01-0.2 | 0.4 | 890 | 890 |
| Tween 20 | 2.96 | 0.998 | 0.01-0.05 | 0.75 | 700 | 700 |
| Tween 85 | 3.62 | 0.975 | 0.01-0.05 | 0.7 | 860 | 860 |
| Span 20 | 4.13 | 0.989 | 0.01-0.05 | 0.12 | 1060 | 1060 |
| CTAB | 4.31 | 0.999 | 0.01-0.05 | 0.39 | 1090 | 1110 |
| SDBS (0.6 M NaCl) | 2.62 | 0.945 | 0.01-0.2 | 0.2 | 680 | 680 |
| SDBS (0.3 M NaCl) | 4.19 | 0.987 | 0.01-0.2 | 0.8 | 980 | 990 |

# REFERENCES


[1] T. Tong, M. Elimelech, The Global Rise of Zero Liquid Discharge for Wastewater Management: Drivers, Technologies, and Future Directions, Environ. Sci. Technol. 50 (2016) 6846–6855. doi:10.1021/acs.est.6b01000.

[2] K.B. Gregory, R.D. Vidic, D. a. Dzombak, Water management challenges associated with the production of shale gas by hydraulic fracturing, Elements. 7 (2011) 181–186. doi:10.2113/gselements.7.3.181.

[3] S.G. Osborn, A. Vengosh, N.R. Warner, R.B. Jackson, Methane contamination of drinking water accompanying gas-well drilling and hydraulic fracturing., Proc. Natl. Acad. Sci. U. S. A. 108 (2011) 8172–8176. doi:10.1073/pnas.1109270108.

[4] EIA, Annual Energy Outlook 2017, Eia. (2017).

[5] IEA, World Energy Outlook 2011 Special Report - Are We Entering a Golden Age of Gas?, 2011. doi:10.1515/reveh-2014-0002.

[6] R.W. Howarth, A. Ingraffea, T. Engelder, Natural gas: Should fracking stop?, Nature. 477 (2011) 271–275. doi:10.1038/477271a.

[7] L.M. McKenzie, R.Z. Witter, L.S. Newman, J.L. Adgate, Human health risk assessment of air emissions from development of unconventional natural gas resources, Sci. Total Environ. 424 (2012) 79–87. doi:10.1016/j.scitotenv.2012.02.018.

[8] R.D. Vidic, S.L. Brantley, J.M. Vandenbossche, D. Yoxtheimer, J.D. Abad, Impact of shale gas development on regional water quality., Science. 340 (2013) 1235009. doi:10.1126/science.1235009.

[9] United States Environmental Protection Agency, The Hydraulic Fracturing Water Cycle, EPA's Study Hydraul. Fract. Its Potential Impact Drink. Water Resour. (2016) 1–666. https://www.epa.gov/hfstudy/hydraulic-fracturing-water-cycle%0Ahttps://www.epa.gov/sites/production/files/2016-12/documents/hfdwa_executive_summary.pdf.

[10] C. Clark, J. Veil, Produced Water Volumes and Management Practices in the United States, Argonne Natl. Lab. Rep. (2009) 64. doi:10.2172/1007397.

[11] B.G. Rahm, J.T. Bates, L.R. Bertoia, A.E. Galford, D. a. Yoxtheimer, S.J. Riha, Wastewater management and Marcellus Shale gas development: Trends, drivers, and planning implications, J. Environ. Manage. 120 (2013) 105–113. doi:10.1016/j.jenvman.2013.02.029.

[12] A. Vengosh, R.B. Jackson, N. Warner, T.H. Darrah, A. Kondash, A critical review of the risks to water resources from unconventional shale gas development and hydraulic fracturing in the United States, Env. Sci Technol. 48 (2014) 8334–8348. doi:10.1021/es405118y.

[13] D.L. Shaffer, L.H. Arias Chavez, M. Ben-Sasson, S. Romero-Vargas Castrillón, N.Y. Yip, M. Elimelech, Desalination and reuse of high-salinity shale gas produced water: drivers, technologies, and future directions., Environ. Sci. Technol. 47 (2013) 9569–83. doi:10.1021/es401966e.

[14] C. Fritzmann, J. Löwenberg, T. Wintgens, T. Melin, State-of-the-art of reverse osmosis desalination, Desalination. 216 (2007) 1–76. doi:10.1016/j.desal.2006.12.009.

[15] M. Elimelech, W. a Phillip, The future of seawater desalination: energy, technology, and the environment., Science. 333 (2011) 712–717. doi:10.1126/science.1200488.

[16] K.W. Lawson, D.R. Lloyd, Membrane distillation, J. Memb. Sci. 124 (1997) 1–25. doi:10.1016/S0376-7388(96)00236-0.

[17] a. M. Alklaibi, N. Lior, Membrane-distillation desalination: Status and potential, Desalination. 171 (2005) 111–131. doi:10.1016/j.desal.2004.03.024.

[18] E. Curcio, E. Drioli, Membrane Distillation and Related Operations—A Review, Sep. Purif. Rev. 34 (2005) 35–86. doi:10.1081/SPM-200054951.

[19] A. Alkhudhiri, N. Darwish, N. Hilal, Membrane distillation: A comprehensive review, Desalination. 287 (2012) 2–18. doi:10.1016/j.desal.2011.08.027.

[20] C.R. Martinetti, A.E. Childress, T.Y. Cath, High recovery of concentrated RO brines using forward osmosis and membrane distillation, J. Memb. Sci. 331 (2009) 31–39. doi:10.1016/j.memsci.2009.01.003.

[21] S. Lin, N.Y. Yip, M. Elimelech, Direct contact membrane distillation with heat recovery: Thermodynamic insights from module scale modeling, J. Memb. Sci. 453 (2014) 498–515. doi:10.1016/j.memsci.2013.11.016.

[22] M.S. El-Bourawi, Z. Ding, R. Ma, M. Khayet, A framework for better understanding membrane distillation separation process, J. Memb. Sci. 285 (2006) 4–29. doi:10.1016/j.memsci.2006.08.002.

[23] L.D. Tijing, Y.C. Woo, J.S. Choi, S. Lee, S.H. Kim, H.K. Shon, Fouling and its control in membrane distillation-A review, J. Memb. Sci. 475 (2015) 215–244. doi:10.1016/j.memsci.2014.09.042.

[24] W. Gao, H. Liang, J. Ma, M. Han, Z. Chen, Z. Han, et al., Membrane fouling control in ultra fi ltration technology for drinking water production : A review, Desalination. 272 (2011) 1–8. doi:10.1016/j.desal.2011.01.051.

[25] F. Meng, S.R. Chae, A. Drews, M. Kraume, H.S. Shin, F. Yang, Recent advances in membrane bioreactors (MBRs): Membrane fouling and membrane material, Water Res. 43 (2009) 1489–1512. doi:10.1016/j.watres.2008.12.044.

[26] Q. She, R. Wang, A.G. Fane, C.Y. Tang, Membrane fouling in osmotically driven membrane processes : A review, J. Memb. Sci. 499 (2016) 201–233. doi:10.1016/j.memsci.2015.10.040.

[27] D.M. Warsinger, J. Swaminathan, E. Guillen-Burrieza, H. a. Arafat, J.H. Lienhard V, Scaling and fouling in membrane distillation for desalination applications: A review, Desalination. 356 (2014) 294–313. doi:10.1016/j.desal.2014.06.031.

[28] M. Gryta, Fouling in direct contact membrane distillation process, J. Memb. Sci. 325 (2008) 383–394. doi:10.1016/j.memsci.2008.08.001.

[29] J. Israelachvili, R. Pashley, The hydrophobic interaction is long range, decaying exponentially with distance., Nature. 300 (1982) 341–342. doi:10.1038/300341a0.

[30] Y. Tsao, D. Evans, H. Wennerstrom, Long-range attractive force between hydrophobic surfaces observed by atomic force microscopy, Science (80-. ). 262 (1993) 547–550. doi:10.1126/science.8211182.

[31] E.E. Meyer, K.J. Rosenberg, J. Israelachvili, Recent progress in understanding hydrophobic interactions., Proc. Natl. Acad. Sci. U. S. A. 103 (2006) 15739–15746. doi:10.1073/pnas.0606422103.

[32] M. Gryta, M. Tomaszewska, J. Grzechulska, a. W. Morawski, Membrane distillation of NaCl solution containing natural organic matter, J. Memb. Sci. 181 (2001) 279–287. doi:10.1016/S0376-7388(00)00582-2.

[33] G. Zuo, R. Wang, Novel membrane surface modification to enhance anti-oil fouling property for membrane distillation application, J. Memb. Sci. 447 (2013) 26–35. doi:10.1016/j.memsci.2013.06.053.

[34] A. El-abbassi, A. Ha, M. Khayet, M.C. García-payo, Integrated direct contact membrane distillation for olive mill wastewater treatment, 323 (2013) 31–38. doi:10.1016/j.desal.2012.06.014.

[35] L.D. Nghiem, T. Cath, A scaling mitigation approach during direct contact membrane distillation, Sep. Purif. Technol. 80 (2011) 315–322. doi:10.1016/j.seppur.2011.05.013.

[36] G. Chen, X. Yang, R. Wang, A.G. Fane, Performance enhancement and scaling control with gas bubbling in direct contact membrane distillation, Desalination. 308 (2013) 47–55. doi:10.1016/j.desal.2012.07.018.

[37] B.J. Privett, J. Youn, S.A. Hong, J. Lee, J. Han, J.H. Shin, et al., Antibacterial Fluorinated Silica Colloid Superhydrophobic Surfaces, Langmuir. (2011) 9597–9601. doi:10.1021/la201801e.

[38] F. He, K.K. Sirkar, J. Gilron, Effects of antiscalants to mitigate membrane scaling by direct contact membrane distillation, J. Memb. Sci. 345 (2009) 53–58. doi:10.1016/j.memsci.2009.08.021.

[39] S. Srisurichan, R. Jiraratananon, A.G. Fane, Humic acid fouling in the membrane distillation process, Desalination. 174 (2005) 63–72. doi:10.1016/j.desal.2004.09.003.

[40] A.C.M. Franken, J.A.M. Nolten, M.H. V Mulder, D. Bargeman, C.A. Smolders, Wetting criteria for the applicability of membrane distillation, J. Memb. Sci. 33 (1987) 315–328.

doi:10.1016/S0376-7388(00)80288-4.

[41] S. Goh, J. Zhang, Y. Liu, A.G. Fane, Fouling and wetting in membrane distillation (MD) and MD-bioreactor (MDBR) for wastewater reclamation, Desalination. 323 (2013) 39–47. doi:10.1016/j.desal.2012.12.001.

[42] E. Guillen-Burrieza, M.O. Mavukkandy, M.R. Bilad, H.A. Arafat, Understanding wetting phenomena in membrane distillation and how operational parameters can affect it, J. Memb. Sci. 515 (2016) 163–174. doi:10.1016/j.memsci.2016.05.051.

[43] M. Rezaei, D.M. Warsinger, J.H. Lienhard V, W.M. Samhaber, Wetting prevention in membrane distillation through superhydrophobicity and recharging an air layer on the membrane surface, J. Memb. Sci. 530 (2017) 42–52. doi:10.1016/j.memsci.2017.02.013.

[44] S. Lin, S. Nejati, C. Boo, Y. Hu, C.O. Osuji, M. Elimelech, Omniphobic Membrane for Robust Membrane Distillation, Environ. Sci. Technol. Lett. 1 (2014) 443–447. doi:10.1021/ez500267p.

[45] G. Naidu, S. Jeong, S.J. Kim, I.S. Kim, S. Vigneswaran, Organic fouling behavior in direct contact membrane distillation, Desalination. 347 (2014) 230–239. doi:10.1016/j.desal.2014.05.045.

[46] A. Razmjou, E. Arifin, G. Dong, J. Mansouri, V. Chen, Superhydrophobic modification of TiO2 nanocomposite PVDF membranes for applications in membrane distillation, J. Memb. Sci. 415–416 (2012) 850–863. doi:10.1016/j.memsci.2012.06.004.

[47] Y. Liao, R. Wang, A.G. Fane, Engineering superhydrophobic surface on poly(vinylidene fluoride) nanofiber membranes for direct contact membrane distillation, J. Memb. Sci. 440 (2013) 77–87. doi:10.1016/j.memsci.2013.04.006.

[48] C. Boo, J. Lee, M. Elimelech, Engineering Surface Energy and Nanostructure of Microporous Films for Expanded Membrane Distillation Applications, Environ. Sci. Technol. 50 (2016) 8112–8119. doi:10.1021/acs.est.6b02316.

[49] J. Lee, C. Boo, W.H. Ryu, A.D. Taylor, M. Elimelech, Development of Omniphobic Desalination Membranes Using a Charged Electrospun Nanofiber Scaffold, ACS Appl. Mater. Interfaces. 8 (2016) 11154–11161. doi:10.1021/acsami.6b02419.

[50] C. Boo, J. Lee, M. Elimelech, Omniphobic Polyvinylidene Fluoride (PVDF) Membrane for Desalination of Shale Gas Produced Water by Membrane Distillation, Environ. Sci. Technol. 50 (2016) 12275–12282. doi:10.1021/acs.est.6b03882.

[51] Y.C. Woo, Y. Chen, L.D. Tijing, S. Phuntsho, T. He, J.S. Choi, et al., CF4plasma-modified omniphobic electrospun nanofiber membrane for produced water brine treatment by membrane distillation, J. Memb. Sci. 529 (2017) 234–242. doi:10.1016/j.memsci.2017.01.063.

[52] P. Peng, A.G. Fane, X. Li, Desalination by membrane distillation adopting a hydrophilic membrane, Desalination. 173 (2005) 45–54. doi:10.1016/j.desal.2004.06.208.

[53] X. Yang, R. Wang, L. Shi, A.G. Fane, M. Debowski, Performance improvement of PVDF hollow fiber-based membrane distillation process, J. Memb. Sci. 369 (2011) 437–447. doi:10.1016/j.memsci.2010.12.020.

[54] D.M. Warsinger, A. Servi, S. Van Belleghem, J. Gonzalez, J. Swaminathan, J. Kharraz, et al., Combining air recharging and membrane superhydrophobicity for fouling prevention in membrane distillation, J. Memb. Sci. 505 (2016) 241–252. doi:10.1016/j.memsci.2016.01.018.

[55] A.B.D. Cassie, S. Baxter, Wettability of porous surfaces, Trans. Faraday Soc. 40 (1944) 546. doi:10.1039/tf9444000546.

[56] J.F. Joanny, P.G. de Gennes, P.G. De Gennes, P.G. de Gennes, P.G. De Gennes, A model for contact angle hysteresis, J. Chem. Phys. 81 (1984) 552. doi:10.1063/1.447337.

[57] C.N.C. Lam, R. Wu, D. Li, M.L. Hair, A.W. Neumann, Study of the advancing and receding contact angles: Liquid sorption as a cause of contact angle hysteresis, Adv. Colloid Interface Sci. 96 (2002) 169–191. doi:10.1016/S0001-8686(01)00080-X.

[58] L. Gao, T.J. McCarthy, Contact angle hysteresis explained, Langmuir. 22 (2006) 6234–6237. doi:10.1021/la060254j.

[59] G. McHale, N.J. Shirtcliffe, M.I. Newton, Contact-angle hysteresis on super-hydrophobic surfaces, Langmuir. 20 (2004) 10146–10149. doi:10.1021/la0486584.

[60] P. Roach, N.J. Shirtcliffe, M.I. Newton, Progess in superhydrophobic surface development, Soft Matter. 4 (2008) 224. doi:10.1039/b712575p.

[61] M. Ma, R.M. Hill, Superhydrophobic surfaces, Curr. Opin. Colloid Interface Sci. 11 (2006) 193–202. doi:10.1016/j.cocis.2006.06.002.

[62] P. Patel, C.K. Choi, D.D. Meng, Superhydrophilic Surfaces for Antifogging and Antifouling Microfluidic Devices, JALA - J. Assoc. Lab. Autom. 15 (2010) 114–119. doi:10.1016/j.jala.2009.10.012.

[63] K. Tadanaga, J. Morinaga, A. Matsuda, T. Minami, Superhydrophobic - Superhydrophilic micropatterning on flowerlike alumina coating film by the sol - Gel method, Chem. Mater. 12 (2000) 590–592. doi:10.1021/cm990643h.

[64] J. Drelich, E. Chibowski, Superhydrophilic and superwetting surfaces: Definition and mechanisms of control, Langmuir. 26 (2010) 18621–18623. doi:10.1021/la1039893.

[65] A.K. Kota, J.M. Mabry, A. Tuteja, Superoleophobic surfaces: design criteria and recent studies., Surf. Innov. 1 (2013) 71–83. doi:10.1680/si.12.00017.

[66] K. Liu, Y. Tian, L. Jiang, Bio-inspired superoleophobic and smart materials: Design, fabrication, and application, Prog. Mater. Sci. 58 (2012) 503–564. doi:10.1016/j.pmatsci.2012.11.001.

[67] A.K. Kota, Y. Li, J.M. Mabry, A. Tuteja, Hierarchically structured superoleophobic

surfaces with ultralow contact angle hysteresis, Adv. Mater. 24 (2012) 5838–5843. doi:10.1002/adma.201202554.

[68] T.-S. Wong, S.H. Kang, S.K.Y. Tang, E.J. Smythe, B.D. Hatton, A. Grinthal, et al., Bioinspired self-repairing slippery surfaces with pressure-stable omniphobicity, Nature. 477 (2011) 443–447. doi:10.1038/nature10447.

[69] A. Tuteja, W. Choi, J.M. Mabry, G.H. McKinley, R.E. Cohen, Robust omniphobic surfaces., Proc. Natl. Acad. Sci. U. S. A. 105 (2008) 18200–18205. doi:10.1073/pnas.0804872105.

[70] L. Zhai, M.C. Berg, F.Ç. Cebeci, Y. Kim, J.M. Milwid, M.F. Rubner, et al., Patterned superhydrophobic surfaces: Toward a synthetic mimic of the namib desert beetle, Nano Lett. 6 (2006) 1213–1217. doi:10.1021/nl060644q.

[71] R.P. Garrod, L.G. Harris, W.C.E. Schofield, J. McGettrick, L.J. Ward, D.O.H. Teare, et al., Mimicking a Stenocara beetle's back for microcondensation using plasmachemical patterned superhydrophobic-superhydrophilic surfaces, Langmuir. 23 (2007) 689–693. doi:10.1021/la0610856.

[72] Y.C. Jung, B. Bhushan, Wetting behaviour during evaporation and condensation of water microdroplets on superhydrophobic patterned surfaces, J. Microsc. 229 (2008) 127–140. doi:10.1111/j.1365-2818.2007.01875.x.

[73] A.M. Kietzig, S.G. Hatzikiriakos, P. Englezos, Patterned superhydrophobic metallic surfaces, Langmuir. 25 (2009) 4821–4827. doi:10.1021/la8037582.

[74] E. Wischerhoff, K. Uhlig, A. Lankenau, H.G. Börner, A. Laschewsky, C. Duschl, et al., Controlled cell adhesion on PEG-based switchable surfaces, Angew. Chemie - Int. Ed. 47 (2008) 5666–5668. doi:10.1002/anie.200801202.

[75] L. Zhang, Z. Zhang, P. Wang, Smart surfaces with switchable superoleophilicity and superoleophobicity in aqueous media: toward controllable oil/water separation, NPG Asia Mater. 4 (2012) 1–8. doi:10.1038/am.2012.14.

[76] S. Liang, Y. Kang, A. Tiraferri, E.P. Giannelis, X. Huang, M. Elimelech, Highly hydrophilic polyvinylidene fluoride (PVDF) ultrafiltration membranes via postfabrication grafting of surface-tailored silica nanoparticles, ACS Appl. Mater. Interfaces. 5 (2013) 6694–6703. doi:10.1021/am401462e.

[77] S.S. Madaeni, N. Ghaemi, a. Alizadeh, M. Joshaghani, Influence of photo-induced superhydrophilicity of titanium dioxide nanoparticles on the anti-fouling performance of ultrafiltration membranes, Appl. Surf. Sci. 257 (2011) 6175–6180. doi:10.1016/j.apsusc.2011.02.026.

[78] H. Guo, Y. Ma, P. Sun, S. Cui, Z. Qin, Y. Liang, Self-Cleaning and Antifouling Nanofiltration Membranes-Superhydrophilic Multilayered Polyelectrolyte/CSH Composite Films Towards Rejection of Dyes, RSC Adv. 5 (2015) 63429–63438. doi:10.1039/C5RA11438A.

[79] A.R. Roudman, F. a. Digiano, Surface energy of experimental and commercial nanofiltration membranes: Effects of wetting and natural organic matter fouling, J. Memb. Sci. 175 (2000) 61–73. doi:10.1016/S0376-7388(00)00409-9.

[80] G. Kang, M. Liu, B. Lin, Y. Cao, Q. Yuan, A novel method of surface modification on thin-film composite reverse osmosis membrane by grafting poly(ethylene glycol), Polymer (Guildf). 48 (2007) 1165–1170. doi:10.1016/j.polymer.2006.12.046.

[81] L. Zou, I. Vidalis, D. Steele, A. Michelmore, S.P. Low, J.Q.J.C. Verberk, Surface hydrophilic modification of RO membranes by plasma polymerization for low organic fouling, J. Memb. Sci. 369 (2011) 420–428. doi:10.1016/j.memsci.2010.12.023.

[82] A. Tiraferri, Y. Kang, E.P. Giannelis, M. Elimelech, Superhydrophilic thin-film composite forward osmosis membranes for organic fouling control: Fouling behavior and antifouling mechanisms, Environ. Sci. Technol. 46 (2012) 11135–11144. doi:10.1021/es3028617.

[83] S. Romero-Vargas Castrillón, X. Lu, D.L. Shaffer, M. Elimelech, Amine enrichment and poly(ethylene glycol) (PEG) surface modification of thin-film composite forward osmosis membranes for organic fouling control, J. Memb. Sci. 450 (2014) 331–339. doi:10.1016/j.memsci.2013.09.028.

[84] D.L. Shaffer, H. Jaramillo, S. Romero-Vargas Castrillón, X. Lu, M. Elimelech, Post-fabrication modification of forward osmosis membranes with a poly(ethylene glycol) block copolymer for improved organic fouling resistance, J. Memb. Sci. 490 (2015) 209–219. doi:10.1016/j.memsci.2015.04.060.

[85] X. Zhu, W. Tu, K.H. Wee, R. Bai, Effective and low fouling oil/water separation by a novel hollow fiber membrane with both hydrophilic and oleophobic surface properties, J. Memb. Sci. 466 (2014) 36–44. doi:10.1016/j.memsci.2014.04.038.

[86] X. Zhu, H.E. Loo, R. Bai, A novel membrane showing both hydrophilic and oleophobic surface properties and its non-fouling performances for potential water treatment applications, J. Memb. Sci. 436 (2013) 47–56. doi:10.1016/j.memsci.2013.02.019.

[87] M. Khayet, T. Matsuura, Membrane Distillation, 2011. doi:10.1016/B978-0-444-53126-1.10016-8.

[88] F. Banat, N. Jwaied, Economic evaluation of desalination by small-scale autonomous solar-powered membrane distillation units, Desalination. 220 (2008) 566–573. doi:10.1016/j.desal.2007.01.057.

[89] S. Al-Obaidani, E. Curcio, F. Macedonio, G. Di Profio, H. Al-Hinai, E. Drioli, Potential of membrane distillation in seawater desalination: Thermal efficiency, sensitivity study and cost estimation, J. Memb. Sci. 323 (2008) 85–98. doi:10.1016/j.memsci.2008.06.006.

[90] Y.D. Kim, K. Thu, N. Ghaffour, K. Choon Ng, Performance investigation of a solar-assisted direct contact membrane distillation system, J. Memb. Sci. 427 (2013) 345–364. doi:10.1016/j.memsci.2012.10.008.

[91] J. Bundschuh, N. Ghaffour, H. Mahmoudi, M. Goosen, S. Mushtaq, J. Hoinkis, Low-cost

low-enthalpy geothermal heat for freshwater production: Innovative applications using thermal desalination processes, Renew. Sustain. Energy Rev. 43 (2015) 196–206. doi:10.1016/j.rser.2014.10.102.

[92] N. Ghaffour, J. Bundschuh, H. Mahmoudi, M.F.A. Goosen, Renewable energy-driven desalination technologies: A comprehensive review on challenges and potential applications of integrated systems, Desalination. 356 (2014) 94–114. doi:10.1016/j.desal.2014.10.024.

[93] L.M. Camacho, L. Dumée, J. Zhang, J. De Li, M. Duke, J. Gomez, et al., Advances in membrane distillation for water desalination and purification applications, Water (Switzerland). 5 (2013) 94–196. doi:10.3390/w5010094.

[94] D.M. Kargbo, R.G. Wilhelm, D.J. Campbell, Natural gas plays in the marcellus shale: Challenges and potential opportunities, Environ. Sci. Technol. 44 (2010) 5679–5684. doi:10.1021/es903811p.

[95] S.M. Olmstead, L. a Muehlenbachs, J. Shih, Z. Chu, A.J. Krupnick, Shale gas development impacts on surface water quality in Pennsylvania, Proc. Natl Acad. Sci. USA. 110 (2013) 4962–4967. doi:10.1073/pnas.1213871110/-/DCSupplemental.www.pnas.org/cgi/doi/10.1073/pnas.1213871110.

[96] N.R. Warner, C. a. Christie, R.B. Jackson, A. Vengosh, Impacts of shale gas wastewater disposal on water quality in Western Pennsylvania, Environ. Sci. Technol. 47 (2013) 11849–11857. doi:10.1021/es402165b.

[97] J. Zhang, N. Dow, M. Duke, E. Ostarcevic, J.D. Li, S. Gray, Identification of material and physical features of membrane distillation membranes for high performance desalination, J. Memb. Sci. 349 (2010) 295–303. doi:10.1016/j.memsci.2009.11.056.

[98] F. Liu, N.A. Hashim, Y. Liu, M.R.M. Abed, K. Li, Progress in the production and modification of PVDF membranes, J. Memb. Sci. 375 (2011) 1–27. doi:10.1016/j.memsci.2011.03.014.

[99] A. Hausmann, P. Sanciolo, T. Vasiljevic, M. Weeks, K. Schroën, S. Gray, et al., Fouling of dairy components on hydrophobic polytetrafluoroethylene (PTFE) membranes for membrane distillation, J. Memb. Sci. 442 (2013) 149–159. doi:10.1016/j.memsci.2013.03.057.

[100] G. Zuo, R. Wang, Novel membrane surface modification to enhance anti-oil fouling property for membrane distillation application, J. Memb. Sci. 447 (2013) 26–35. doi:10.1016/j.memsci.2013.06.053.

[101] W. Orem, C. Tatu, M. Varonka, H. Lerch, A. Bates, M. Engle, et al., Organic substances in produced and formation water from unconventional natural gas extraction in coal and shale, Int. J. Coal Geol. 126 (2014) 20–31. doi:10.1016/j.coal.2014.01.003.

[102] S. Nishimoto, B. Bhushan, Bioinspired self-cleaning surfaces with superhydrophobicity, superoleophobicity, and superhydrophilicity, RSC Adv. (2012) 671–690.

doi:10.1039/c2ra21260a.

[103] M. Liu, S. Wang, Z. Wei, Y. Song, L. Jiang, Bioinspired design of a superoleophobic and low adhesive water/solid interface, Adv. Mater. 21 (2009) 665–669. doi:10.1002/adma.200801782.

[104] X. Liu, J. Zhou, Z. Xue, J. Gao, J. Meng, S. Wang, et al., Clam's shell inspired high-energy inorganic coatings with underwater low adhesive superoleophobicity, Adv. Mater. 24 (2012) 3401–3405. doi:10.1002/adma.201200797.

[105] Z. Xue, S. Wang, L. Lin, L. Chen, M. Liu, L. Feng, et al., A novel superhydrophilic and underwater superoleophobic hydrogel-coated mesh for oil/water separation, Adv. Mater. 23 (2011) 4270–4273. doi:10.1002/adma.201102616.

[106] Q. Wen, J.C. Di, L. Jiang, J.H. Yu, R.R. Xu, Zeolite-coated mesh film for efficient oil-water separation, Chem. Sci. 4 (2013) 591–595. doi:10.1039/c2sc21772d.

[107] Y. Zhu, F. Zhang, D. Wang, X.F. Pei, W. Zhang, J. Jin, A novel zwitterionic polyelectrolyte grafted PVDF membrane for thoroughly separating oil from water with ultrahigh efficiency, J. Mater. Chem. A. 1 (2013) 5758–65. doi:10.1039/c3ta01598j.

[108] K. Rohrbach, Y. Li, H. Zhu, Z. Liu, J. Dai, J. Andreasen, et al., A cellulose based hydrophilic, oleophobic hydrated filter for water/oil separation, Chem. Commun. 50 (2014) 13296–13299. doi:10.1039/C4CC04817B.

[109] V. Hejazi, A.E. Nyong, P.K. Rohatgi, M. Nosonovsky, Wetting transitions in underwater oleophobic surface of brass, Adv. Mater. 24 (2012) 5963–5966. doi:10.1002/adma.201202516.

[110] S.S. Chhatre, A. Tuteja, W. Choi, A. Revaux, D. Smith, J.M. Mabry, et al., Thermal annealing treatment to achieve switchable and reversible oleophobicity on fabrics., Langmuir. 25 (2009) 13625–32. doi:10.1021/la901997s.

[111] P.S. Brown, O.D.L. a Atkinson, J.P.S. Badyal, Ultrafast oleophobic-hydrophilic switching surfaces for antifogging, self-cleaning, and oil-water separation, ACS Appl. Mater. Interfaces. 6 (2014) 7504–7511. doi:10.1021/am500882y.

[112] Z. Wang, M. Elimelech, S. Lin, Environmental Applications of Interfacial Materials with Special Wettability, Environ. Sci. Technol. 50 (2016) 2132–3150.

[113] Y. Liao, R. Wang, A.G. Fane, Fabrication of bioinspired composite nanofiber membranes with robust superhydrophobicity for direct contact membrane distillation, Environ. Sci. Technol. 48 (2014) 6335–6341. doi:10.1021/es405795s.

[114] J. Zhang, Z. Song, B. Li, Q. Wang, S. Wang, Fabrication and characterization of superhydrophobic poly (vinylidene fluoride) membrane for direct contact membrane distillation, Desalination. 324 (2013) 1–9. doi:10.1016/j.desal.2013.05.018.

[115] M. Khayet, J.I. Mengual, T. Matsuura, Porous hydrophobic/hydrophilic composite membranes: Application in desalination using direct contact membrane distillation, J.

Memb. Sci. 252 (2005) 101–113. doi:10.1016/j.memsci.2004.11.022.

[116] M. Qtaishat, D. Rana, M. Khayet, T. Matsuura, Preparation and characterization of novel hydrophobic/hydrophilic polyetherimide composite membranes for desalination by direct contact membrane distillation, J. Memb. Sci. 327 (2009) 264–273. doi:10.1016/j.memsci.2008.11.040.

[117] M. Qtaishat, M. Khayet, T. Matsuura, Novel porous composite hydrophobic/hydrophilic polysulfone membranes for desalination by direct contact membrane distillation, J. Memb. Sci. 341 (2009) 139–148. doi:10.1016/j.memsci.2009.05.053.

[118] S. Bonyadi, T.S. Chung, Flux enhancement in membrane distillation by fabrication of dual layer hydrophilic-hydrophobic hollow fiber membranes, J. Memb. Sci. 306 (2007) 134–146. doi:10.1016/j.memsci.2007.08.034.

[119] Y. Liu, J. Tang, X. Chen, J.H. Xin, Decoration of carbon nanotubes with chitosan, Carbon N. Y. 43 (2005) 3178–3180. doi:10.1016/j.carbon.2005.06.020.

[120] J. Yang, H. Song, X. Yan, H. Tang, C. Li, Superhydrophilic and superoleophobic chitosan-based nanocomposite coatings for oil/water separation, Cellulose. 21 (2014) 1851–1857. doi:10.1007/s10570-014-0244-0.

[121] M. Khayet, T. Matsuura, Preparation and characterization of polyvinylidene fluoride membranes for membrane distillation, Ind. Eng. Chem. …. 40 (2001) 5710–5718. doi:10.1021/ie010553y.

[122] K. Smolder, A. Franken, Terminology for Membrane Distillation, Desalination. 72 (1989) 249–262.

[123] K. Liu, J. Du, J. Wu, L. Jiang, Superhydrophobic gecko feet with high adhesive forces towards water and their bio-inspired materials, Nanoscale. 4 (2012) 768. doi:10.1039/c1nr11369k.

[124] X. Yao, J. Gao, Y. Song, L. Jiang, Superoleophobic Surfaces with Controllable Oil Adhesion and Their Application in Oil Transportation, Adv. Funct. Mater. 21 (2011) 4270–4276. doi:10.1002/adfm.201100775.

[125] L. Heng, J. Su, J. Zhai, Q. Yang, L. Jiang, Dual high adhesion surface for water in air and for oil underwater, Langmuir. 27 (2011) 12466–12471. doi:10.1021/la202692c.

[126] R.N. Wenzel, Resistance of solid surfaces to wetting by water., J. Ind. Eng. Chem. (Washington, D. C.). 28 (1936) 988–994. doi:10.1021/ie50320a024.

[127] R.N. Wenzel, Surface Roughness and Contact Angle, J. Phys. Colloid Chem. 53 (1949) 1466–1467. doi:10.1021/j150474a015.

[128] J. a Howarter, J.P. Youngblood, Amphiphile grafted membranes for the separation of oil-in-water dispersions., J. Colloid Interface Sci. 329 (2009) 127–32. doi:10.1016/j.jcis.2008.09.068.

[129] J. a. Howarter, K.L. Genson, J.P. Youngblood, Wetting behavior of oleophobic polymer coatings synthesized from fluorosurfactant-macromers, ACS Appl. Mater. Interfaces. 3 (2011) 2022–2030. doi:10.1021/am200255v.

[130] M. Rinaudo, Chitin and chitosan: Properties and applications, Prog. Polym. Sci. 31 (2006) 603–632. doi:10.1016/j.progpolymsci.2006.06.001.

[131] D. Anjali Devi, B. Smitha, S. Sridhar, T.M. Aminabhavi, Pervaporation separation of isopropanol/water mixtures through crosslinked chitosan membranes, J. Memb. Sci. 262 (2005) 91–99. doi:10.1016/j.memsci.2005.03.051.

[132] S. Chen, L. Li, C. Zhao, J. Zheng, Surface hydration: Principles and applications toward low-fouling/nonfouling biomaterials, Polymer (Guildf). 51 (2010) 5283–5293. doi:10.1016/j.polymer.2010.08.022.

[133] A.C.M. Franken, J.A.M. Nolten, M.H.V. Mulder, D. Bargeman, C.A. Smolders, Wetting criteria for the applicability of membrane distillation, J. Memb. Sci. 33 (1987) 315–328. doi:10.1016/S0376-7388(00)80288-4.

[134] D. Langevin, S. Poteau, I. Hénaut, J.F. Argillier, Crude Oil Emulsion Properties and Their Application to Heavy Oil Transportation, Oil Gas Sci. Technol. 59 (2004) 511–521. doi:10.2516/ogst:2004036.

[135] A.P. Sullivan, P.K. Kilpatrick, The Effects of Inorganic Solid Particles on Water and Crude Oil Emulsion Stability, Ind. Eng. Chem. Res. 41 (2002) 3389–3404. doi:10.1021/ie010927n.

[136] L. Martínez-Díez, M.. Vázquez-González, Temperature and concentration polarization in membrane distillation of aqueous salt solutions, J. Memb. Sci. 156 (1999) 265–273. doi:10.1016/S0376-7388(98)00349-4.

[137] M. Qtaishat, T. Matsuura, B. Kruczek, M. Khayet, Heat and mass transfer analysis in direct contact membrane distillation, Desalination. 219 (2008) 272–292. doi:10.1016/j.desal.2007.05.019.

[138] M.K. Souhaimi, T. Matsuura, Membrane Distillation: Principles and Applications, Elsevier, Amsterdam, 2011.

[139] E. Shaulsky, C. Boo, S. Lin, M. Elimelech, Membrane-based osmotic heat engine with organic solvent for enhanced power generation from low-grade heat, Environ. Sci. Technol. 49 (2015) 5820–5827. doi:10.1021/es506347j.

[140] G. Zuo, R. Wang, R. Field, A.G. Fane, Energy efficiency evaluation and economic analyses of direct contact membrane distillation system using Aspen Plus, Desalination. 283 (2011) 237–244. doi:10.1016/j.desal.2011.04.048.

[141] Z. Wang, D. Hou, S. Lin, Composite Membrane with Underwater-Oleophobic Surface for Anti-Oil-Fouling Membrane Distillation, Environ. Sci. Technol. (2016) acs.est.5b05976. doi:10.1021/acs.est.5b05976.

[142] S. Kim, D.W. Lee, J. Cho, Application of direct contact membrane distillation process to treat anaerobic digestate, J. Memb. Sci. 511 (2016) 20–28. doi:10.1016/j.memsci.2016.03.038.

[143] J. Genzer, K. Efimenko, Recent developments in superhydrophobic surfaces and their relevance to marine fouling: a review., Biofouling. 22 (2006) 339–360. doi:10.1080/08927010600980223.

[144] S. Pechook, K. Sudakov, I. Polishchuk, I. Ostrova, V. Zakin, B. Pokroy, et al., Bioinspired Passive Anti-biofouling Surfaces Preventing Biofilm Formation, J. Mater. Chem. B. 4 (2014) 1166–1169. doi:10.1039/b000000x.

[145] S.S. Chhatre, A. Tuteja, W. Choi, A. Revaux, D. Smith, J.M. Mabry, et al., Thermal annealing treatment to achieve switchable and reversible oleophobicity on fabrics, Langmuir. 25 (2009) 13625–13632. doi:10.1021/la901997s.

[146] R.M. Pashley, Hydration forces between mica surfaces in aqueous electrolyte solutions, J. Colloid Interface Sci. 80 (1981) 153–162. doi:10.1016/0021-9797(81)90171-5.

[147] R.M. Pashley, DLVO and hydration forces between mica surfaces in Li+, Na+, K+, and Cs+ electrolyte solutions: A correlation of double-layer and hydration forces with surface cation exchange properties, J. Colloid Interface Sci. 83 (1981) 531–546. doi:10.1016/0021-9797(81)90348-9.

[148] A. V. Dudchenko, J. Rolf, L. Shi, L. Olivas, W. Duan, D. Jassby, Coupling Underwater Superoleophobic Membranes with Magnetic Pickering Emulsions for Fouling-Free Separation of Crude Oil/Water Mixtures: An Experimental and Theoretical Study, ACS Nano. 9 (2015) 9930–9941. doi:10.1021/acsnano.5b04880.

[149] H. Fe, D. Lu, W. Cheng, T. Zhang, X. Lu, Q. Liu, et al., Hydrophilic Fe2O3 dynamic membrane mitigating fouling of support ceramic membrane in ultrafiltration of oil/water emulsion, Sep. Purif. Technol. 165 (2016) 1–9. doi:10.1016/j.seppur.2016.03.034.

[150] P.-C. Chen, Z.-K. Xu, Mineral-coated polymer membranes with superhydrophilicity and underwater superoleophobicity for effective oil/water separation., Sci. Rep. 3 (2013) 2776. doi:10.1038/srep02776.

[151] H. Shi, Y. He, Y. Pan, H. Di, G. Zeng, L. Zhang, et al., A modified mussel-inspired method to fabricate TiO2 decorated superhydrophilic PVDF membrane for oil/water separation, J. Memb. Sci. 506 (2016) 60–70. doi:http://dx.doi.org/10.1016/j.memsci.2016.01.053.

[152] J. Zeng, Z. Guo, Superhydrophilic and underwater superoleophobic MFI zeolite-coated film for oil/water separation, Colloids Surfaces A Physicochem. Eng. Asp. 444 (2014) 283–288. doi:10.1016/j.colsurfa.2013.12.071.

[153] C.J. Van Oss, M.K. Chaudhury, R.J. Good, Interfacial Lifshitz-van der Waals and polar interactions in macroscopic systems, Chem. Rev. 88 (1988) 927–941. doi:10.1021/cr00088a006.

[154] C.J. van Oss, R.F. Giese, P.M. Costanzo, DLVO and Non-DLVO Interactions in Hectorite, Clays Clay Miner. 38 (1990) 151–159. doi:10.1346/CCMN.1990.0380206.

[155] C.J. van Oss, Acid-base interfacial interactions in aqueous media, Colloids Surfaces A Physicochem. Eng. Asp. 78 (1993) 1–49. doi:10.1016/0927-7757(93)80308-2.

[156] H.-C. Yang, K.-J. Liao, H. Huang, Q.-Y. Wu, L.-S. Wan, Z.-K. Xu, Mussel-inspired modification of a polymer membrane for ultra-high water permeability and oil-in-water emulsion separation, J. Mater. Chem. A. 2 (2014) 10225. doi:10.1039/c4ta00143e.

[157] N. Liu, Mussel power, Nature. 7 (2008) 2–3.

[158] P.S. Brown, B. Bhushan, Mechanically durable, superomniphobic coatings prepared by layer-by-layer technique for self-cleaning and anti-smudge, J. Colloid Interface Sci. 456 (2015) 210–218. doi:10.1016/j.jcis.2015.06.030.

[159] D. Hou, G. Dai, J. Wang, H. Fan, L. Zhang, Z. Luan, Preparation and characterization of PVDF/nonwoven fabric flat-sheet composite membranes for desalination through direct contact membrane distillation, Sep. Purif. Technol. 101 (2012) 1–10. doi:10.1016/j.seppur.2012.08.031.

[160] D. Hou, G. Dai, J. Wang, H. Fan, Z. Luan, C. Fu, Boron removal and desalination from seawater by PVDF flat-sheet membrane through direct contact membrane distillation, Desalination. 326 (2013) 115–124. doi:10.1016/j.desal.2013.07.023.

[161] H. Xie, T. Saito, M.A. Hickner, Zeta potential of ion-conductive membranes by streaming current measurements, Langmuir. 27 (2011) 4721–4727. doi:10.1021/la105120f.

[162] A. V. Delgado, F. González-Caballero, R.J. Hunter, L.K. Koopal, J. Lyklema, Measurement and interpretation of electrokinetic phenomena, J. Colloid Interface Sci. 309 (2007) 194–224. doi:10.1016/j.jcis.2006.12.075.

[163] M. Elimelech, W.H. Chen, J.J. Waypa, Measuring the zeta (electrokinetic) potential of reverse osmosis membranes by a streaming potential analyzer, Desalination. 95 (1994) 269–286. doi:10.1016/0011-9164(94)00064-6.

[164] K. Boussu, Y. Zhang, J. Cocquyt, P. Van der Meeren, A. Volodin, C. Van Haesendonck, et al., Characterization of polymeric nanofiltration membranes for systematic analysis of membrane performance, J. Memb. Sci. 278 (2006) 418–427. doi:10.1016/j.memsci.2005.11.027.

[165] D.L. Shaffer, J.R. Werber, H. Jaramillo, S. Lin, M. Elimelech, Forward osmosis: Where are we now?, Desalination. 356 (2014) 271–284. doi:10.1016/j.desal.2014.10.031.

[166] J. Israelachvili, Intermolecular and Surface Forces, 3rd Edition, 2010. doi:10.1016/B978-0-12-375182-9.10025-9.

[167] J.A. Brant, A.E. Childress, Colloidal adhesion to hydrophilic membrane surfaces, J. Memb. Sci. 241 (2004) 235–248. doi:10.1016/j.memsci.2004.04.036.

[168] E.M. V Hoek, S. Bhattacharjee, M. Elimelech, Effect of membrane surface roughness on colloid-membrane DLVO interactions, Langmuir. 19 (2003) 4836–4847. doi:10.1021/la027083c.

[169] A. Subramani, E.M. V Hoek, Direct observation of initial microbial deposition onto reverse osmosis and nanofiltration membranes, J. Memb. Sci. 319 (2008) 111–125. doi:10.1016/j.memsci.2008.03.025.

[170] S. Lin, M.R. Wiesner, Paradox of stability of nanoparticles at very low ionic strength, Langmuir. 28 (2012) 11032–11041. doi:10.1021/la3016589.

[171] J.A. Brant, A.E. Childress, Assessing short-range membrane-colloid interactions using surface energetics, J. Memb. Sci. 203 (2002) 257–273. doi:10.1016/S0376-7388(02)00014-5.

[172] C. Van Oss, R. Good, M. Chaudhury, C. Oss, Additive and nonadditive surface tension components and the interpretation of contact angles, Langmuir. 4 (1988) 884–891. doi:10.1021/la00082a018.

[173] E. Drioli, A. Ali, F. Macedonio, Membrane distillation: Recent developments and perspectives, Desalination. 356 (2015) 56–84. doi:10.1016/j.desal.2014.10.028.

[174] M. Khayet, T. Matsuura, J.I. Mengual, M. Qtaishat, Design of novel direct contact membrane distillation membranes, Desalination. 192 (2006) 105–111. doi:10.1016/j.desal.2005.06.047.

[175] A. Deshmukh, C. Boo, V. Karanikola, S. Lin, A.P. Straub, T. Tong, et al., Membrane Distillation at the Water-Energy Nexus: Limits, Opportunities, and Challenges, Energy Environ. Sci. (2018). doi:10.1039/C8EE00291F.

[176] Z. Wang, S. Lin, Membrane fouling and wetting in membrane distillation and their mitigation by novel membranes with special wettability, Water Res. 112 (2017) 38–47. doi:http://dx.doi.org/10.1016/j.watres.2017.01.022.

[177] P.D. Dongare, A. Alabastri, S. Pedersen, K.R. Zodrow, N.J. Hogan, O. Neumann, et al., Nanophotonics-enabled solar membrane distillation for off-grid water purification, Proc. Natl. Acad. Sci. 114 (2017) 6936–6941. doi:10.1073/pnas.1701835114.

[178] J. Wu, K.R. Zodrow, P.B. Szemraj, Q. Li, Photothermal Nanocomposite Membranes for Direct Solar Membrane Distillation, J. Mater. Chem. A. (2017). doi:10.1039/C7TA04555G.

[179] M.R. Qtaishat, T. Matsuura, 13 - Modelling of pore wetting in membrane distillation compared with pervaporation, 2015. doi:http://dx.doi.org.proxy2.library.illinois.edu/10.1016/B978-1-78242-246-4.00013-1.

[180] Y. Liao, R. Wang, A.G. Fane, Engineering superhydrophobic surface on poly(vinylidene fluoride) nanofiber membranes for direct contact membrane distillation, J. Memb. Sci. 440 (2013) 77–87. doi:10.1016/j.memsci.2013.04.006.

[181] Y. Chen, Z. Wang, K. Jennings, S. Lin, Probing Pore Wetting in Membrane Distillation using Impedance: Early Detection and Mechanism of Surfactant-induced Wetting, Environ. Sci. Technol. Lett. 4 (2017) 505–510. doi:10.1021/acs.estlett.7b00372.

[182] M. Gryta, Long-term performance of membrane distillation process, J. Memb. Sci. 265 (2005) 153–159. doi:10.1016/j.memsci.2005.04.049.

[183] M. Gryta, M. Barancewicz, Influence of morphology of PVDF capillary membranes on the performance of direct contact membrane distillation, J. Memb. Sci. 358 (2010) 158–167. doi:10.1016/j.memsci.2010.04.044.

[184] F.E. Ahmed, B.S. Lalia, R. Hashaikeh, Membrane-based detection of wetting phenomenon in direct contact membrane distillation, J. Memb. Sci. 535 (2017) 89–93. doi:10.1016/j.memsci.2017.04.035.

[185] J.M. Kavanagh, S. Hussain, T.C. Chilcott, H.G.L. Coster, Fouling of reverse osmosis membranes using electrical impedance spectroscopy: Measurements and simulations, Desalination. 236 (2009) 187–193. doi:10.1016/j.desal.2007.10.066.

[186] E. Barsoukov, J.R. Macdonald, Impedance Spectroscopy, 2005. doi:10.1002/0471716243.

[187] J.C. Tuberquia, W.S. Song, G.K. Jennings, Investigating the superhydrophobic behavior for underwater surfaces using impedance-based methods, Anal. Chem. 83 (2011) 6184–6190. doi:10.1021/ac200650z.

[188] J.C. Tuberquia, N. Nizamidin, G.K. Jennings, Effect of superhydrophobicity on the barrier properties of polymethylene films, Langmuir. 26 (2010) 14039–14046. doi:10.1021/la102312w.

[189] C.A. Escobar, A.R. Zulkifli, C.J. Faulkner, A. Trzeciak, G.K. Jennings, Composite fluorocarbon membranes by surface-initiated polymerization from nanoporous gold-coated alumina, ACS Appl. Mater. Interfaces. 4 (2012) 906–915. doi:10.1021/am201565b.

[190] S. Bannwarth, H. Breisig, V. Houben, C. Oberschelp, M. Wessling, Membrane impedance porometry, J. Memb. Sci. 542 (2017) 352–366. doi:10.1016/j.memsci.2017.08.019.

[191] Y. Gao, W. Li, W.C.L. Lay, H.G.L. Coster, A.G. Fane, C.Y. Tang, Characterization of forward osmosis membranes by electrochemical impedance spectroscopy, Desalination. 312 (2013) 45–51. doi:10.1016/j.desal.2012.03.006.

[192] J.S. Ho, J.H. Low, L.N. Sim, R.D. Webster, S.A. Rice, A.G. Fane, et al., In-situ monitoring of biofouling on reverse osmosis membranes: Detection and mechanistic study using electrical impedance spectroscopy, J. Memb. Sci. 518 (2016) 229–242. doi:10.1016/j.memsci.2016.06.043.

[193] J.S. Ho, L.N. Sim, R.D. Webster, B. Viswanath, H.G.L. Coster, A.G. Fane, Monitoring fouling behavior of reverse osmosis membranes using electrical impedance spectroscopy: A field trial study, Desalination. 407 (2017) 75–84. doi:10.1016/j.desal.2016.12.012.

[194] A. Antony, T. Chilcott, H. Coster, G. Leslie, In situ structural and functional

characterization of reverse osmosis membranes using electrical impedance spectroscopy, J. Memb. Sci. 425–426 (2013) 89–97. doi:10.1016/j.memsci.2012.09.028.

[195] M.T. Darestani, T.C. Chilcott, H.G.L. Coster, Electrical impedance spectroscopy study of piezoelectric PVDF membranes, J. Solid State Electrochem. 18 (2014) 595–605. doi:10.1007/s10008-013-2286-x.

[196] H.G.L. Coster, T.C. Chilcott, A.C.F. Coster, Impedance spectroscopy of interfaces, membranes and ultrastructures, in: Bioelectrochemistry Bioenerg., 1996: pp. 79–98. doi:10.1016/0302-4598(96)05064-7.

[197] H.G.L. Coster, K.J. Kim, K. Dahlan, J.R. Smith, C.J.D. Fell, Characterisation of ultrafiltration membranes by impedance spectroscopy. I. Determination of the separate electrical parameters and porosity of the skin and sublayers, J. Memb. Sci. 66 (1992) 19–26. doi:10.1016/0376-7388(92)80087-Z.

[198] V.S.T. Sim, J. Cen, T.H. Chong, A.P.S. Yeo, W.B. Krantz, H.G.L. Coster, et al., Novel Monitors Enable Early Detection of RO System Fouling, IDA J. Desalin. Water Reuse. 4 (2012) 36–48. doi:10.1179/ida.2012.4.3.36.

[199] E.M. V Hoek, M. Elimelech, Cake-Enhanced Concentration Polarization: A New Fouling Mechanism for Salt-Rejecting Membranes, Environ. Sci. Technol. 37 (2003) 5581–5588. doi:10.1021/es0262636.

[200] J.S. Park, T.C. Chilcott, H.G.L. Coster, S.H. Moon, Characterization of BSA-fouling of ion-exchange membrane systems using a subtraction technique for lumped data, J. Memb. Sci. 246 (2005) 137–144. doi:10.1016/j.memsci.2004.07.022.

[201] M.M.C. Garcia-Payo, M.A.M. Izquierdo-Gil, C. Fernandez-Pineda, Wetting Study of Hydrophobic Membranes via Liquid Entry Pressure Measurements with Aqueous Alcohol Solutions, J. Colloid Interface Sci. 230 (2000) 420–431. doi:10.1006/jcis.2000.7106.

[202] D.E.M. Warsinger, A. Servi, G.B. Connors, M.O. Mavukkandy, H.A. Arafat, K. Gleason, et al., Reversing membrane wetting in membrane distillation: comparing dryout to backwashing with pressurized air, Environ. Sci. Water Res. Technol. 3 (2017) 930–939. doi:10.1039/C7EW00085E.

[203] N.G.P. Chew, S. Zhao, C.H. Loh, N. Permogorov, R. Wang, Surfactant effects on water recovery from produced water via direct-contact membrane distillation, J. Memb. Sci. 528 (2017) 126–134. doi:10.1016/j.memsci.2017.01.024.

[204] A. Tuteja, W. Choi, M. Ma, J.M. Mabry, S. a Mazzella, G.C. Rutledge, et al., Designing superoleophobic surfaces., Science. 318 (2007) 1618–1622. doi:10.1126/science.1148326.

[205] A.K. Kota, W. Choi, A. Tuteja, Superomniphobic surfaces: Design and durability, MRS Bull. 38 (2013) 383–390. doi:10.1557/mrs.2013.101.

[206] E.J. Lee, B.J. Deka, J. Guo, Y.C. Woo, H.K. Shon, A.K. An, Engineering the Re-Entrant Hierarchy and Surface Energy of PDMS-PVDF Membrane for Membrane Distillation Using a Facile and Benign Microsphere Coating, Environ. Sci. Technol. 51 (2017) 10117–

10126. doi:10.1021/acs.est.7b01108.

[207] Y.G. Zmievskii, Determination of critical pressure in membrane distillation process, Pet. Chem. 55 (2015) 308–314. doi:10.1134/S0965544115040118.

[208] N.V. Churaev, G.A. Martynov, V.M. Starov, Z.M. Zorin, Some features of capillary imbibition of surfactant solutions, Colloid Polym. Sci. 259 (1981) 747–752.

[209] V.M. Starov, S.A. Zhdanov, M.G. Velarde, Capillary imbibition of surfactant solutions in porous media and thin capillaries: Partial wetting case, J. Colloid Interface Sci. 273 (2004) 589–595. doi:10.1016/j.jcis.2004.02.033.

[210] M.S. Romero-Cano, A. Martín-Rodríguez, F.J. de las Nieves, Adsorption and Desorption of Triton X-100 in Polystyrene Particles with Different Functionality: I. Adsorption Study, J. Colloid Interface Sci. 227 (2000) 322–328. doi:http://dx.doi.org/10.1006/jcis.2000.6862.

[211] A. Martín-Rodríguez, M.A. Cabrerizo-Vílchez, R. Hidalgo-Álvarez, A comparative study on the adsorption of Triton X-100 and Tween 20 onto latexes with different interfacial properties, J. Colloid Interface Sci. 187 (1997) 139–147. doi:10.1006/jcis.1996.4681.

[212] M.S. Romero-Cano, A. Martín-Rodríguez, F.J. de las Nieves, Adsorption and Desorption of Triton X-100 in Polystyrene Particles with Different Functionality: I. Adsorption Study, J. Colloid Interface Sci. 227 (2000) 322–328. doi:http://dx.doi.org/10.1006/jcis.2000.6862.

[213] J. Landers, G.Y. Gor, A. V Neimark, Colloids and Surfaces A: Physicochemical and Engineering Aspects, Colloids Surfaces A Physicochem. Eng. Asp. 437 (2013) 3–32. doi:10.1016/j.colsurfa.2013.01.007.

[214] J.D. Berry, M.J. Neeson, R.R. Dagastine, D.Y.C. Chan, R.F. Tabor, Measurement of surface and interfacial tension using pendant drop tensiometry, J. Colloid Interface Sci. 454 (2015) 226–237. doi:10.1016/j.jcis.2015.05.012.

[215] M.G. Cabezas, A. Bateni, J.M. Montanero, A.W. Neumann, A new drop-shape methodology for surface tension measurement, in: Appl. Surf. Sci., 2004: pp. 480–484. doi:10.1016/j.apsusc.2004.05.250.

[216] Z. Wang, S. Lin, Membrane fouling and wetting in membrane distillation and their mitigation by novel membranes with special wettability, Water Res. 112 (2017) 38–47. doi:10.1016/j.watres.2017.01.022.

[217] M.R. Qtaishat, T. Matsuura, Modelling of pore wetting in membrane distillation compared with pervaporation, in: Pervaporation, Vap. Permeat. Membr. Distill. Princ. Appl., 2015: pp. 385–413. doi:10.1016/B978-1-78242-246-4.00013-1.

[218] Z. Wang, S. Lin, Membrane fouling and wetting in membrane distillation and their mitigation by novel membranes with special wettability, Water Res. 112 (2017) 38–47. doi:http://dx.doi.org/10.1016/j.watres.2017.01.022.

[219] Z. Wang, Y. Chen, X. Sun, R. Duddu, S. Lin, Mechanism of Pore Wetting in Membrane Distillation with Alcohol vs. Surfactant, J. Memb. Sci. 559 (2018) 183–195. doi:10.1016/j.memsci.2018.04.045.

[220] N.G.P. Chew, S. Zhao, C. Malde, R. Wang, Polyvinylidene fluoride membrane modification via oxidant-induced dopamine polymerization for sustainable direct-contact membrane distillation, J. Memb. Sci. 563 (2018) 31–42. doi:10.1016/j.memsci.2018.05.035.

[221] M. Elimelech, J. Gregory, X. Jia, R.A. Williams, Modelling of particle deposition onto ideal collectors, Part. Depos. Aggreg. - Meas. Model. Simul. (1995). doi:http://dx.doi.org/10.1016/B978-075067024-1/50005-4.

[222] M. Khayet, Membranes and theoretical modeling of membrane distillation: A review, Adv. Colloid Interface Sci. 164 (2011) 56–88. doi:10.1016/j.cis.2010.09.005.

[223] M.C. García-Payo, M.A. Izquierdo-Gil, C. Fernández-Pineda, Wetting study of hydrophobic membranes via liquid entry pressure measurements with aqueous alcohol solutions, J. Colloid Interface Sci. 230 (2000) 420–431. doi:http://dx.doi.org/10.1006/jcis.2000.7106.

[224] R.W. Schofield, A.G. Fane, C.J.D. Fell, R. Macoun, Factors affecting flux in membrane distillation, Desalination. 77 (1990) 279–294. doi:10.1016/0011-9164(90)85030-E.

[225] N. Mikati, S. Wall, Diffusion of Sodium Dodecyl Sulfate Studied by a Steady-State Technique, Langmuir. 9 (1993) 113–116. doi:10.1021/la00025a026.

[226] M. Sudoh, K. Takuwa, H. Iizuka, K. Nagamatsuya, Effects of thermal and concentration boundary layers on vapor permeation in membrane distillation of aqueous lithium bromide solution, J. Memb. Sci. 131 (1997) 1–7. doi:10.1016/S0376-7388(97)00109-9.

[227] C.H. Chang, E.I. Franses, Adsorption dynamics of surfactants at the air/water interface: a critical review of mathematical models, data, and mechanisms, Colloids Surfaces A Physicochem. Eng. Asp. 100 (1995) 1–45. doi:10.1016/0927-7757(94)03061-4.

[228] J.R. McCutcheon, M. Elimelech, Influence of concentrative and dilutive internal concentration polarization on flux behavior in forward osmosis, J. Memb. Sci. 284 (2006) 237–247. doi:10.1016/j.memsci.2006.07.049.

[229] G.T. Gray, J.R. McCutcheon, M. Elimelech, Internal concentration polarization in forward osmosis: role of membrane orientation, Desalination. 197 (2006) 1–8. doi:10.1016/j.desal.2006.02.003.

[230] M.C. Porter, Concentration Polarization with Membrane Ultrafiltration, Ind. Eng. Chem. Prod. Res. Dev. 11 (1972) 234–248. doi:10.1021/i360043a002.

[231] N.R. Biswal, S. Paria, Wetting of PTFE and glass surfaces by aqueous solutions of cationic and anionic double-chain surfactants, Ind. Eng. Chem. Res. 51 (2012) 10172–10178. doi:10.1021/ie301198k.

[232] P.E. Levitz, Adsorption of non ionic surfactants at the solid/water interface, Colloids Surfaces A Physicochem. Eng. Asp. 205 (2002) 31–38. doi:10.1016/S0927-7757(01)01139-6.

[233] M.J. Rosen, A.W. Cohen, M. Dahanayake, X.Y. Hua, Relationship of structure to properties in surfactants. 10. Surface and thermodynamic properties of 2-dodecyloxypoly(ethenoxyethanol)s, C12H25(OC2H4)xOH, in aqueous solution, J. Phys. Chem. 86 (1982) 541–545. doi:10.1021/j100393a025.

[234] B. Dong, N. Li, L. Zheng, L. Yu, T. Inoue, Surface adsorption and micelle formation of surface active ionic liquids in aqueous solution, Langmuir. 23 (2007) 4178–4182. doi:10.1021/la0633029.

[235] Y.X. Huang, Z. Wang, J. Jin, S. Lin, Novel Janus Membrane for Membrane Distillation with Simultaneous Fouling and Wetting Resistance, Environ. Sci. Technol. 51 (2017) 13304–13310. doi:10.1021/acs.est.7b02848.

[236] D. Hou, Z. Wang, K. Wang, J. Wang, S. Lin, Composite membrane with electrospun multiscale-textured surface for robust oil-fouling resistance in membrane distillation, J. Memb. Sci. 546 (2018) 179–187. doi:10.1016/j.memsci.2017.10.017.

[237] Y. Kwon, N. Patankar, J. Choi, J. Lee, Design of surface hierarchy for extreme hydrophobicity, Langmuir. 25 (2009) 6129–6136. doi:10.1021/la803249t.

[238] Z. Wang, Y. Chen, S. Lin, Kinetic model for surfactant-induced pore wetting in membrane distillation, J. Memb. Sci. 564 (2018) 275–288. doi:10.1016/j.memsci.2018.07.010.

[239] Z. Wang, D. Hou, S. Lin, Composite Membrane with Underwater-Oleophobic Surface for Anti-Oil-Fouling Membrane Distillation, Environ. Sci. Technol. 50 (2016) 3866–3874. doi:10.1021/acs.est.5b05976.

[240] Z. Wang, J. Jin, D. Hou, S. Lin, Tailoring surface charge and wetting property for robust oil-fouling mitigation in membrane distillation, J. Memb. Sci. 516 (2016) 113–122. doi:10.1016/j.memsci.2016.06.011.

[241] J. Israelachvili, Intermolecular and Surface Forces, 3rd ed., Elsevier Inc, Waltham, MA, 2011.

[242] A.K. Kota, G. Kwon, A. Tuteja, The design and applications of superomniphobic surfaces, NPG Asia Mater. 6 (2014) e109. doi:10.1038/am.2014.34.

[243] H. Meng, S. Wang, J. Xi, Z. Tang, L. Jiang, Facile means of preparing superamphiphobic surfaces on common engineering metals, J. Phys. Chem. C. 112 (2008) 11454–11458. doi:10.1021/jp803027w.

[244] D. Nyström, J. Lindqvist, E. Östmark, P. Antoni, A. Carlmark, A. Hult, et al., Superhydrophobic and self-cleaning bio-fiber surfaces via ATRP and subsequent postfunctionalization, ACS Appl. Mater. Interfaces. 1 (2009) 816–823. doi:10.1021/am800235e.

[245] A. Ceria, P.J. Hauser, Atmospheric plasma treatment to improve durability of a water and oil repellent finishing for acrylic fabrics, Surf. Coatings Technol. 204 (2010) 1535–1541. doi:10.1016/j.surfcoat.2009.09.077.

[246] A. Vilčnik, I. Jerman, A.Š. Vuk, M. Koželj, B. Orel, B. Tomšič, et al., Structural properties and antibacterial effects of hydrophobic and oleophobic sol-gel coatings for cotton fabrics, Langmuir. 25 (2009) 5869–5880. doi:10.1021/la803742c.

[247] M. Hikita, K. Tanaka, T. Nakamura, T. Kajiyama, A. Takahara, Super-liquid-repellent surfaces prepared by colloidal silica nanoparticles covered with fluoroalkyl groups, Langmuir. 21 (2005) 7299–7302. doi:10.1021/la050901r.

[248] C.T. Hsieh, Y.S. Cheng, S.M. Hsu, J.Y. Lin, Water and oil repellency of flexible silica-coated polymeric substrates, Appl. Surf. Sci. 256 (2010) 4867–4872. doi:10.1016/j.apsusc.2010.01.081.

[249] Z. Wang, S. Lin, The Impact of Low-surface-energy Functional Groups on Oil Fouling Resistance in Membrane Distillation, J. Memb. Sci. 527 (2016) 68–77. doi:10.1016/j.memsci.2016.12.063.

[250] W. Chen, Y. Su, J. Peng, Y. Dong, X. Zhao, Z. Jiang, Engineering a robust, versatile amphiphilic membrane surface through forced surface segregation for ultralow flux-decline, Adv. Funct. Mater. 21 (2011) 191–198. doi:10.1002/adfm.201001384.

[251] W. Chen, Y. Su, J. Peng, X. Zhao, Z. Jiang, Y. Dong, et al., Efficient wastewater treatment by membranes through constructing tunable antifouling membrane surfaces, Environ. Sci. Technol. 45 (2011) 6545–6552. doi:10.1021/es200994n.

[252] J.R. Werber, C.O. Osuji, M. Elimelech, Materials for next-generation desalination and water purification membranes, Nat. Rev. Mater. (2016) 16018. doi:10.1038/natrevmats.2016.18.

[253] H.F. Hoefnagels, D. Wu, G. De With, W. Ming, Biomimetic superhydrophobic and highly oleophobic cotton textiles, Langmuir. 23 (2007) 13158–13163. doi:10.1021/la702174x.

[254] X. Feng, L. Jiang, Design and creation of superwetting/antiwetting surfaces, Adv. Mater. 18 (2006) 3063–3078. doi:10.1002/adma.200501961.

[255] L. Ostrovskaya, H. Diamant, T.A. Witten, M. Poujade, C. Guthmann, E. Rolley, et al., Roughness-induced non-wetting, Europhys. Lett. 52 (2000) 165–170.

[256] J. Yang, Z. Zhang, X. Xu, X. Zhu, X. Men, X. Zhou, Superhydrophilic–superoleophobic coatings, J. Mater. Chem. 22 (2012) 2834. doi:10.1039/c2jm15987b.

[257] L. Wang, X. Li, G. Zhang, J. Dong, J. Eastoe, Oil-in-water nanoemulsions for pesticide formulations, J. Colloid Interface Sci. 314 (2007) 230–235. doi:10.1016/j.jcis.2007.04.079.

[258] B. Abismaïl, J.P. Canselier, A.M. Wilhelm, H. Delmas, C. Gourdon, Emulsification by ultrasound: Drop size distribution and stability, Ultrason. Sonochem. 6 (1999) 75–83.

doi:10.1016/S1350-4177(98)00027-3.

[259] Y. Li, Y. Su, X. Zhao, X. He, R. Zhang, J. Zhao, et al., Antifouling, high-flux nanofiltration membranes enabled by dual functional polydopamine, ACS Appl. Mater. Interfaces. 6 (2014) 5548–5557. doi:10.1021/am405990g.

[260] X. Zhao, Y. Su, W. Chen, J. Peng, Z. Jiang, Grafting perfluoroalkyl groups onto polyacrylonitrile membrane surface for improved fouling release property, J. Memb. Sci. 415–416 (2012) 824–834. doi:10.1016/j.memsci.2012.05.075.

[261] Y. Li, Y. Su, X. Zhao, R. Zhang, J. Zhao, X. Fan, et al., Surface fluorination of polyamide nanofiltration membrane for enhanced antifouling property, J. Memb. Sci. 455 (2014) 15–23. doi:10.1016/j.memsci.2013.12.060.

[262] S. Rajesh, K.H. Shobana, S. Anitharaj, D.R. Mohan, Preparation, morphology, performance, and hydrophilicity studies of poly(amide-imide) incorporated cellulose acetate ultrafiltration membranes, Ind. Eng. Chem. Res. 50 (2011) 5550–5564. doi:10.1021/ie1019613.

[263] G. Kang, H. Ko, C. Choi, Chemical Bond Structure of a-C:F Films with a Low Dielectric Constant Deposited by Using CH4/CF4 ICPCVD, 42 (2003) 676–681.

[264] J. Serra, P. Gonz??lez, S. Liste, C. Serra, S. Chiussi, B. Le??n, et al., FTIR and XPS studies of bioactive silica based glasses, J. Non. Cryst. Solids. 332 (2003) 20–27. doi:10.1016/j.jnoncrysol.2003.09.013.

[265] B.P. Singh, D. Singh, R.B. Mathur, T.L. Dhami, Influence of surface modified MWCNTs on the mechanical, electrical and thermal properties of polyimide nanocomposites, Nanoscale Res. Lett. 3 (2008) 444–453. doi:10.1007/s11671-008-9179-4.

[266] S. Mallakpour, A. Zadehnazari, Nanostructure Formation in Chiral Poly(amide-imide)s Based on Dopamine Moiety and N-Trimellitylimido-L-Amino Acids in the Main Chain, J. Chil. Chem. Soc. 57 (2012) 1248–1252.

[267] Y. Wu, M. Yan, X. Liu, P. Lv, J. Cui, M. Meng, et al., Accelerating the design of multi-component nanocomposite imprinted membranes by integrating a versatile metal–organic methodology with a mussel-inspired secondary reaction platform, Green Chem. 17 (2015) 3338–3349. doi:10.1039/C5GC00453E.

[268] V.K. Thakur, M.-F. Lin, E.J. Tan, P.S. Lee, Green aqueous modification of fluoropolymers for energy storage applications, J. Mater. Chem. 22 (2012) 5951. doi:10.1039/c2jm15665b.

[269] B.J. Kirby, Micro- and Nanoscale Fluid Mechanics: Transport in Microfluidic Devices, Brian. (2010) 512. doi:10.1007/s13398-014-0173-7.2.

[270] H. Bruus, Theoretical microfluidics, Physics (College. Park. Md). 18 (2008) 363. doi:10.1111/j.1574-6968.2009.01808.x.

[271] K. Streletzky, G.D.J. Phillies, Temperature Dependence of Triton X-100 Micelle Size and

Hydration, Langmuir. 11 (1995) 42–47. doi:10.1021/la00001a011.

[272] H.H. Paradies, Shape and size of a nonionic surfactant micelle. Triton X-100 in aqueous solution, J. Phys. Chem. 84 (1980) 599–607. doi:10.1021/j100443a008.

[273] C.H. Chang, E.I. Franses, Modified Langmuir-Hinselwood kinetics for dynamic adsorption of surfactants at the air/water interface, Colloids and Surfaces. 69 (1992) 189–201. doi:10.1016/0166-6622(92)80230-Y.

[274] A.B. Mandal, B.U. Nair, Cyclic voltammetric technique for the determination of the critical micelle concentration of surfactants, self-diffusion coefficient of micelles, and partition coefficient of an electrochemical probe, J. Phys. Chem. 95 (1991) 9008–9013. doi:10.1021/j100175a106.

[275] F. Luschtinetz, C. Dosche, Determination of micelle diffusion coefficients with fluorescence correlation spectroscopy (FCS), J. Colloid Interface Sci. 338 (2009) 312–315. doi:10.1016/j.jcis.2009.06.064.

[276] D. Attwood, G. Ktistis, Y. Mccormick, M.J. Story, Solubilization of Indomethacin by Polysorbate 80 in Mixed Water-Sorbitol Solvents, J. Pharm. Pharmacol. (1989) 83–86.

[277] J.R. Campanelli, X. Wang, Comments on modelling the diffusion-controlled adsorption of surfactants, Can. J. Chem. Eng. 76 (1998) 51–57. doi:10.1002/cjce.5450760107.

[278] D.C.H. Cheng, E. Gulari, Micellization and intermicellar interactions in aqueous sodium dodecyl benzene sulfonate solutions, J. Colloid Interface Sci. 90 (1982) 410–423. doi:10.1016/0021-9797(82)90308-3.